



VNIVERSITAT
DE VALÈNCIA

FACULTAD DE CIENCIAS BIOLÓGICAS

Departamento de Biología Celular, Biología Funcional y Antropología Física.
Instituto Universitario de Biotecnología y Biomedicina (BIOTECMED).

Doctorado en Biomedicina y Biotecnología

Unveiling neural stem cell quiescence: a crosstalk with the extracellular matrix

Laura Blasco Chamarro

Directora de la Tesis Doctoral:
Isabel Fariñas Gómez

València, enero 2023

Dña. Isabel Fariñas Gómez, catedrática del Departamento de Biología Celular, Biología Funcional y Antropología Física de la Universitat de València, y miembro del Instituto Universitario de Biotecnología y Biomedicina (BIOTECMED), como directora.

D. Andrés Cervantes Ruipérez, catedrático de Medicina de la Universitat de València y director científico del Instituto de Investigación Sanitaria INCLIVA, como tutor.

INFORMAN QUE:

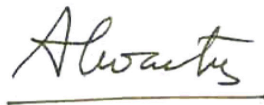
Dña. Laura Blasco Chamarro ha realizado bajo la dirección de Isabel Fariñas Gómez la tesis doctoral titulada “Unveiling neural stem cell quiescence: a crosstalk with the extracellular matrix”, y que hallándose concluida, autorizan su presentación a fin de que pueda ser juzgada por el tribunal correspondiente para la obtención del grado de Doctora por la Universitat de València.

Y para que conste, en cumplimiento de la legislación, firman el presente informe.

València, enero 2023



Dra. Isabel Fariñas Gómez



Dr. Andrés Cervantes Ruipérez

A mis padres, Ángela y Óscar.

A mi hermana, Sara.

A Pere.

*“Research is to see what everybody else has seen,
and to think what nobody else has thought.”*

-Albert Szent-Gyorgyi

Index

<i>Abbreviation list</i>	15
<i>Introduction</i>	21
1. Studying stem cells: from homeostasis to tumorigenesis	23
2. The neurogenic niche at a glance	25
3. NSC coexist and transit between three actively regulated states	28
4. BuMPing to quiescence	31
5. Multi-level regulation through SEZ vasculature	34
6. BM structures as signal integrators	37
7. The role of YAP/TAZ	42
<i>Objectives</i>	47
<i>Material and Methods</i>	51
1. Mouse strains and handling	53
2. <i>In vivo</i> methods	53
2.1 <i>In utero</i> electroporation	53
2.2 FACS strategy to characterize the neurogenic lineage	54
2.3 Animal perfusion and brain processing	56
2.4 Immunohistochemistry	56
3. Microscopy techniques	56
3.1 Fluorescence microscopy	56
3.2 CLARITY-based tissue clearing	57
3.3 Expansion microscopy	57
3.4 Transmission electron microscopy	58
4. <i>In vitro</i> NSC cell culture methods	59
4.1 Establishment of NSC primary cultures	59
4.2 NSC subculture	59
4.3 NSC treatments and culture over CM matrices	60
4.4 aNSC sorting	61
4.5 Neurosphere formation assay	61

4.6 Evaluation of NSC proliferation by FACS: DFFDA and EdU	62
4.7 Immunocytochemistry	63
4.8 NSC nucleofections	63
5. EC culture methods	65
5.1 Primary EC isolation with CD31 ⁺ magnetic beads	65
5.2 Endothelial cell line maintenance	66
5.3 Direct NSC-EC co-culture and treatments	66
6. Molecular methods	67
6.1 RNA extraction and qPCR	67
6.2 Laminin immunoprecipitation and western blot	68
6.3. Proteomics of BMP4-treated NSCs	68
6.3.1 Sample processing and digestion	68
6.3.2 LC-MS/MS in differential proteomics	69
6.3.3 Protein identification and quantification	69
7. Bioinformatic analyses	70
8. Image analyses	71
9. Statistical analyses	72
Results	75

1. BMP4 as a model of NSC quiescence <i>in vitro</i>	77
1.1 BMP4 response is EGF-dependent and favors NSC adhesion	77
1.2 BMP4-treated NSCs resemble <i>in vivo</i> quiescent cells	79
2. BMP4 in ECM secretion	82
2.1 BMP4 proteomics reveal changes in ECM components	82
2.2 Quiescent NSCs display a shared ECM-related signature	84
2.3 BMP4 induces LM secretion	87
3. qNSC disposition in the SEZ niche	88
3.1 qNSC display heterogeneous apico-basal positions	88
3.2 qNSCs closely interact with LM-enriched BM structures	90
4. Quiescent NSC are preferentially adhered to LM ⁺ BM	93
4.1 <i>In vivo</i> quiescent NSCs are differentially surrounded by LM	93

4.2 qNSCs are differentially co-isolated with BVs	94
5. Vascular regulation of NSCs	96
5.1 Direct co-culture with ECs induces NSC quiescence	96
5.2 LM-integrin interactions are enhanced in co-culture	98
5.3 BMP4 participates in co-culture induced quiescence	100
6. Study of the role of NSC self-assembled ECM	100
6.1 BMP4-CM matrix favors a reversible cell cycle arrest	100
6.2 Integrin α 6 conditions quiescence over self-assembled ECM	103
7. Downstream mechanisms regulating adhesion to self-assembled ECM	105
7.1 NSC spreading and quiescence induction depends on ROCK	105
7.2 YAP-TEAD activity is enhanced over self-assembled ECM	108
7.3 Constitutive YAP activation induces NSC arrest	110
<i>Discussion</i>	113
<i>Conclusions</i>	127
<i>Resumen</i>	131
<i>Bibliography</i>	147
<i>Annex</i>	171
<i>Agradecimientos</i>	183

Figure index

Introduction

Figure 1. Stem cell potency and self-renewal.	23
Figure 2. Adult subependymal zone niche.	26
Figure 3. Main molecular traits of NSC populations.	30
Figure 4. Canonical and non-canonical BMP signaling pathways and BMP sources in the SEZ niche.	32
Figure 5. EC-derived signals.	36
Figure 6. BM composition in the SEZ.	39
Figure 7. The ECM as a signal integrator.	41
Figure 8. RhoA/ROCK and Hippo pathway in the activation of YAP/TAZ.	44

Material and Methods

Graphical Method 1. <i>In utero</i> electroporation strategy.	54
Graphical Method 2. FACS strategy for lineage characterization.	55
Graphical Method 3. Methodologies to increase microscopy resolution.	58
Graphical Method 4. Experimental pipeline for studying BMP4-induced NSC self-assembled matrix.	60
Graphical Method 5. NSC-EC co-cultures.	66

Results

Figure 1. BMP4-induced quiescence depends on mitogenic stimulation and induces NSC adhesion.	78
Figure 2. Proteomic analysis of BMP4-treated NSCs.	79
Figure 3. BMP4-treated NSCs resemble DFFDA ^{high} cells.	80
Figure 4. BMP4 mimics the molecular profile of <i>in vivo</i> qNSCs.	81
Figure 5. Matrisome-associated and SEZ-specific proteomes are affected after BMP4 treatment.	82
Figure 6. BMP4 tightly regulates ECM protein levels.	83
Figure 7. qNSCs have increased expression of matrisome genes.	85

Figure 8. LM receptors are enriched in qNSCs.	86
Figure 9. BMP4 regulates LM transcription and protein secretion.	87
Figure 10. Apico-basal distribution of IUE-labelled qNSC.	89
Figure 11. qNSC contact LM ⁺ BVs.	91
Figure 12. qNSC interaction with vascular and speckled BM.	92
Figure 13. qNSCs display higher levels of LM.	93
Figure 14. qNSCs are co-isolated with ECs.	94
Figure 15. qNSC-EC binding is mediated by integrin $\alpha 6$.	96
Figure 16. Direct EC co-culture induces NSC quiescence.	97
Figure 17. ITGA6-LM interactions in co-culture.	99
Figure 18. Noggin reverts co-culture induced quiescence and LM desposition.	100
Figure 19. Culturing over BMP4-CM matrix favors NSC adhesion and quiescence.	101
Figure 20. BMP4-CM matrix causes a reversible NSC cell cycle arrest.	102
Figure 21. Integrin $\alpha 6$ conditions NSC proliferation and spreading over self-assembled matrix.	104
Figure 22. STRING analysis of BMP4 upregulated proteins from adhesion-related GO categories.	106
Figure 23. Adhesion to self-assembled matrix is dependent on ROCK activity.	107
Figure 24. YAP signature in NSC populations.	108
Figure 25. YAP/TEAD transcriptional activity is induced over BMP4-CM matrix.	109
Figure 26. NSCs nucleofected with constitutively active YAP adhere over uncoated wells and reduce their proliferation.	111
Figure 27. BMP4-induced NSC adhesion depends on YAP/TEAD activity.	111

Abbreviation list

ACN:	acetonitrile
ADAM:	a desintegrin and metalloproteinase
aNSCs:	activated neural stem cells
AR:	aspect ratio
Ara-C:	cytosine arabinoside
BBB:	blood-brain barrier
BDNF:	brain-derived neurotrophic factor
bFGF:	basic fibroblast growth factor
BM:	basement membrane
BMP:	bone morphogenetic protein
BMPR:	BMP receptor
BSA:	bovine serum albumin
BV:	blood vessel
CD:	cluster of differentiation
CDC42:	cell division control protein 42 homolog
cDNA:	complementary DNA
CM:	conditioned media
CMV:	cytomegalovirus
CSF:	cerebrospinal fluid
CXCR4:	receptor de quimiocina C-X-C 4
DAPI:	4',6-diamidino-2-phenylindole
DE:	differentially expressed
DIA:	data-independent acquisition
DIV:	days <i>in vitro</i>
DMSO:	dimethyl sulphoxyde
DNA:	deoxyribonucleic acid
E:	embryonic day
EC:	endothelial cell

ECM:	extracellular matrix
EdU:	5-Ethynyl-2'-deoxyuridine
EDTA:	ethylenediaminetetraacetic acid
e.g:	<i>exempli gratia</i> , “for example”
FA:	focal adhesion
FACS:	fluorescence activated cell sorting
FAK:	focal adhesion kinase
FC:	fold change
FDR:	false discovery rate
GAP:	GTPase activating protein
GDI:	guanine nucleotide dissociation inhibitors
GD/TP:	guanosine di/triphosphate
GFAP:	glial fibrillary acidic protein
GFP:	green fluorescent protein
GLAST:	glutamate aspartate transporter
GO:	gene ontology
GP:	glycoprotein
GPCR:	G-protein coupled receptor
HS:	heparan sulfate
HSC:	hematopoietic stem cell
HUVEC:	human umbilical vein endothelial cell
H2B:	histone 2B
ICC:	immunocytochemistry
IHC:	immunohistochemistry
IP:	immunoprecipitation
IUE:	<i>in utero</i> electroporation
i.e:	<i>id est</i> , “in other words”
i.p:	intraperitoneal
JNK:	c-Jun N-terminal kinase
kDa:	kilodalton
LATS:	large tumor suppression kinase
LIF:	leukemia inhibitory factor
LIMK:	LIM kinase
LV:	lateral ventricle
MAPK:	MAP kinase

MFI:	median fluorescence intensity
MMP:	matrix metalloproteinase
MOB:	mps1-binder-related
mRNA:	messenger ribonucleic acid
MS:	mass spectrometry
MST:	mammalian STE20-like protein kinase
NB:	neuroblast
NPC:	neural progenitor cells
NSC:	neural stem cell
NVU:	neuro-vascular unit
OB:	olfactory bulb
PBS:	phosphate buffer saline
PCA:	principal component analysis
PEDF:	pigmented epithelium-derived factor
PIGF:	placental growth factor
pNSCs:	primed NSCs
qNSCs:	quiescent NSCs
qPCR:	quantitative polymerase chain reaction
Rac1:	Ras-related C3 botulinum toxin substrate 1
Ref.:	reference
RFP:	red fluorescent protein
RGC:	radial glia cells
Rho:	Ras homolog
RhoA:	Ras homolog family member A
RMS:	rostral migratory stream
RNA:	ribonucleic acid
ROCK:	Rho associated coiled-coil containing kinase
RT:	room temperature
R-SMAD:	receptor-regulated SMAD
SAV:	salvador homolog
SC:	stem cell
SDF:	stromal derived growth factor
SEM:	standard error of the mean
SEZ:	subependymal zone

SGZ:	subgranular zone
SHH:	sonic hedgehog
SWATH:	sequential window acquisition of all theoretical mass spectra
TAZ:	transcriptional coactivator with PDZ-binding motif
TBS-T:	tris buffer saline-tween
TEAD:	TEA domain family member
TEM:	transmission electron microscopy
TF:	transcription factor
TFA:	trifluoroacetic acid
TGF:	transforming growth factor
vs.:	<i>versus</i>
WB:	western blot
WT:	wild-type
YAP:	YES-associated protein
ZO:	zonula occludens

Introduction



1. Studying stem cells: from homeostasis to tumorigenesis

Resident somatic stem cells (SCs) in adult tissues, although constituting a small pool of cells, bear the brunt of having to regulate tissue maintenance in homeostasis and after damage throughout life (Barker *et al.*, 2010; Simons & Clevers, 2011). SCs have in common their ability to self-renew, a process by which they divide to give rise to daughter cells with SC properties, and to differentiate into at least one mature tissue-specific cell type. For most SCs, divisions are essentially asymmetrical (Bonaguidi *et al.*, 2011), giving rise to two daughter cells, one with self-renewing potential, and another one that is either differentiated or at least more committed to generate mature progeny. This type of division will enable the preservation of the SC pool without expanding it, for which symmetrical divisions would be required. Symmetric consuming divisions can also occur, which produce two differentiated cells that should be correctly balanced with self-renewing divisions in order to avoid the depletion of the SC pool (**Figure 1**).

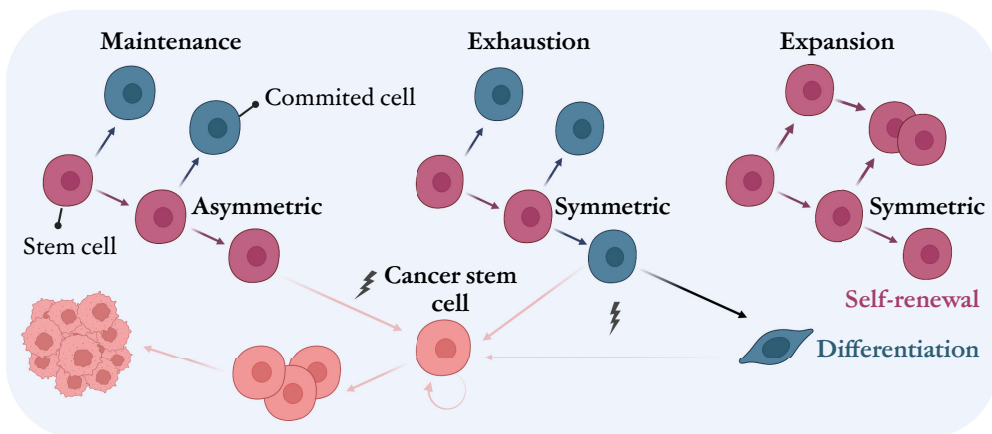


Figure 1. Stem cell potency and self-renewal. Asymmetric divisions give rise to a SC (magenta) and a more committed or differentiated cell (blue), favoring an equilibrium that promotes their maintenance. Self-renewing divisions (see *self-renewal* in figure) and terminal divisions (*differentiation* in figure) should be correctly balanced to enable tissue homeostasis. Unbalanced symmetrical divisions can lead to SC pool expansion or exhaustion. Furthermore, potential harmful mutations in SCs, or in partially or fully committed cells can favor the acquisition of cancer SC properties with uncontrolled proliferation potential that may prone for tumorigenesis. SC: stem cell. Figure adapted from (Ito & Suda, 2014). Created with BioRender.com.

Undoubtedly, maintaining a regulated balance between self-renewal and differentiation is key to accomplish a correct tissue homeostasis. Therefore, the study of the mechanisms by which this is regulated have been, for many years, in the spotlight of SC research. Nevertheless, the study of SCs is far from a one-size-fits-all approach, as its

Introduction

behavior is tightly conditioned by the specific function of the tissue in which they reside. For example, SCs from the intestine or the skin are constantly exposed to environmental assault, requiring higher rates of cell replacement (Barker *et al.*, 2010). Instead, the generation of new neurons from neural stem cells (NSCs) occurs, although continuously, at a slower pace, and in this case, hardly participating in brain repair (Goodell & Rando, 2015).

As occurs with most cell types, SCs do not remain unchanged with time, and lose their potential and self-renewal capacities with aging (Kalamakis *et al.*, 2019), making it more difficult to avoid SC pool consumption. The aging process is complex, as there are its consequences. SC dysregulation clearly contributes to the generation of the aging phenotype, while at the same time, other cellular and molecular disturbances occurring in parallel in the aged tissue, directly condition the SC detrimental phenotype. There are different factors that can cause injurious changes in SCs: genetic mutations, epigenetic changes, and/or extrinsic factors (Goodell & Rando, 2015). Mutations can, in addition, be carried forward to the differentiated progeny, which is especially alarming when they imply functional deficiencies with survival advances, as they could prime for tumor formation (**Figure 1**). It should be noted that, in a physiological context, there are multiple shared pathways between cancer cells and SC development (Reya *et al.*, 2001). For example, overexpression of oncogene *Bcl-2* by hematopoietic stem cells (HSCs) favor cell number increase *in vivo* by preventing apoptosis (Domen & Weissman, 2000). However, such mechanisms must be tightly controlled, as its imbalance could lead to tumorigenesis.

The potential dysregulation of this pathways is, besides, worsened by the fact that adult SCs are the longest living proliferative cells in multicellular organisms, which highly increases the risk of accumulating detrimental mutations spontaneously generated through cell divisions (Blokzijl *et al.*, 2016; Ermolaeva *et al.*, 2018). Transformed HSCs, for example, can initiate certain types of leukemia, and recent genetic evidence shows that glioblastoma, which is the most aggressive tumor in the brain, can arise from NSCs in the subependymal zone (SEZ) (Alcantara-Laguno *et al.*, 2009; Alcantara-Llaguno *et al.*, 2016; Lee *et al.*, 2018). Bearing this in mind, we consider that the study of the basic mechanisms regulating SC behavior are of great value both to better understand SC biology in the context of homeostasis and disease, and to hold better prospects for finding targets to potentially interfere with tissue rejuvenation and potential SC-derived tumorigenic processes. In this thesis, we will specifically focus on the study of NSCs in the adult SEZ, and the mechanisms that regulate their maintenance in a physiological context.

2. The neurogenic niche at a glance

NSCs are multipotent self-renewing cells that give rise, during embryonic development, to the complete pool of neurons and glial cells in the brain and spinal cord (Urbán *et al.*, 2019). The dogma encountered regarding NSC function being limited to embryonic stages, was called into question more than 50 years ago by John Altman's discoveries, which suggested that new neurons could also be formed during adulthood (Altman, 1962; Altman & Das, 1965). However, adult neurogenesis remained controversial and was further confirmed decades later by the studies of Nottebohm and colleagues demonstrating, in songbirds, the formation of new neurons that integrated in the song-control nuclei (Burd & Nottebohm, 1985; Paton & Nottebohm, 1984). Although it is true that most NSCs disappear at late embryonic or early postnatal stages as they generate differentiated progeny, in most mammal species, NSCs are maintained in specialized brain regions or *niches*, where they are subjected to specific environmental cues needed for their long-term maintenance (Obernier & Alvarez-Buylla, 2019; Urbán *et al.*, 2019). These unique microenvironments are located in two specialized regions in the brain: the subgranular zone (SGZ) in the hippocampus, and in the SEZ, which will be specifically addressed in this thesis.

The SEZ, which lines the walls of the lateral ventricles (LVs), is the largest and most active germinal niche in the adult mammalian brain. It homes thousands of NSCs that give rise to millions of neurons throughout lifespan, both in homeostasis and after injury (Obernier *et al.*, 2018; Obernier & Alvarez-Buylla, 2019). Albeit 20% of NSC divisions are self-renewing, most of them are consuming (Obernier & Alvarez-Buylla, 2019; Ponti *et al.*, 2013) and will initiate a hierarchical lineage progression that starts with the formation of two transit-amplifying neural progenitor cells (NPCs). NPCs will divide symmetrically 3-4 times to give rise to more committed early neuroblasts (NB1), that will still go through 1-2 rounds of division to amplify the number of young neurons generated (Ponti *et al.*, 2013), to finally generate non-proliferative migrating late NBs (also named NB2). NB2 will form the rostral migratory stream (RMS) and travel relatively long distances (3-8 mm in mouse) to head towards the olfactory bulb (OB), where they will generate interneurons that will integrate into pre-existing circuits and participate in the refinement of the processes of odor discrimination and odor-reward association. In addition to neurogenesis, NSCs also participate in gliogenesis to a lesser extent, as they can form astrocytes and oligodendrocytes, conferring the brain with a certain degree of plasticity (Obernier & Alvarez-Buylla, 2019; Urbán *et al.*, 2019).

To fulfill the complex process that is neurogenesis, NSCs go through different steps which are tightly regulated by both cell-intrinsic and cell-extrinsic mechanisms, the latter

Introduction

originated from the unique microenvironment in which they reside (Morante-Redolat & Porlan, 2019; Quaresima *et al.*, 2022). To understand the signals to which NSCs are subjected, we should first consider the origin and disposition of these cells in their niche.

At the cellular level, NSCs are unique multipotent astrocytes that are specified at mid embryonic (E) stages (E15.5) from radial glial cells (RGCs) (Fuentelba *et al.*, 2015). Recent transcriptome analyses have revealed that the core signature linked to NSC identity is widely shared between RGCs and adult SEZ NSCs (Yuzwa *et al.*, 2017). Moreover, NSCs inherit some of the RGCs morphological and biochemical features, such as their elongated bipolar radial morphology and the expression of specific astrocytic markers such as glial acidic fibrillary protein (GFAP) and glutamate transporter (GLAST). Remarkably, they also retain the characteristic apico-basal polarity of an epithelial niche, that confers them with a unique compartmentalized cytoarchitecture that favors multiple interactions with other constituents (i.e. the ependyma in the apical side and the vascular compartment in the basal) (**Figure 2**) (Chaker *et al.*, 2016; Doetsch *et al.*, 1999; Doetsch *et al.*, 2003).

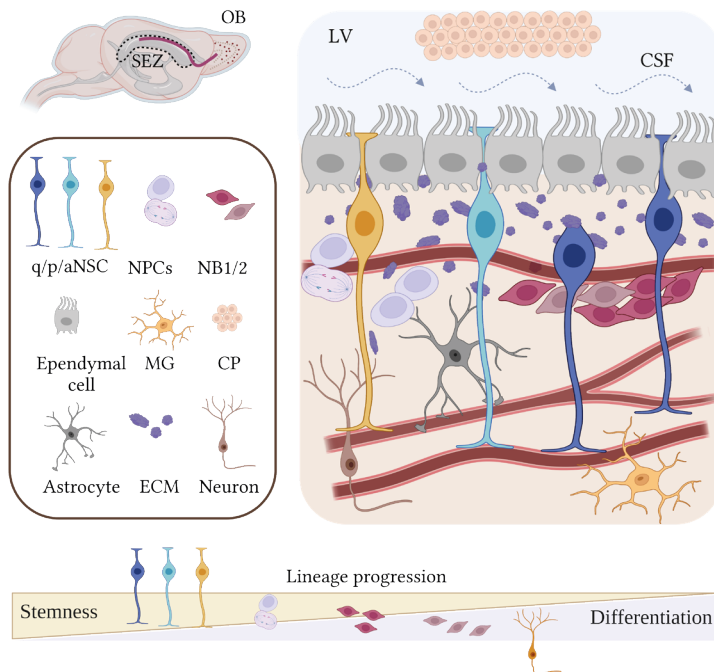


Figure 2. Adult subependymal zone niche. NSCs are located beneath the ependymal cell layer that lines the LV. Their primary cilium intercalates into the ependyma to access the LV, and they emit a basal projection that terminate in vasculature. They are regulated by multiple cell types with which they coexist, such as their progeny, microglia or mature astrocytes. q/p/aNSCs: quiescent/primed/activated NSCs; MG: microglia; CP: choroid plexus; CSF: cerebrospinal fluid. ECM: extracellular matrix. Created with BioRender.com.

Indeed, NSCs have a privileged position beneath the ependymal cells, which are multi-ciliated glial cells that form an epithelial barrier at the interface between the cerebrospinal fluid (CSF) and the brain parenchyma. Most NSCs have an apical extension that they project through the ependyma ending as a primary cilium (**Figure 2**). These interactions form specialized *rosette*-shaped structures, named as pinwheels, in which multiple ependymal cells surround a NSC process (Codega *et al.*, 2014; Mirzadeh *et al.*, 2008). The primary cilium acts as a source of regulatory signals at two different levels. The first one, by mediating direct contact with ependymocytes. This interactions are regulated, for example, by N-cadherin, which has been shown to be essential for maintaining NSC quiescence (Morante-Redolat & Porlan, 2019; Porlan *et al.*, 2014). The second level of regulation is mediated through the direct exposure of NSCs to the CSF, which constitutes a rich source of regulatory signals. Among them, we can find sonic hedgehog (SHH), basic fibroblast growth factors (bFGF) or leukemia inhibitory factor (LIF), among others (Zappaterra & Lehtinen, 2012). Regarding their basal compartment, NSC projections directly terminate in the basal lamina of blood vessels (BVs), which also reminds us of its RGCs origin. Interestingly, SEZ BV have specialized properties, and regulate NSCs through soluble and adhesion-mediated signals that will be explained in other sections of this thesis (Karakatsani *et al.*, 2019; Shen *et al.*, 2008; Tavazoie *et al.*, 2008).

NSCs coexist with multiple other cell types which actively sustain NSC maintenance and the neurogenic output (Cope & Gould, 2019). For example, NSCs are regulated by their progeny, NPCs and NBs, or by differentiated cells as SEZ microglia (Sirerol-Piquer *et al.*, 2019), mature astrocytes, or even neuronal terminals (Berg *et al.*, 2013; Perez-Villalba *et al.*, 2018). In addition to the cellular components, NSC are embedded in a specialized extracellular matrix (ECM), the role of which will be further discussed (Morante-Redolat & Porlan, 2019). It is pertinent to note that some of the abovementioned SEZ constituents have distinguished traits and functions when compared to other non-neurogenic brain regions (e.g., BV, microglia or the ECM), suggesting that this region is conferred with specialized regulatory mechanisms to maintain NSC homeostasis.

It is not surprising that, due to the diverse intrinsic and extrinsic regulators of NSCs in the niche, the NSC pool is found to be heterogeneous, both regarding the activation state and the interaction with other SEZ constituents. Indeed, NSC diversity is already evidenced when considering NSC disposition in the niche: the antero-posterior and dorso-ventral positioning conditions the neurogenic output, with NSCs giving rise to different subtypes of OB interneurons depending on their original location (Chaker *et al.*, 2016; Merkle *et al.*, 2007, 2014). In addition, the distance to the LV has also been shown to be a determinant factor for the neurogenic activity (Kazanis *et al.*, 2010). In this regard, there are some NSCs (originally named as B2) that, although retaining the BV contact, do not

Introduction

display a primary cilium and do not contact the apical side of the SEZ (Baur *et al.*, 2022; Obernier *et al.*, 2018). Recent discoveries have shown that this basally located NSCs have reduced Notch activity compared to apical cells and they differentially contribute to OB neurogenesis (Baur *et al.*, 2022).

As to NSC states of activation, recent advances in transcriptomic and single-cell analyses have shed some light on the understanding of the different molecular identities coexisting in the niche, which will be discussed in detail in the following section (Belenguer *et al.*, 2021a; Codega *et al.*, 2014; Llorens-Bobadilla *et al.*, 2015).

3. NSC coexist and transit between three actively regulated states

It is widely accepted that NSCs can accomplish long-term self-renewal, enabling the formation of new progeny during lifespan. Taking into consideration that most NSC divisions are symmetrical and consuming, this sustained neurogenesis could only be explained by the fact that most NSC remain in a quiescent state until adulthood, as it occurs in other SC niches (van Velthoven & Rando, 2019). Indeed, early studies supported the idea that most NSCs are quiescent, as they were shown to be resistant to anti-mitotic treatments such as cytosine arabinoside (Ara-C) (Doetsch *et al.*, 1999). However, a small subset of NSCs was found to be proliferative: they expressed cell cycle markers such as Ki67 and could be traced by the incorporation of nucleotide analogs as 5-Ethynyl-2-deoxyuridine (EdU) in short pulse-chase regimes (i.e., 1h) (Codega *et al.*, 2014; Ponti *et al.*, 2013). Alternatively, repeated injections of the analogs combined with long chasing times (21-28 days) have been commonly used to trace more quiescent NSCs. After this time, while proliferating cells would have diluted the nucleoside or differentiated and migrated towards the OB, slow-cycling NSCs would have divided only a few times and would, hence, retain the analogs. However, genetic and nucleoside-based cumulative label studies suggested certain degree of cycling heterogeneity among NSCs (Ponti *et al.*, 2013), with a pool of cells being maintained in a deeply quiescent state since developmental stages (Fuentelba *et al.*, 2015). This called into question the use of these traditional strategies to target quiescent cells, as nucleoside analogs require cell cycle entry for its incorporation, and thus, would not apply to those cells that have not divided. Since this controversy emerged, many groups raised their interest in the development of new tools to unequivocally identify the different NSC states and study the transitions from one another.

In this regard, fluorescence activated cell sorting (FACS) analyses have allowed great advances in the field. Indeed, isolation and transcriptional studies based on GLAST levels or GFAP-based reporters, combined with the use of fluorescently-labeled epidermal

growth factor (EGF), have unveiled the existence of two different NSC states of activation: quiescent (qNSCs), and activated NSCs (aNSCs). While they both express GLAST/GFAP, they display distinguishable EGF receptor (EGFR) levels, which are high in aNSCs and found very low or absent in qNSCs (Codega *et al.*, 2014; Pastrana *et al.*, 2009). Moreover, recent advances in single-cell RNA sequencing have gone even deeper and disclosed that the quiescent population is, *per se*, heterogeneous. The work by Llorens-Bobadilla and colleagues described that NSCs can be found in two different levels of quiescence: deep quiescence and *shallow* quiescence. NSCs displaying a more shallow quiescence were named as *primed* NSCs (pNSCs) (Llorens-Bobadilla *et al.*, 2015). This primed state resembled the G_{alert} state that was defined as an alerting mechanism for muscle SCs to enable faster future responses following a systemic injury (Rodgers *et al.*, 2014).

NSC states differ both transcriptionally and phenotypically, and have also diverse behaviors *in vitro* (Basak *et al.*, 2018; Belenguer *et al.*, 2021a; Codega *et al.*, 2014). However, the different states are not independent and constitute an ordered progression, from deeply quiescent NSCs, to pNSCs, to the active state and back (Basak *et al.*, 2018; Belenguer *et al.*, 2021a). To enable fine studies of these NSC states, our laboratory has developed a strategy to analyze the complete neurogenic lineage by FACS (Belenguer *et al.*, 2021a, b), based on the relative expression of different markers (GLAST/cluster of differentiation (CD) 9/CD24/EGFR). With this strategy we have, in addition, sorted the different populations to perform RNA-seq analyses of the complete neurogenic lineage (Belenguer *et al.*, 2021a), data that has been used during the development of this thesis.

Gene Ontology (GO) analyses have revealed that NSC states have specialized traits, which are clearly related to their specific function in the niche and go far beyond evident differences in cell cycle genes. Indeed, the progression from dormancy to activation appears associated with an up and down-regulation of a significant number of genes related to specific signaling pathways (summarized in **Figure 3**) (Belenguer *et al.*, 2021a; Chaker *et al.*, 2016; Codega *et al.*, 2014; Leeman *et al.*, 2018; Llorens-Bobadilla *et al.*, 2015). Interestingly, one of the main distinguishable traits between q/a NSCs is their metabolism: while qNSCs rely on glycolysis and fatty acid catabolism, proliferation of aNSCs depend on oxidative phosphorylation. Further, qNSCs upregulate specific signaling pathways compared to aNSCs, as for example the G-protein coupled receptor (GPCR) pathway, and display enhanced cell-cell and cell-ECM interactions. This suggests a differential regulation from extrinsic elements in the niche, as it is also evidenced by their increased response to inflammation. Pathways related to protein homeostasis also differ between q/a pools, with qNSCs showing enhanced autophagy and lysosomal activity. This can be exemplified by the work of Kobayashi, which showed that enhanced EGFR degradation by the lysosomal pathway is necessary for maintaining quiescence (Kobayashi *et al.*, 2019). Besides, it has also

Introduction

been shown that qNSC have a distinct lysosome-mediated protein quality control signaling which conditions qNSCs/aNSCs transitions (Leeman *et al.*, 2018). Regarding aNSCs, they have, as expected, increased expression of cell cycle genes, together with increased protein synthesis or DNA repair mechanisms (Chaker *et al.*, 2016). Remarkably, pNSCs, although having a similar profile to qNSC, are molecularly distinct, and are usually categorized as an intermediate stage between qNSCs and aNSCs. Albeit they clearly resemble qNSCs, this pool of cells is more prepared for activation, as they present higher ribosomal activity and an incipient, although low, expression of cell cycle genes and *Egfr*.

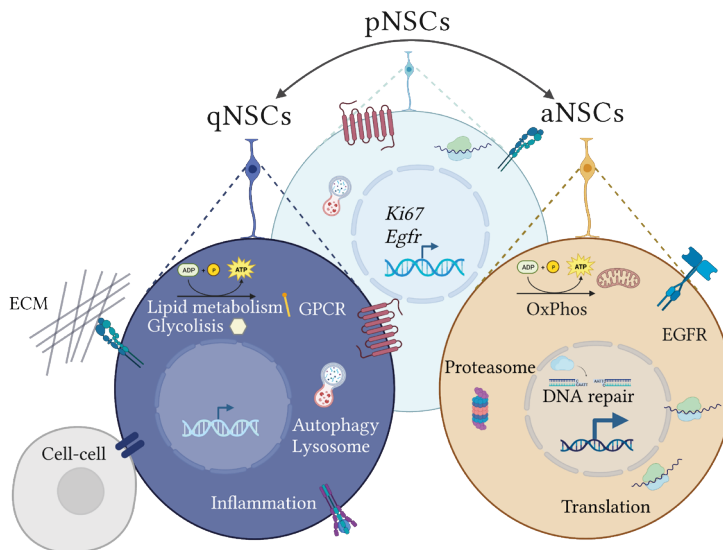


Figure 3. Main molecular traits of NSC populations. Representation of some of the main characteristic traits of NSC in different states of activation (qNSCs, pNSCs and aNSCs), encompassing GO analysis from published transcriptomic and functional data. Differences in metabolism, autophagy-lysosomal pathway, adhesion, or specific receptors are represented. OxPhos.: Oxidative phosphorylation. Created with BioRender.com.

Since the first research paper reported that primary NSC can be isolated, expanded and maintained in culture (Reynolds & Weiss, 1992; Vescovi *et al.*, 1993), many groups have worked in the refinement of the process (Belenguer *et al.*, 2016). NSCs respond to EGF and bFGF *in vitro* and divide clonally to give rise to floating neurospheres. When assessing their cellular identity by comparing neurosphere transcriptomes with the ones from the different populations *in vivo*, we showed that neurospheres highly resemble aNSCs, as they are mostly composed of activated cells and NPCs (Belenguer *et al.*, 2021a). Nevertheless, NSC heterogeneity is also evident *in vitro*, as we have found that neurospheres contain a small pool of cells with slow-cycling dynamics that transcriptionally resemble *in vivo* pNSCs (Belenguer *et al.*, 2021a). We have named this population as *DFFDA^{high}* due to their

low DFFDA-tracer dilution rates compared to highly proliferative (*DFFDA^{low}*) neurosphere cells. The study of *DFFDA^{high}* cells, which are maintained along cell passages (Belenguer *et al.*, 2021a), have enabled us to model quiescent-like cells *in vitro*, as *in vivo* sorted qNSCs cannot be maintained for longer than 48h in culture (Belenguer *et al.*, 2021a).

Overall, this section about NSC heterogeneity raises the idea of q/p/a NSCs as well-defined actively regulated states. This is especially interesting for quiescence, that, far from being a passive state, relies on multiple signaling mechanisms that keep them away from activation. The transitions from quiescence to activation require profound changes in cellular physiology and constitute the first level of regulation to which NSCs are subjected. The study of the mechanisms regulating this process will be one of the main goals of this thesis as we consider it to be essential to understand the basis of neurogenesis and gain potential insights in the understanding of its decline over time.

4. BuMPing to quiescence

Much effort has been done to unveil signaling pathways related to quiescence-induction and maintenance (Urbán *et al.*, 2019). Among the different extrinsic signals associated with NSC quiescence, bone morphogenetic proteins (BMPs), have been extensively studied (Le Dréau, 2022; Schmierer & Hill, 2007). They are evolutionarily conserved proteins that were first described in the context of bone formation, and are part of the large transforming growth factor β (TGF β) cytokine superfamily, with more than 20 members described so far (Derynck & Zhang, 2003; Schmierer & Hill, 2007). BMPs are pleiotropic molecules, and have diverse essential functions that range from dorsoventral patterning and specification in vertebrate neural development, to neurogenesis and gliogenesis regulation in the adult brain (Le Dréau, 2022).

Regarding its mechanism of action, BMP ligands are secreted to the extracellular milieu as dimers, where they bind to serine/threonine kinase BMP receptors (BMPRI and BMPRII). BMP ligand binding favors the transphosphorylation of BMPRI by constitutively active BMPRII, which induces the recruitment of proteins that will propagate the signaling cascade intracellularly through canonical or non-canonical pathways (**Figure 4**). The canonical BMP pathway starts with the recruitment of receptor-regulated SMAD proteins (R-SMADs) and its activation by phosphorylation. Then, R-SMADs bind to their common mediator, SMAD4, for stabilization. R-SMADs/SMAD4 complexes are then translocated to the nucleus where they directly regulate the expression of target genes in cooperation with other transcription factors (TFs), coactivators and corepressors (Derynck & Zhang, 2003; Schmierer & Hill, 2007). A negative feedback of the pathway is mediated

Introduction

by inhibitory SMADs, including SMAD6 and 7 (Itoh & ten Dijke, 2007). On the other side of the story, non-canonical pathways are not so well understood. They are mediated by the binding of different proteins to BMPRs, that initiate diverse SMAD-independent intracellular cascades, such as the mediated by c-Jun N-terminal kinase (JNK), p-38, Erk/Map kinase (MAPK), Ras homolog (Rho) family member A (RhoA)/Rho associated coiled-coil containing kinase (ROCK), among others (Derynck & Zhang, 2003) (**Figure 4**).

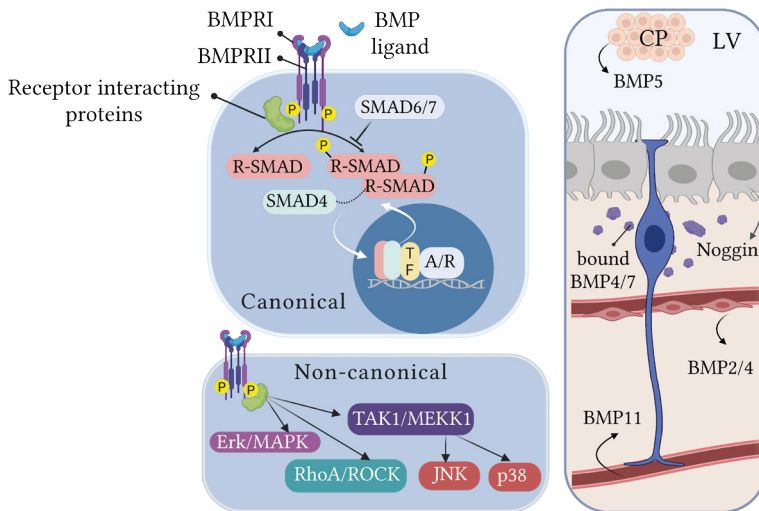


Figure 4. Canonical and non-canonical BMP signaling pathways and BMP sources in the SEZ niche. In the canonical pathway, BMP receptors activate R-SMADs by phosphorylation, which is also regulated by receptor-interacting proteins. Then, activated R-SMADs bind to SMAD4 forming heterodimers or heterotrimers and are translocated to the nucleus to regulate gene expression in collaboration with specific TFs and coactivators/corepressors (A/R). SMADs can also shuttle back to the cytoplasm. Some non-canonical BMP pathways are shown in the lower panel. Sources of BMP ligands and antagonists in the SEZ are shown in the right side panel. Created with BioRender.com.

BMP signaling has an important role in regulating NSC activation state and neurogenesis (Urbán *et al.*, 2019; Yousef *et al.*, 2015). Transcriptional and *pseudotime* analyses of NSC populations have shown that BMP transcripts are overexpressed in quiescent NSCs (Llorens-Bobadilla *et al.*, 2015) and transitions from quiescence to activation occur concomitant with a downregulation of BMP signaling pathways. It has been demonstrated *in vivo* in the SGZ, that BMP signaling supports hippocampal NSC quiescence (Bond *et al.*, 2014; Mira *et al.*, 2010), as blocking BMP canonical signaling induced NSC self-amplification causing NSC depletion and an impairment in the production of newborn granular neurons (Bonaguidi *et al.*, 2008; Mira *et al.*, 2010). However, while its role in the SGZ has been widely studied (Blomfield *et al.*, 2019; Bond *et al.*, 2014; Urbán *et al.*, 2019), its function in the SEZ is still less well understood.

Indeed, NSCs in the SEZ also express BMP receptors and show nuclear SMAD activity (Colak *et al.*, 2008; Lim *et al.*, 2000). In fact, the use of anti-TGF β 1 antibodies or receptor inhibitors have been shown to partially rescue proliferation and neurogenesis in aged mice (Daynac *et al.*, 2014; Pineda *et al.*, 2013), suggesting a relevant role of this pathway also in the SEZ. Interestingly, the activation of BMP signaling pathways will be determined by the specific bioavailability of different ligands and antagonists, which generate regions of tightly regulated gradients (**Figure 4**) (Lim *et al.*, 2000; Obernier & Alvarez-Buylla, 2019). BMP5, for example, is present in the CSF of young animals, and can potentially affect NSC behavior by improving the cloning formation capacity of aged aNSCs (Silva-Vargas *et al.*, 2016). Nevertheless, ependymal cells secrete Noggin (Lim *et al.*, 2000) and express low-density receptor-related protein 2 (Gajera *et al.*, 20210), which inhibit BMP signaling and favor neurogenesis. The vasculature constitutes another source of BMP, as it is locally secreted by endothelial cells (ECs) (Mathieu *et al.*, 2008; Pineda *et al.*, 2013) and can also be transported in the blood, as it is the case for BMP11, which has been reported to have rejuvenating effects in older mice (Katsimpardi *et al.*, 2014). Furthermore, NSCs also express BMP ligands, as occurs with BMP2, which is negatively regulated by p21 to avoid differentiation (Porlan *et al.*, 2013). Remarkably, the accessibility of BMP ligands will not only be determined by the secretion from their respective sources, but will also depend on its interaction with the ECM. It has been shown that BMP ligands and also its antagonist Noggin can bind to ECM components, specially heparan sulfate (HS) proteoglycans (PGs) (Kerever *et al.*, 2007, 2021). By this means, the ECM can positively (exposing or releasing) or negatively (sequestering) condition the bioavailability and the responses to soluble factors (Sedlmeier & Sleeman, 2017; Zimmermann *et al.*, 2021) (**Figure 4**).

Unveiling the role of BMP in NSCs has meant a step forward in the aforementioned problem of maintaining qNSCs *in vitro*. Mira and colleagues showed that BMP4 treatment in combination with bFGF favored quiescence induction in primary NSCs cultures from the SGZ (Mira *et al.*, 2010). In this condition, cells were shown to rapidly exit the cell cycle in a reversible manner, a state which could be maintained for weeks while retaining their proliferative and neurogenic potential (Martynoga *et al.*, 2013; Mira *et al.*, 2010; Yirui Sun *et al.*, 2011). Recent reports suggest that treating SEZ NSCs with BMP4 with or without bFGF generates different stable cell states, the first one resembling qNSCs and the latter inducing a state similar to that of pNSCs (Marqués-Torrejón *et al.*, 2021). bFGF and BMP4 have antagonistic functions, as bFGF can inhibit BMP through different mechanisms including the modulation of SMADs (Manzari-Tavakoli *et al.*, 2022). This proposes that very fine interactions occur between BMPs and other signaling pathways, which can generate completely different cellular effects when cultured in the presence of specific mitogens. Remarkably, EGFR and BMP cascades also converge at multiple levels: EGF can induce

Introduction

the expression of some BMP ligands and can regulate intracellular signaling proteins that also participate in BMP-activated pathways (Sun *et al.*, 2020). Still, EGF has never been used in culture in combination with BMP4 for quiescence induction albeit the fact that NSC are subjected to both EGF and bFGF *in vivo* (Weickert *et al.*, 2000). In conclusion, although it is clear that BMP pathway is essential for maintaining NSC quiescence *in vivo* and for modeling quiescence *in vitro*, neither the mechanisms of quiescence-induction nor the specific culture conditions for SEZ NSCs are fully understood.

5. Multi-level regulation through SEZ vasculature

The close association between the neural and vascular system is already evidenced during development, as they are formed in a parallel and coordinated manner in multiple species (Segarra *et al.*, 2019). In fact, the concept ‘neurovascular unit’ (NVU) was established to refer to the functional structure constituted by neurons and blood-brain barrier (BBB) constituents (i.e. astrocytes, pericytes, ECs and the ECM) (Schaeffer & Iadecola, 2021). The different components are anatomically and functionally linked to one another, and have to communicate and function as a whole in order to respond to specific needs such as blood flow oscillations (Iadecola, 2017; Schaeffer & Iadecola, 2021).

Although the classical meaning of the NVU does not refer to the germinal niches, the concept could also be applied to this specific scenario, as it has been shown that cells from the neural lineage strongly interact with BVs, from which they receive multiple signals that actively regulate their behavior (Karakatsani *et al.*, 2019; Quaresima *et al.*, 2022). The adult SEZ is highly irrigated by a dense vascular plexus, mostly composed of branched planar capillaries that run in the basal side of the SEZ, in parallel to the ependyma. SEZ BVs have a specialized structure and function that makes them distinguishable from non-neurogenic areas (Culver *et al.*, 2013; Shen *et al.*, 2008; Tavazoie *et al.*, 2008). Specifically, some pioneer studies showed that BV encountered reduced astrocyte and pericyte coverage in the SEZ compared to cortex BVs, making the region more permeable to blood-derived molecules (Tavazoie *et al.*, 2008). This same study also unveiled that progenitors are located the closest to BVs, in sites bereft of astrocytes and pericytes, suggesting that they possibly rely on blood-borne molecules to proliferate. NPCs are followed in proximity to BV by active NSCs, while proliferating neuroblasts are located at further distances (Shen *et al.*, 2004; Tavazoie *et al.*, 2008). More committed non-proliferating late neuroblasts again approach vasculature to use BVs as scaffolds for migration towards the OB (Martončíková *et al.*, 2021; Whitman *et al.*, 2009) (**Figure 5**). However, it is worth noting that these studies, although informative, did not distinguish between specific NSC populations.

Instead, NSCs were identified by general GFAP and LeX markers, which stain for neurosphere-forming cells (activated NSC and NPCs) (Capela & Temple, 2002). Furthermore, they used classical long-chase pulses that, as already introduced before, will not stain those cells that have remained fully quiescent since their embryonic specification (Shen *et al.*, 2008; Tavazoie *et al.*, 2008). We consider, thus, that due to the limitations of the histological identification of quiescent NSCs this topic should be further addressed using new methodologies that could better contemplate this population, as for example *in utero* electroporation (IUE) with fluorescent episomal plasmids.

Indeed, the proximity and interaction of cells from the neural lineage to vasculature is highly relevant, as it makes them susceptible to receive regulatory signals from it. Further, the nature and complexity of the vascular system and the cells that are part of it, enable multiple levels of regulation (**Figure 5**): the mediated by soluble factors (blood-derived molecules or locally secreted factors), or by adhesion-related cues (mediated by direct cell-cell contacts or adhesion to basement membrane (BM) structures). In addition, although research has mostly focused on describing specific molecular interactions, more holistic processes such as blood flow oscillations or shear stress have been also described to affect NSCs (reviewed in Karakatsani *et al.*, 2019).

As already mentioned, the SEZ vasculature enables the trespass of molecules derived from the blood (Tavazoie *et al.*, 2008), and both positive and negative regulators of neurogenesis have been described in the context of young and aged blood, respectively (Katsimpari *et al.*, 2014; Rojas-Vázquez *et al.*, 2021). Soluble factors are also locally secreted by BBB components, specially ECs. Among these molecules, named *angiocrine factors*, brain-derived neurotrophic factor (BDNF) was the first one described to increase neurogenesis in the adult songbird brain (Louissaint *et al.*, 2002). After this, different research groups have made big efforts to unveil different EC-derived regulatory molecules, which have been associated with surprisingly diverse effects in NSCs (Karakatsani *et al.*, 2019). Our laboratory described pigmented epithelium-derived factor (PEDF) as the first factor that could affect neurogenesis by selectively enhancing NSC self-renewal through Notch pathway activity (Andreu-Agulló *et al.*, 2009; Ramírez-Castillejo *et al.*, 2006). Thereafter, EC-derived betacellulin (Gómez-Gavira *et al.*, 2012) or placental growth factor 2 (PlGF-2) (Crouch *et al.*, 2015) have also been shown to promote NSC proliferation. Nevertheless, other soluble factors, as for example neurotrophin-3 (Delgado *et al.*, 2014) or TGF β (Daynac *et al.*, 2014; Mathieu *et al.*, 2008; Pineda *et al.*, 2013) appear to actively participate in quiescence maintenance by diverse mechanisms. A third level of regulation is the one related to cell-cell or cell-matrix adhesion which has been considerably less studied (Morante-Redolat & Porlan, 2019). Direct NSC-EC contacts have been shown to induce

Introduction

quiescence by EphrinB2/Ephs, Dll1-Dll4/Notch and Jagged1/Notch-mediated interactions (Bicker *et al.*, 2017; Kawaguchi *et al.*, 2013; Ottone *et al.*, 2014) (Figure 5).

Regarding ECM interactions, the role of integrins in NSC binding to BV BMs was described for the first time more than a decade ago (Shen *et al.*, 2008). This family of proteins, which will be described in more detail the following sections, are key in regulating cell adhesion, as they favor both structural support and the initiation and propagation of ECM responses intracellularly (Morgan *et al.*, 2007). Integrin $\alpha 6$ blocking was shown to affect NSC interaction with BVs *in vivo*, as it favored NSC relocation at further distances from vasculature concomitant with an increase in proliferation (Shen *et al.*, 2008). However, cell responses to vasculature are diverse, as active proliferating cells seem to contradictorily require close proximity with BV to divide (Tavazoie *et al.*, 2008). Furthermore, it has been described that soluble factor stromal-derived factor 1 (SDF1) (Kokovay *et al.*, 2010), which is heterogeneously expressed by SEZ capillaries (Zhu *et al.*, 2017), interacts with

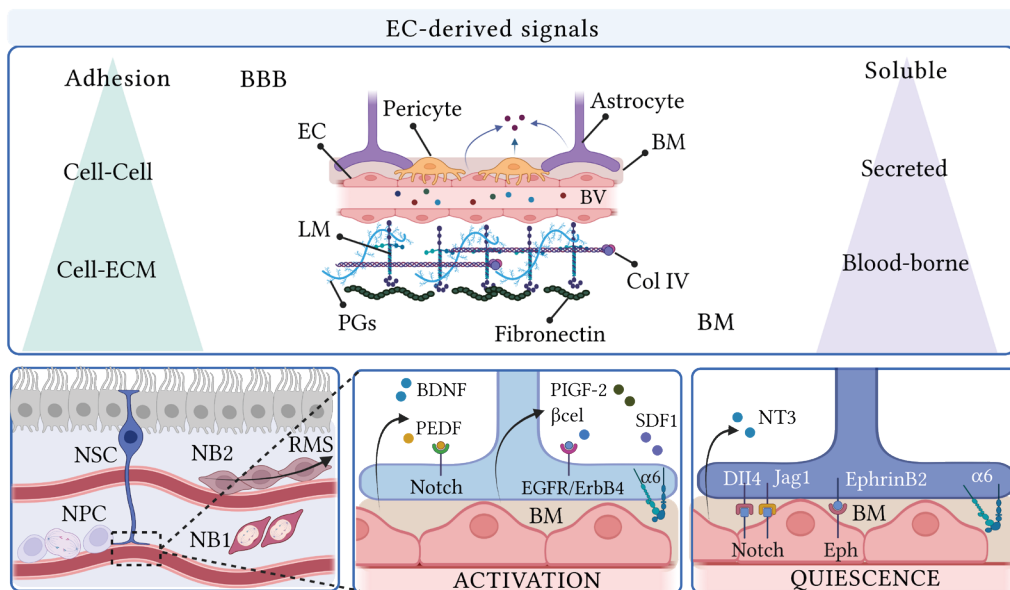


Figure 5. EC-derived signals. Upper panel shows different types of EC-derived signals (soluble and adhesion-mediated). The image displayed at the center represents BBB cell constituents and vascular BM composition. Lower panel shows, from left to right: 1) the interaction of cells from the neural lineage with BVs: NPCs lie the closest, followed by NSCs. Early NBs (NB1) locate at further distances and late NBs (NB2) interact with vasculature to migrate. 2) Different soluble factors related to NSC activation: BDNF affects self-renewal, and PEDF, PIGF-2 and β Celulin, proliferation. SDF-1 favors aNSC and NPC interaction with BV through ITGA6. 3) Molecular signals inducing quiescence, including soluble ligand NT3, cell-cell adhesion molecules, and ITGA6 binding to BV BM. Betacellulin: β cel. $\alpha 6$: integrin $\alpha 6$. Created with BioRender.com.

C-X-C chemokine receptor type 4 (CXCR4) in EGFR⁺ NSCs and NPCs increasing the expression of integrin $\alpha 6$. In this case, integrin $\alpha 6$ enabled NSC binding to BV to allow the maintenance of the proliferative pool (Kokovay *et al.*, 2010; Zhu *et al.*, 2019). The fact that integrin $\alpha 6$ has been reported as a pro-proliferative signal in these and other reports (Rosa *et al.*, 2016), unveils certain controversy regarding the role of integrin interactions in the niche, which differ among NSC with different states of activation.

6. BM structures as signal integrators

The ECM can be defined as a complex cell-secreted macromolecular network that provides structural support and biochemical signals to cells, tissues and organs (Naba *et al.*, 2016). In the brain, it constitutes around 20% of its total volume, and is primarily composed of glycosaminoglycans (e.g. hyaluronan), PGs (e.g. neurocan and brevican), glycoproteins (GPs) (e.g. tenascin-R, laminins (LMs) and fibronectin), and low levels of fibrous proteins (e.g. collagen) (Dityatev *et al.*, 2010). Emerging discoveries have led to the actual conception of the ECM, which is viewed as a multivalent signal integrator that regulate essential processes such as proliferation, differentiation, or migration both during development and in adult tissues (Cope & Gould, 2019; Hynes, 2009). The mammalian ECM matrix comprises 300 different proteins that are organized in two different structures with a specific location, composition, and function: the interstitial connective tissue, which surrounds cells and provides structural support, and the BMs. As to the brain, ECM also organizes into perineural nets, which favors synaptic functions (Cope & Gould, 2019; Deepa *et al.*, 2006). Interestingly, the interaction between presynaptic and postsynaptic neurons, glia and the ECM is such that this interaction is commonly referred as a functional unit named the *tetrapartite synapse* (Cope & Gould, 2019; Dityatev & Rusakov, 2011).

The BM is a specific type of ECM that forms sheet-like fibrous structures that line the basal side of epithelial and ECs, separating them from the stroma (Khalilgharibi & Mao, 2021). Its function is in part facilitated by its location at the interface between cells, and its specialized biochemical and mechanical properties makes it an ideal signaling platform to modulate cell responses (Bonnans *et al.*, 2014). Its composition is phylogenetically conserved, and is mainly composed of LM, collagen IV, GPs nidogen and the HSPG perlecan and/or agrin (Khalilgharibi & Mao, 2021; LeBleu *et al.*, 2007; Sekiguchi & Yamada, 2018). Further, mutations that promote changes in composition can lead to the development of detrimental conditions affecting multiple organs and structures across embryonic and postnatal stages (Sekiguchi & Yamada, 2018). Its components are usually secreted by tissue

Introduction

resident cells, which also participate in its assembly, a process that requires the organized recruitment of different ECM components and the generation of specific interactions among them and cell-ECM receptors (Yurchenco *et al.*, 2004). The historical conception of the ECM as an invariable structure has been challenged over time and it is now widely accepted that its composition and structure can be subjected to active remodeling through synthesis, degradation, reassembly and chemical modifications (Bonnans *et al.*, 2014). Nonetheless, these processes usually occur leisurely, as BM components have slow turnover rates and long half-lives that range from several hours to even months (Khalilgharibi & Mao, 2021). To maintain a correct homeostasis of the tissues, ECM remodeling must be tightly controlled, as its dysregulation may favor disease progression. For example, an abnormal deposition of ECM and an increased ECM stiffness is observed during cancer progression (Bonnans *et al.*, 2014; Ferrer-Ferrer & Dityatev, 2018; Pintér & Alpár, 2022).

Interestingly, the SEZ niche is the only region in the brain in which there are two types of BMs: the vascular BM, which is common to all BVs from different brain regions, and a very specialized extravascular BM that is only restricted to this region, originally named as *fractones* (Kerever *et al.*, 2007; Leonhardt & Desaga, 1975; Mercier *et al.*, 2002, 2003). Fractones are generated at postnatal day (P) 3-7 (Nascimento *et al.*, 2018), and have historically been thought to emerge from BV forming two different structures, *stems* and *bulbs*. They both lack the characteristic BM-laminar organization, with stems constituting fingerlike thin fibrous processes that emerge from BVs and profusely branch as they approach the LV, and bulbs referring to large amorphous round deposits that form rounded speckled structures close to the ependymal layer in the LV wall (Mercier *et al.*, 2002, 2003). During this work we will focus on the extravascular BM fractone bulbs, and from now on we will name them as *speckles*, referring to their rounded shape.

Whether or not speckles were part of the vascular BM was under debate for years, until more recent studies elucidated that they are independent BM structures with no contact with BVs and with some differences in its composition and function (Nascimento *et al.*, 2018; Sato *et al.*, 2019). LMs are one of the main functional constituents of the BMs, both from speckles (Kerever *et al.*, 2007; Sato *et al.*, 2019) and BV BMs, together with nidogen, HSPGs, collagen IV, among others (**Figure 6**). LMs are high molecular weight (400-900 kDa) glycoproteins structurally organized as heterotrimers, composed by the assembly of three different polypeptide chains (α , β and γ). To date 5 α , 3 β , and 3 γ variants have been described in mouse and human, that can combine to generate the 16 isoforms identified so far (Barros *et al.*, 2020; LeBleu *et al.*, 2007; Nirwane & Yao, 2018). It is worth noting that speckles and vascular BM have a unique composition regarding LM isoforms (**Figure 6**). While polypeptide $\alpha 3$ is only present in speckles, LM $\alpha 2$ and $\alpha 4$ are restricted to vascular BMs (Sato *et al.*, 2019), which hints to the existence of potential

different functions of specific LM subtypes. This is, however, very difficult to determine, as the genetic disturbance of a specific polypeptide chain is usually compensated by an increase in another one, as it is the case for LM $\alpha 5$ with LM $\alpha 2$ or $\alpha 3$ (Nascimento *et al.*, 2018; Sato *et al.*, 2019). These α , β and γ chains interact to form a characteristic cross-shaped protein structure that display two or three short arms and a triple α helical coiled-coil domain formed by a combination of the three chains, which constitute the LM long arm.

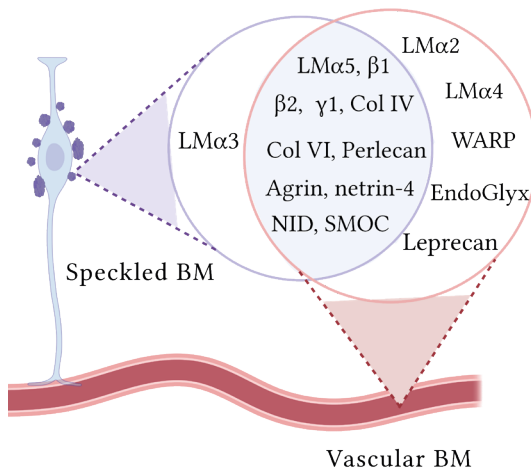


Figure 6. BM composition in the SEZ. NSCs contact vascular BM through their basal end-feet and are surrounded by speckles on their apical side. The main components of speckled and vascular BMs are described in the figure. Although there are some components that are unique to one or the other BM structure, most of them are common. Figure adapted from (Sato *et al.*, 2019). Col: collagen; NID: nidogen; SMOC: SPARC Related Modular Calcium Binding; WARP: von Willebrand factor A-domain-related protein. Created with BioRender.com.

Although the old nomenclature which followed the order of discovery (LM 1-15) is still used, these proteins are commonly identified by the combination of their three polypeptide chains (i.e. LM $\alpha 5\beta 1\gamma 1$, or the simplified version LM 511) (Aumailley *et al.*, 2005). Regarding its function, LM is an especially interesting component of BMs, as it favors the interaction of other ECM components to enable the assembly of stable BM structures (Barros *et al.*, 2020; Hohenester & Yurchenco, 2013; McKee *et al.*, 2007, 2017). In addition, it induces different biological responses related to adhesion, migration, differentiation or neurite outgrowth, among others (Barros *et al.*, 2020; Hohenester, 2019; Nirwane & Yao, 2018).

LM immunostaining in the SEZ displays speckles as amorphous rounded structures. However, transmission electron microscopy (TEM) studies have revealed that they are actually highly branched structures that contact multiple cell types at strategic locations at the end of the interstitial clefts between ependymal cells (Mercier *et al.*, 2002, 2003). They are essentially located in the apical side of the SEZ, occupying the center of pinwheel structures (Nascimento *et al.*, 2018), from where they contact nearby ependymocytes, NSC, progenitors and astrocytes (Kerever *et al.*, 2007; Mercier *et al.*, 2002). These interactions have been shown to regulate NSC behavior, both in a physiological and an aging context (Kerever *et al.*, 2015; Nascimento *et al.*, 2018; Sato *et al.*, 2019). For example, Nascimento

Introduction

and colleagues showed that genetic disturbance of LM $\alpha 5$ increased the number of proliferating cells concomitant with a reduction in the number of label-retaining NSCs (Nascimento *et al.*, 2018). Interestingly, speckles increase in size during aging and change their composition and cellular interactions, directly affecting NSC behavior (Kerever *et al.*, 2015; Nascimento *et al.* 2018).

Due to its close interaction with multiple cell types, the cellular origin of this speckled BM has been under debate for years (Kazanis *et al.*, 2010; Nascimento *et al.*, 2018; Sato *et al.*, 2019). While Nascimento *et al.* suggested an ependymal origin, others argued that speckles are NSC-derived (Kjell *et al.*, 2020; Sato *et al.*, 2019). Both groups have shown that disturbing LM $\alpha 5$ deposition by ependymal (Foxj1-Cre;Lama5^{fl/fl}) or GFAP⁺ NSC (Gfap-Cre;Lama5^{fl/fl}) affected the composition of speckles (Nascimento *et al.*, 2018; Sato *et al.*, 2019), suggesting that secretion might not be restricted to one cell type. However, the contribution and relevance of each of the sources is still fully unveiled.

Regarding ECM-NSCs interactions, it has been shown that NSCs express different LM-binding receptors, among which integrins are the most well-studied (Kazanis & Ffrench-Constant, 2011; Lathia *et al.*, 2007). Integrins are heterodimers composed by combinations of two subunits (α and β), with a total of 24 dimers described so far (Hynes, 2002; Takada *et al.*, 2007). Among them, LM-binding integrins $\alpha 6\beta 1$, $\alpha 3\beta 1$ and $\alpha 7\beta 1$ have been shown to bind speckles by *in situ* hybridization (Sato *et al.*, 2019). Interestingly, the genetic disruption of the ability to bind integrins in speckled BM (Gfap-Cre;Lamc1^{cEQ/cEQ}) have shown that correct LM-integrin interactions are needed for the proper assembly of these structures and a correct NSC attachment. This disturbed adhesion was, in addition, associated with a defect in the ability to form neurospheres *in vitro* (Sato *et al.*, 2019). However, the effect of NSC detachment *in vivo* and the mechanisms by which LM–integrin interactions in speckles regulate NSC behavior, are still unexplored.

A different level of regulation mediated through speckles is the one related to its ability to bind and expose soluble factors (**Figure 7**). In this context, it is worth mentioning that the SEZ fractones have a unique HS composition (Kerever & Arikawa-Hirasawa, 2021), which will regulate the bioavailability of heparin-binding ligands in the niche and promote growth factor-mediated signaling (Kerever *et al.*, 2007, 2021; Kerever & Arikawa-Hirasawa, 2021). For example, it has been demonstrated that speckles bind bFGF (Kerever *et al.*, 2014) and BMP4/7 (Douet *et al.*, 2012; Mercier & Douet, 2014), which have antagonistic effects increasing and reducing proliferation, respectively. For bFGF and BMP7, its function is dependent on their binding to HS chains in HSPG, as it favors cell bioavailability (Douet *et al.*, 2012; Kerever *et al.*, 2014; Mercier and Douet, 2014). Instead, for BMP4, their binding to speckles moderate its effect when injected *in vivo*,

suggesting that speckles sequester this factor reducing its biological function (Mercier and Douet, 2014). Interestingly, isoforms bound to speckles can be released through matrix remodeling, thereby finely regulating its accessibility in the niche (Bonnans *et al.*, 2014; Sedlmeier & Sleeman, 2017).

Finally, ECM composition can confer unique mechanical properties to the tissues (**Figure 7**), such as stiffness or elasticity, which can be sensed and transmitted intracellularly affecting different cell responses (Sun *et al.*, 2012; Vining & Mooney, 2017). For example, fate decisions of adult SCs, such as muscle or mesenchymal SCs, are conditioned by mechanical properties (Engler *et al.*, 2006; Gilbert *et al.*, 2010; Zhu *et al.*, 2019). Remarkably, the brain constitutes one of the softest tissues in the body (Tyler, 2012), which makes the fact that the SEZ possesses higher overall stiffness compared to non-neurogenic regions, even more interesting (Kjell *et al.*, 2020). It is known that NSCs are mechanosensitive, as they possess ion-channels that can respond to mechanical cues that affect, in response, self-renewal and differentiation (Pathak *et al.*, 2014; Petrik *et al.*, 2018).

However, this topic is still considerably unexplored, especially regarding the contribution of speckled or vascular BM structures to potential NSC mechanoresponses. Besides, the fact that integrins participate in NSCs adhesion to speckles opens a potential

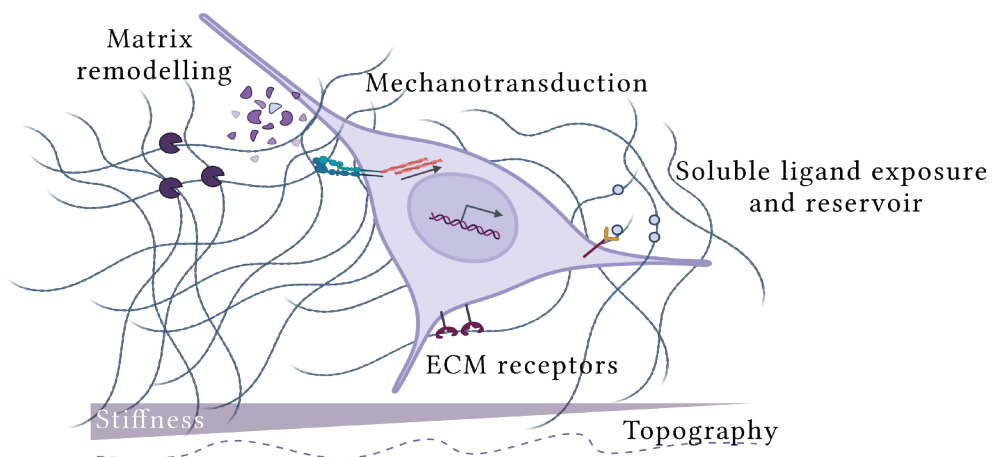


Figure 7. The ECM as a signal integrator. Schematic drawing showing cell signals derived from the ECM. ECM composition will determine mechanical properties such as the stiffness or topography to which cells can respond. Besides the recognition of matrix elements by ECM receptors, ECM also expose soluble ligands to the cells which can be, in addition, affected by enzyme remodeling. Integrin binding can modulate cytoskeletal dynamics that can lead to the regulation of transcription. Created with BioRender.com.

Introduction

wide regulation downstream this binding, as integrins are the main regulators in the formation of focal adhesion (FA) complexes, that link the ECM with the cell cytoskeleton (Kechagia *et al.*, 2019). In this regard, FAs and its downstream effectors have been shown to mediate NSCs adhesive responses, especially through affecting cell specification and commitment (Discher *et al.*, 2009; Keung *et al.*, 2011; McBeath *et al.*, 2004). In the last section, we will focus on understanding the basis of mechanotransduction and the different players involved in the response.

7. The role of YAP/TAZ

Mechanotransduction refers to the process by which cells sense mechanical properties of the environment, named as mechanosensing, and convert them into biochemical cues that propagate intracellularly (Vining & Mooney, 2017; Wagh *et al.*, 2021). Mechanical signals can be originated in both directions, from the cells to the ECM (inside-out) or *vice versa* (outside-in signaling). Mechanical forces triggered intracellularly are usually mediated by proteins associated to the cytoskeleton and actomyosin contractility, and the generated forces will affect surrounding ECM and neighboring cells. Alternatively, extrinsic forces can be applied by shear or tension and/or compression, or can be derived from intrinsic mechanical cues from the environment (e.g, stiffness, topography, cell density or shape) (Engler *et al.*, 2006; Petzold & Gentleman, 2021). Cells can sense this signals by diverse mechanisms, including mechanically gated ion channels, receptor–ligand binding, deformation of the cytoskeleton and/or through primary cilia (Vinning and Mooney, 2017; Wagh *et al.*, 2021). The responses of the cell to these forces will be diverse and dependent on the biological and cellular context and the physical and biochemical properties of the microenvironment (Wagh *et al.*, 2021).

Although different receptors can regulate mechanoresponses, including GPCRs or cadherins, integrins are the main players in sensing and transducing ECM-derived cues (Case & Waterman, 2015; Elosegui-Artola *et al.*, 2014; Kechagia *et al.*, 2019). Integrins regulate the formation of FAs, which are dynamic protein bonds that connect the cell cytoskeleton to extracellular ECM, controlling the tensional equilibrium between the cell and the forces applied by/to the surrounding microenvironment. When integrins activate, they acquire an active conformation and start to cluster in the membrane, forming *nascent adhesions*. This type of adhesions are unstable and can either disassemble, or progress to form more stable *focal complexes*. These complexes can then form FAs, which are the larger, most stable and mature adhesions. The dynamic association between the integrins bound to the ECM and the force-generating actomyosin cytoskeleton is commonly named as the *molecular clutch* (Kechagia *et al.*, 2019; Mitchison & Kirschner, 1988; Zhiqi Sun *et al.*,

2016). This clutch is mediated by cytosolic proteins that are recruited to the intracellular integrin domains, which are globally named as *adaptor proteins*, among which we can find vinculin, talin or tensin (reviewed in Kechagia *et al.*, 2019) (**Figure 8**). They function as linkers between integrins and the actin cytoskeleton, thus participating in the generation of cytoskeletal tension. Furthermore, they favor the recruitment of key proteins that initiate intracellular signaling cascades downstream integrin signaling, such as FA kinase (FAK) or Src non-receptor protein kinase (Böttcher *et al.*, 2017; Kim & Gumbiner, 2015; Morgan *et al.*, 2007) (**Figure 8**).

The formation of the actin cytoskeletal stress fibers is tightly regulated by the Rho GTPases family (Keung *et al.*, 2011; Marjoram *et al.*, 2014; Morgan *et al.*, 2007). Although there are many members described, the three canonical most well studied proteins are RhoA, Ras-related C3 botulinum toxin substrate 1 (Rac1) and cell division control protein 42 homolog (Cdc42). Their activation is dependent on Rho-guanine nucleotide exchange factors (Rho-GEFs), Rho-GTPases activating proteins (Rho-GAPs) and guanine nucleotide dissociation inhibitors (GDIs) (Lawson & Burrridge, 2014). While the latter forms a complex with the GDP-bound form of Rho GTPases to inhibit their activation and maintain a cytosolic pool of Rho GTPases, the other two actively participate in the regulation of the state of activation. Specifically, Rho-GEFs are responsible for the guanosine diphosphate (GDP) to guanosine triphosphate (GTP) exchange needed to activate the proteins and Rho-GAPs promote their inactivation by activating the intrinsic GTPase protein activity, that will exchange GTP to GDP keeping the proteins in an inactive state (Marjoram *et al.*, 2014; Lawson and Burrridge, 2014).

In more mature adhesions, RhoA activity is increased thanks to specific RhoA activating GEFs, leading to actin filamentous polymerization and myosin-containing stress fiber formation. This process is mediated by the main effector of RhoA, ROCK, which conditions cell contractility and cytoskeletal reinforcement by diverse mechanisms. On the one hand, ROCK increases myosin activity through direct phosphorylation of the regulatory myosin light chain and inhibition of myosin phosphatases. On the other hand, it promotes the activation of its main target, LIM kinases (LIMK1, 2). LIMK favors the inactivation of the actin filament destabilizing protein Cofilin, thereby enhancing actin polymerization and stability (Case & Waterman, 2015; Kechagia *et al.*, 2019; Ohashi *et al.*, 2017).

Once we have introduced the main players of FAs, we can now discuss how these signals can ultimately mediate cell behavior. The main output of ECM mechanoresponses is to regulate gene expression, which mostly occurs through the activation of YES-associated protein (YAP) and transcriptional activator with PDZ-binding motif (TAZ) (Aragona *et al.*, 2013; Dupont *et al.*, 2011; Panciera *et al.*, 2017).

Introduction

Both proteins are structurally similar and have overlapping functions that compensate each other, being usually studied together as YAP/TAZ. Despite multiple pathways converge in YAP/TAZ regulation, their main regulator is the Hippo pathway (Dey *et al.*, 2020; Moya & Halder, 2019) (**Figure 8**).

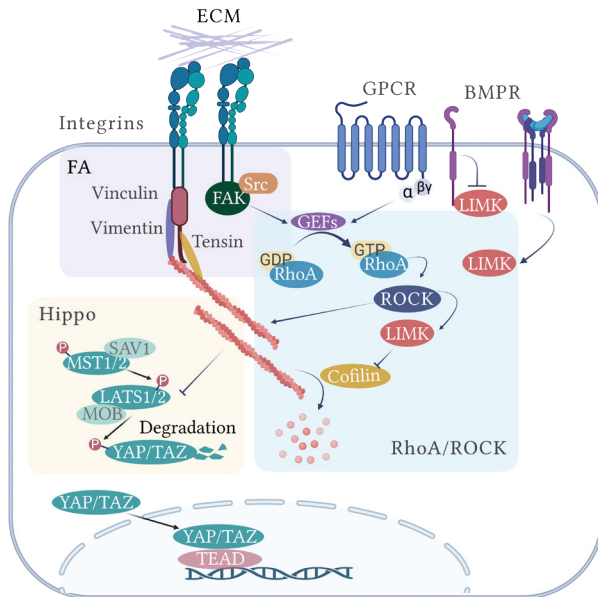


Figure 8. RhoA/ROCK and Hippo pathway in the activation of YAP/TAZ. Integrin activation favors the recruitment of adapter proteins that directly interact with actin cytoskeleton. Recruited FAK or SRC will mediate different signaling responses, including the activation of RhoA/ROCK pathway through GEFs. ROCK activity will determine stress fiber formation by different mechanisms including Cofilin inhibition through LIMK. The inactivation of the Hippo pathway and activation of RhoA/ROCK converge in YAP/TAZ translocation to the nucleus in its unphosphorylated form to act as co-activators of TEAD TFs. Created with BioRender.com.

It is a highly conserved signaling route that involves more than 30 proteins, which has an essential role in regulating growth and regeneration in multiple tissues (Johnson & Halder, 2014; Nguyen & Yi, 2019). In brief, the activation of the route converges, upstream YAP/TAZ, in a core of kinases: mammalian STE20-like kinase 1 (MST1) and MST2, large tumor suppressor kinase 1 (LATS1) and LATS2, and their cofactors, Salvador 1 (SAV1) and Mps1-binder-related (MOB) kinase activators MOB1A and MOB1B. When Hippo signaling is activated, MST kinases will phosphorylate and activate SAV1 and MOB cofactors that will assist in the recruitment and activation of LATS kinases. Phosphorylated LATS will, in turn, phosphorylate YAP/TAZ, favoring its retention at cellular junctions and/or its targeting for proteasomal degradation. Alternatively, when the Hippo pathway is inactive, unphosphorylated YAP/TAZ will translocate to the nucleus and perform its regulatory function as a transcriptional co-activator (**Figure 8**). In the nucleus, they bind to TFs with TEA DNA-binding domains (TEAD1-4), which will ultimately lead to the activation/repression of specific gene programs (Wagh *et al.*, 2021). Although most of the studied effects have been shown to be mediated through TEADs, YAP/TAZ can also bind and regulate other TFs, such as SMADs (Alarcón *et al.*, 2009), or T-box 3 transcription

factor (Rosenbluh *et al.*, 2012). These changes can generate different responses depending on the context and cell type, and affect essential processes such as proliferation, migration, stemness, fate, cell morphology or survival (Moya & Halder, 2019).

The Hippo pathway integrates multiple cellular and extracellular cues to regulate gene expression. It can be activated through cell-cell binding, including zonula occludens 1 (ZO1) tight junctions or α -Catenin-mediated adherens junctions, cell polarity, or different ligand-receptor interactions as Wnt-Frizzled or GPCRs. Interestingly, YAP/TAZ regulation by mechanotransduction pathways can be mediated by Hippo-dependent and independent mechanisms (**Figure 8**) (Rausch & Hansen, 2020). Both integrin-recruited kinases in FAs, such as FAK or Src, and Rho GTPases can activate YAP/TAZ by diverse mechanisms (Ege *et al.*, 2018; Lachowski *et al.*, 2018; Rausch & Hansen, 2020). Interestingly, recent reports show that actomyosin forces can induce cell stretching forcing YAP/TAZ entry through nuclear pores (Elosegui-Artola *et al.*, 2017; Andreu *et al.*, 2022). Besides, cell spreading (Nardone *et al.*, 2017) or substrate stiffness (Dupont *et al.*, 2011; Yubing Sun *et al.*, 2014) can also activate YAP/TAZ nuclear translocation. Aside from FAs, GPCRs or even BMPRII can converge in the activation of Rho GTPases, thus also affecting YAP/TAZ signaling. Regarding its interaction with BMP pathway, it has been shown that ROCK-effector LIMK, can be recruited to BMPRII (Foletta *et al.*, 2003), and BMP ligand binding will induce LIMK activation, favoring stress fiber formation and YAP/TAZ activity.

In summary, cells can sense the ECM both at the biochemical and biomechanical level and can translate these signals to transcriptional changes, mostly through the regulation of YAP/TAZ activity. Different pathways converge in the activation of YAP/TAZ which are, in addition, interconnected to one another and work coordinately to regulate adhesion-mediated cell responses.

Objectives



In this project, we set out to assess the mechanisms regulating NSC behavior, especially focusing on NSCs quiescence maintenance. This process is tightly controlled by extrinsic signals derived from the specialized niche in which they reside. Among them, the interactions mediated by the ECM, specifically by vascular and speckled BMs, are found to be particularly relevant and still not fully understood (Nascimento *et al.*, 2018; Sato *et al.*, 2019). In line with this, recent publications have suggested that NSCs could participate in the generation of their own ECM niche (Kjell *et al.*, 2020). However, there is still a lack of evidence regarding the triggers for ECM deposition and the effectors downstream ECM-mediated responses.

Hence, we proposed the following specific objectives:

1. To analyze the contribution of NSCs to the ECM niche.
2. To study the interaction of specific NSC populations with BM structures.
3. To evaluate the role of adhesion to vascular ECM in NSC regulation.
4. To assess the mechanisms by which NSC self-generated ECM modulates NSC behavior.

Material and Methods



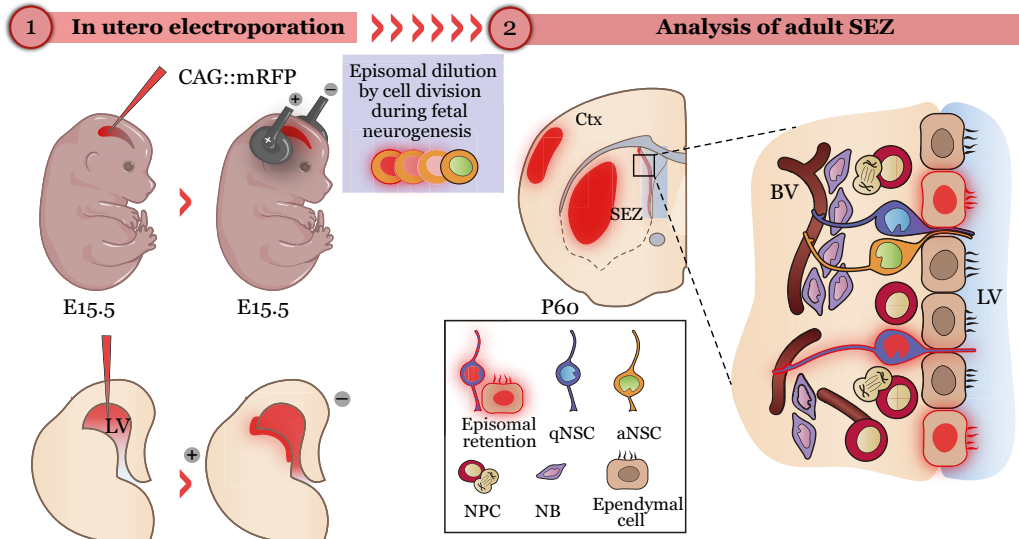
1. Mouse strains and handling

Adult C57BL/6J wild-type (WT) mice were obtained from the Jackson Laboratory (stock no. 000664) and were bred and housed at the animal housing facility (Universitat de València, Servei Central de Suport a la Investigació Experimental – SCSIE, Burjassot) according to the European Union 2010/63/UE and Spanish RD-53/2013 guidelines and under official veterinary supervision. Litters were weaned 21 days after birth, and housing established 12 h periods of light/darkness, room temperature (RT) of 20–22°C and a free accessible diet of pellets and water. All experimental procedures were approved by the Ethics Committee of Universitat de València (CEEA: 2015/VSC/PEA/00132 and 00133). When using highly invasive techniques was inevitable, mice were deeply anesthetized by intraperitoneal (i.p.) injection of a mixture of medetomidine (0.5–1 mg *per* kilogram of body weight) and ketamine (50–75 mg/kg) diluted in saline solution (0.9% NaCl). For all *in vivo* and *in vitro* experiments, adult mice ranging from 2 to 4 months of age were used.

2. *In vivo* methods

2.1 *In utero* electroporation

In order to label quiescent NSCs *in vivo*, we used IUE that was carried out as reported (Mateos-White *et al.*, 2020). This procedure was performed at the Universitat de València animal facility by researchers with expertise in the technique and under the supervision of a veterinarian. The main objective was to introduce genetic constructs in the cells lining the LV using a micropipette and a pair of electrodes to direct the desoxyribonucleic acid (DNA) and enable the incorporation of the plasmids in the cells. As NSCs are specified early in development, before E15.5, IUE was performed at this gestational time point to target this population and episomal plasmids containing fluorescent proteins (mRFP or GFP) under the control of the constitutive CAG promoter were used. After the incorporation, most cells will continue proliferating and the plasmid will be lost during consecutive divisions. Instead, cells that have not divided, or that have divided only a few times (i.e. quiescent NSCs), will retain the episomal plasmids in the adult (2-month) brain. Also, cells that have exited the cell cycle to differentiate immediately after the plasmid incorporation (i.e., neurons or ependymocytes) will also remain fluorescent (**Graphical Method 1**). Brains from electroporated mice were analyzed at 2 months by FACS (section 2.2) or processed for immunohistochemistry (IHC) for further characterization (section 2.3 and 2.4).







Graphical Method 1. *In utero* electroporation strategy. CAG::mRFP episomal plasmids are introduced in the LV of the embryo at E15.5 using a micropipette and a pair of electrodes. During fetal neurogenesis, episomal plasmids will be diluted through consecutive cell divisions. A coronal section illustrates the regions with episomal plasmid retention (cortex, striatum and SEZ) in the adult mouse brain (P60). In the SEZ, only ependymal cells that differentiate early in development and quiescent NSCs, will display episomal retention of the plasmids and remain fluorescent. Illustration by Ana Domingo-Muelas.

2.2 FACS strategy to characterize the neurogenic lineage

In our laboratory, we have developed a strategy that enables the characterization of the complete neurogenic lineage using FACS (Belenguer *et al.*, 2021a, b). The first step of this strategy is the dissection and digestion of the SEZ to obtain single-cell suspensions. To do so, brains from 2–4-month-old mice were collected in phosphate buffer solution (PBS) on ice and SEZ from both hemispheres were carefully dissected as previously reported (Belenguer *et al.*, 2016) to obtain very thin wholemount preparations. Then, they were cut into 4–5 pieces with sterilized scalpels, and transferred to a gentleMACS C (Reference (Ref.) 130-096-334) tube, removing the remaining PBS to avoid the dilution of the enzymatic solution to be added. For the digestion, Neural Tissue Dissociation kit (T) (Ref. 130-093-231) was used as specified by the supplier. The enzyme solution was composed of two mixes that were prepared independently: Enzyme mix (1) containing 1750 μl of buffer X + 200 μl of trypsin (component T); and mix (2) containing 20 μl of buffer Y + 10 μl of component A. First, 1,950 μl of mix 1 will be added to the tissue in the C tube followed by 30 μl of mix 2 to a final volume of 1,980 μl of enzyme solution *per* sample. Next, automatic digestion of the tissue was performed using the 37C_NTDK_01 program from a GentleMACS™ Octo

Dissociator with Heaters (Ref. 130-042-109), which allows highly reproducible chemical and mechanical disaggregation of the tissue.

To stop digestion, 3 ml of 100 µg/ml trypsin inhibitor (Sigma, Ref. T6522) diluted in FACS blocking buffer (*Table 3 Annex*) was added to each tube and a plastic pipette was used to carefully, but thoroughly, homogenate the remaining pieces of tissue by pipetting up and down. Then, cell suspensions were passed through previously humidified 40 µm filters and pelleted by centrifugation (at 300g, 10 min). Cells were resuspended in 100 µl of blocking buffer containing a combination of antibodies used for lineage characterization for 30 min on ice and protected from light (*Table 1 Annex*). Finally, antibodies were washed by adding 1 ml of FACS buffer and centrifuged (at 300g, 10 min). Cells were resuspended in 500 µl of FACS buffer, counterstained with 4',6-diamidino-2-fenilindol (DAPI) (0.1 µg/ml in distilled water) and analyzed with a LSR-Fortessa cytometer (Becton Dickinson) with 350, 405, 488, 561 and 640 nm lasers (**Graphical method 2**). Briefly, microglia, oligodendrocytes, erythrocytes, and ECs, named as Lin⁺, were first excluded using specific markers conjugated to the same fluorochrome. Then, Lin⁻ cells were stratified into: (1) neuroblasts (NBs: GLAST⁻/CD24^{high}) that are further separated into: NB1 (EGFR⁺) and NB2 (EGFR^{-low}); (2) neural progenitor cells (NPCs) comprised of two different subpopulations: NPC1 (GLAST⁻/CD24^{-low}) and NPC2 (GLAST⁺/CD24^{high}), both EGFR⁺; (3) non-neurogenic astrocytes (GLAST⁺/CD24^{-low}/CD9^{low}), and (4) neural stem cells (NSCs: GLAST⁺/CD24^{-low}/CD9^{high}) which are further divided into quiescent (qNSCs: GLAST^{high}/EGFR^{-low}), primed (pNSCs: GLAST^{low}/EGFR^{-low}) and activated (aNSCs: GLAST^{low}/EGFR⁺) (Belenguer *et al.*, 2021b) (**Graphical method 2**).

1 Lin ⁺				2 From Lin ⁻				
CD45 ⁺	O4 ⁺	Ter119 ⁺	CD31 ⁺	Population	GLAST	CD9	CD24	EGFR
Microglia 	Oligos 	Erythrocytes 	ECs 	Astrocyte	High	Low	-/Low	-/Low
				qNSC	High			-/Low
				pNSC	Low	High	-/Low	-/Low
				aNSC				+
				NPC1	-	High	-/Low	+
				NPC2	+	High	High	+
				NB1		High	High	+
				NB2	-	Low	High	-/Low

Graphical Method 2. FACS strategy for lineage characterization. (1) Markers used for exclusion of microglia, oligodendrocytes, erythrocytes and ECs. (2) Expression and relative intensity of the different markers used to identify the complete neurogenic lineage.

Material and Methods

2.3 Animal perfusion and brain processing

Adult young mice were deeply anesthetized with an i.p injection of a mixture of medetomidine (0.5–1 mg/kg of body weight) and ketamine (50–75 mg/kg) diluted in saline solution (0.9% NaCl). Then, they were perfused at a constant rate of 5.5 ml/min, first with saline solution (28 ml) and then with 4% paraformaldehyde (PFA) (83 ml) for fixation. Brains were extracted and post-fixed for 1h at RT. Prior to processing, brains were thoroughly washed with PBS, and then embedded in 4% agar for vibratome sectioning. Alternatively, they were conserved in PBS with 0.05% azide until its use. Coronal sections (40 µm) were obtained with a Leica VT1000 vibratome, and cuts were serially collected to have sets of sections representative of the whole SEZ. Sections were also kept refrigerated in 0.05% sodium azide to avoid contamination. For wholemount SEZ preparations processing, animals were usually non-perfused, and dissection was performed with fresh tissue and fixed by immersion in 4% PFA with 0.5% Triton-X-100 for 1 h.

2.4 Immunohistochemistry

Vibratome sections that included the SEZ were selected for immunostaining. Sections, or complete SEZ wholemount preparations were permeabilized and blocked for unspecific protein binding by incubating them for 1 h at RT with 10% of horse serum and 0.1-0.2% Triton X-100 in PBS prior to incubation with primary antibodies (*Table 1 Annex*) overnight at 4 °C. The next day, sections were thoroughly washed with PBS and incubated with fluorescence-conjugated secondary antibodies (*Table 2 Annex*) for 1 h at RT in the dark. Finally, nuclei were counterstained with DAPI (1 µg/ml) for 5-7 min, and sections were mounted with FlourSave™ Reagent (Calbiochem, Ref. 345789) for visualization and correct long-term maintenance.

3. Microscopy techniques

3.1 Fluorescence microscopy

For cell cultures, images were randomly acquired using a Nikon ECLIPSE Ni-U microscope (Nikon) with a Zyla 4.2 sCMOS camera (Andor). For live imaging, complete culture wells were automatically photographed using an IN Cell Analyzer 2000 imaging system (GE Healthcare) with controlled temperature and CO₂ conditions. For sections and wholemount preparations, images were acquired with an Olympus FV10i confocal microscope (405, 458, 488 and 633 nm lasers). To increase imaging resolution for the fine study of cell interactions *in vivo*, we performed tissue-clearing and expansion microscopy.

3.2 CLARITY-based tissue clearing

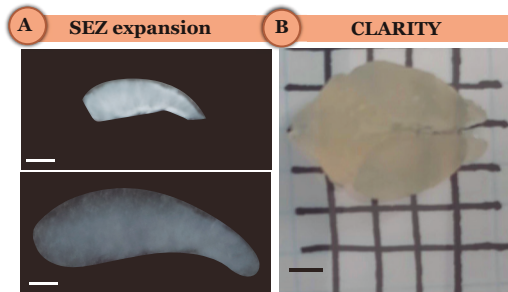
The objective of this process was to obtain optically transparent brain sections (300 μm) or SEZ wholemount preparations to enable high-resolution and deep imaging of the tissue. We used X-Clarity™ (Logos Biosystems), a collection of systems and reagents for tissue clearing based on the system CLARITY. In brief, for this aqueous-based clearing technique, hydrogel monomers (X-CLARITY™ Hydrogel Solution Kit, Ref. C1310X) were added to the sample and polymerized with heat to generate covalent links with the tissue biomolecules to form stable tissue-hydrogel hybrids (X-CLARITY™ Polymerization System, Ref. C20001). Then, electrophoresis (Electrophoretic Tissue Clearing Solution, Ref. C13001) with detergents was performed to remove lipids which will clarify and make the tissue transparent (X-CLARITY™ Tissue Clearing System II, Ref. C3000) (**Graphical Method 3**). This process maintained the direct fluorescence of qNSCs stained by IUE and was combined with immunostaining for LM visualization. Immunostaining was performed using the DeepLabel Antibody Kit (Logos Biosystem, Ref. C33001) following the instructions provided by the supplier, which allows higher antibody penetration. In brief, sections were incubated in rabbit α Laminin (1:500), chicken α GFP (1:500) and mouse α S100 β (1:400) (*Table 1 Annex*) antibodies in DeepLabel solution B for 48 h, washed in DeepLabel Washing solution and then incubated for 48 h with the corresponding secondary antibodies (*Table 2 Annex*). Finally, sections were washed and mounted in X-CLARITY mounting solution for refractive index homogenization. Sections were analyzed in a super-resolution confocal microscope (ZEISS, LCS 980).

3.3 Expansion microscopy

Expansion microscopy is a recently developed technique to allow nanoscale-resolution imaging by causing a physical expansion of the samples (Asano *et al.*, 2018). SEZ wholemount preparations were obtained, fixed and stained with antibodies using conventional immunostaining protocols. Then, they were incubated with Acryloyl-X SE overnight at RT to favor protein cross-linking in MatTek dishes (Ref. P35G-1.5-14-C). Following the cross-linking, gelling solution (*Table 9 Annex*) was added to the samples and incubated for 30 min to enable deep penetration of the solution at 4 °C protected from light. The solution was then removed, and new fresh gelling solution was added to the sample, which was then covered with 15 μm coverslip using a forceps to favor the formation of a flat gel. To allow gel polymerization, the solution was incubated for 2 h in the dark at 37 °C. After removing the coverslip, the gel was first incubated with digestion solution (*Table 10 Annex*) containing proteinase K, and incubated overnight. Then, sample expansion was performed by adding water 3-4 times and waiting for 10-15 min each time for samples to

Material and Methods

progressively expand (**Graphical Method 3**). Agarose at 2% was used to mount the gel with the embedded sample in a Petri dish, that was then covered with water and imaged on an inverted confocal microscope coupled with a water immersion objective (Leica, TCS SP8).



Graphical Method 3. Methodologies to increase microscopy resolution. (A) After SEZ dissection and IHC staining, wholemount preparations are expanded as reported (Asano *et al.*, 2018). Images of the SEZ before and after the expansion are shown. Scale bar: 1mm (Left). (B) Adult mouse brain after clarification with X-CLARITY™ method. Scale bar: 3mm.

3.4 Transmission electron microscopy

TEM was used to study the ultrastructure of qNSC contacts with BMs. 2-month-old mice with IUE-delivered CAG::eGFP episomal plasmids were intracardially perfused with 4% PFA and 0.5% glutaraldehyde to enable a better conservation of the tissue structure while preserving GFP epitopes. Brains were collected and 50 μm sections were obtained using a vibratome (Leica VT1000). Cryopreserved sections in 25% sucrose were permeabilized through successive freeze-thaw cycles. After blocking nonspecific binding for 1 h at RT, sections were incubated with the primary αGFP (1:200, Aves Labs) antibody for 48 h, at 4 °C under mild agitation. Then, sections were washed, blocked again, and incubated with the secondary antibody conjugated to colloidal gold (1:50, Ultrasmall, Aurion). The detection of ultrasmall gold particles with TEM requires a particle enhancement procedure with silver (immunogold-silver staining). Silver is deposited on the gold surface, a process that increases the size of the particles and enables the formation of metallic silver by the reduction of silver ions thanks to the catalytic activity of the gold particles. Sections were incubated in silver enhancement solution (Aurion R-Gent SE-LM, Aurion) in a dark chamber for 20 min. Finally, metallic silver has to be reduced to elemental gold to enable its visualization (process named as gold toning). To do so, an incubation with 0.05% gold chloride for 10 min at 4 °C is followed by an incubation with the 0.3 % reducing agent sodium thiosulfate. The formation of elemental gold can be seen as dark brown electron dense precipitates at the specific antibody-bound sites, which provide high contrast signals for TEM analysis. Further sample preparation to obtain 50-70 nm ultrathin cuts, including Durcupan™ resin embedding and sectioning, was performed by the Microscopy Facility at Universitat de València.

4. *In vitro* NSC cell culture methods

4.1 Establishment of NSC primary cultures

NSC primary cultures were generated as previously reported (Belenguer *et al.*, 2016). In brief, SEZs from C57BL/6J mice were dissected and minced in small pieces with scalpels in sterile PBS under a magnifying glass. For each young adult mouse brain (2-3 month old), the SEZs from both hemispheres were transferred to a 15 ml falcon tube, PBS was removed, and 1 ml of papain enzymatic solution was added. Papain solution was prepared by adding 12 U/ml of papain (Worthington Biochemical Corporation, Ref. LS003120) in Earle's Balanced Salt Solution (Gibco™, Ref. 24010-043) with 0.2 mg/ml L-cysteine hydrochloride (Sigma, Ref. C8277) and 0.2 mg/ml of ethylenediaminetetraacetic acid (EDTA) (Sigma, Ref. E6511) and was previously activated by incubating it for 20 min at 37 °C in a thermostatic bath. Tissue was kept for 30 min with the enzymatic solution in the water bath, assuring a correct penetration by mixing with a gentle vortex each 10 min. To stop the reaction, 3 ml of control medium (*Table 7 Annex*) was added and, to obtain single-cell suspensions, we performed mechanical disaggregation by pipetting up and down with a P1,000 until a homogenate was obtained. Cells were then washed and centrifuged at 200g for 10 min and each cell pellet was resuspended in growth media (i.e, control media supplemented with EGF and bFGF (*Table 8 Annex*)). We brought all cell suspensions to a final volume of 4 ml, with which we seeded 8 p48-well plates (1 cm² growth area, 500 µl/well). Cells were incubated for 7-10 days in an incubator at 37 °C and 5% CO₂, which enables the enrichment in NSCs and progenitors, that will proliferate and grow as floating neurospheres.

4.2 NSC subculture

Primary NSC cultures were maintained by regular subculture in growth media up to passage 7, after which some signs of senescence, such as shortened telomeres, can appear (Ferrón *et al.*, 2004). For NSC maintenance, if the growth was adequate, cells were passed after 5 days *in vitro* (DIV). To do so, neurospheres were collected in a 15 ml falcon tube using a plastic Pasteur pipette and centrifuged at 130g for 7 min. Pelleted neurospheres were resuspended in 200 µl of Accutase® solution (Sigma, Ref. A6964) to allow enzymatic digestion for 10 min at RT. Then, 1 ml of control media was added, and mechanical disaggregation was performed by gently but thoroughly pipetting up and down until a homogeneous solution was observed (20 times approximately). Then, cells were washed by adding control media and centrifuging at 200g for 10 min and finally resuspended in growth media. Cell concentration and viability was determined using an automated ADAM cell counter system and then were seeded at a density of 10,000 cells/cm² for maintenance. For

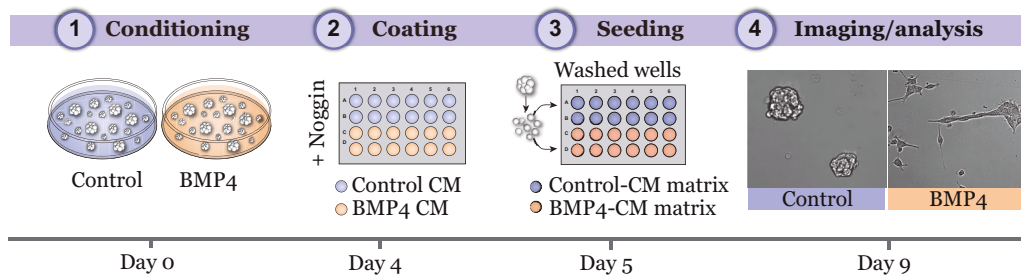
Material and Methods

long-term storage, 1.5 to 2 million single NSCs or, preferably, complete flasks with grown neurospheres at short passages were snap-frozen in control medium with 10% dimethyl sulfoxide (DMSO) using liquid nitrogen and conserved at -80 °C.

4.3 NSC treatments and culture over CM matrices

For quiescence induction, single-cell NSC suspensions were seeded at 10,000 cells/cm² density in growth medium containing 50 ng/ml of recombinant human BMP4 (RYD, Ref. 314-BP) or its vehicle (4 mM HCl with 0.1 % bovine serum albumin (BSA)). After 4 DIV, conditioned media (CM) was collected, centrifuged at 400g for 10 min to remove all cells and debris and the supernatant was conserved at -80 °C until its use. Taking into consideration that BMP4 can bind to the ECM, we decided to add to the CM highly concentrated Noggin (0.4 µg/ml), which acts as a BMP4 antagonist, so that we could sequester the remaining BMP4 in the media before its use.

CM was added to the desired well plates, with adjusted volumes considering the well surface (200 µl/cm²), and then kept overnight at 37 °C. Before seeding the cells, CM was removed and thoroughly washed with distilled water to only keep the deposited matrix. Dissociated neurosphere cells were then seeded at 20,000 cell/cm² in growth medium after their loading with DFFDA or not, depending on the experimental setup. Cells were allowed to grow for 4DIV and then were photographed in an IN Cell Analyzer 2000 with controlled temperature and CO₂ conditions to avoid cell detachment or, alternatively, cells were fixed for immunocytochemistry (ICC) or processed for FACS analysis (**Graphical Method 4**).



Graphical Method 4. Experimental pipeline for studying BMP4-induced NSC self-assembled matrix. (1) Neurosphere cells are seeded in growth media with BMP4 (50ng/ml) or its vehicle, for 4DIV. (2) CM is collected by centrifugation and BMP4-antagonist Noggin is added. Then, this media is used as a coating and maintained overnight. (3) Coated wells are washed and then neurosphere cultures are passed and seeded (10,000 cells/cm²) over the deposited matrix. (4) After 4DIV cells are live-imaged or detached for further analyses.

For evaluating the role of integrins in adhesion to self-generated ECM, we used integrin $\alpha 6$ -blocking GoH3 antibody (Sigma, Ref. MAB1378) and integrin $\beta 1$ -blocking (CD29, Bioscience Ref. KMID) at 40 $\mu\text{g}/\text{ml}$ for 30 min in FACS buffer. Then, cells were washed and seeded for 4DIV. For ROCK, we used Y27632 at 25 μM (Sigma, Ref. Y0503) diluted in growth medium or its vehicle (DMSO) as a control. Y27632 inhibits both ROCK1 ($K_i = 220 \text{ nM}$) and ROCK2 ($K_i = 300 \text{ nM}$) by competing with adenosine triphosphate for binding to the catalytic site (Davies *et al.*, 2000).

4.4 aNSC sorting

For sorting aNSCs, we dissected the SEZ of two C57BL/6J mice that were pooled and disaggregated as explained before. Cells were stained with our FACS panel (see section 2.2), and then aNSCs ($\text{GLAST}^{\text{low}}/\text{EGFR}^+$) were sorted using a BD FACSAria™ Fusion Flow Cytometer, which enables direct cell sorting to a culture dish incorporated in a safety cabin to avoid contamination. To identify how activated NSC responded to self-generated ECM, we coated p48-well culture dishes (1 cm^2) with control or BMP4-CM to which we added BMP4 antagonist Noggin (RyD, 1967) at 0.4 $\mu\text{g}/\text{ml}$ to sequester any remaining BMP4. Then, coatings were washed with distilled water and substituted with 500 μl of growth media in which 300 aNSCs were directly sorted in each well. Cells were kept in the incubator at 37 °C 5% CO_2 and counted manually at 24 h, 48 h, and 72 h for evaluating cell division. Total number of live cells, seen as refringent cells, were counted 24 h after seeding, and each of the three consecutive days we evaluated the number of singlets or the rest (doublets, triplets and small spheres). We showed these categories as a percentage from the total of live sorted cells.

4.5 Neurosphere formation assay

A neurosphere formation assay was used to evaluate the ability of NSC to self-renew after being cultured over control or BMP4-CM for 4 DIV. Single-cell suspensions were obtained as already explained for neurospheres (control-CM). For adhered cells (BMP4-CM), cells were detached by directly adding Accutase® solution (Sigma, Ref. A6964) to the wells, to further collect them and mechanically disaggregate them with the P1,000 pipette. Then, cells were counted and seeded at 5 cells/ μl , which avoids aggregation and assures that neurospheres are formed from a single cell (Ferrón *et al.*, 2004). Specifically, 1,000 cells were plated in 4 wells in p96-well dishes, with 200 μl of growth medium *per* well. Cells were kept in the incubator at 37°C 5% CO_2 for 6 DIV to allow neurosphere formation, avoiding the dish movement as much as possible as it will cause cell aggregation. After that, the complete

Material and Methods

wells were automatically photographed using an InCell analyzer 2000, with controlled temperature and CO₂ conditions. Number and diameter of the neurospheres were counted manually using Fiji. While the number of neurospheres will indicate the ability of the cells to self-renew and form neurospheres, diameter evaluation will depend on NSC proliferation.

4.6 Evaluation of NSC proliferation by FACS: DFFDA and EdU

To assess proliferation in NSC cultures, we used a cell-tracer method that was recently published by our laboratory (Belenguer *et al.*, 2021a). This strategy is based on the use of fluorescent tracer DFFDA (CellTrace™ Oregon Green 488 Carboxy-DFFDA-SE, Ref. C34555), which is diluted by half in each cell division, allowing us to study proliferation by evaluating DFFDA retention after 4 DIV. To load NSCs with DFFDA, single-cell suspensions were obtained as explained before and counted. 10⁶ single cells were washed with PBS, centrifuged at 200g for 10 min and then resuspended in 1 ml of PBS with DFFDA diluted at 1:1,000 (2 µg/ml). If 500,000 cells were used, incubation volumes were reduced to 500 µl with the same DFFDA concentration. Cells were incubated for 7 min in a 37 °C in a thermostatic bath and protected from light, and then washed, resuspended in growth medium and finally seeded at 20,000 cells/cm² in suspension or in adherent conditions: over Matrigel™ (Corning™, Ref. 356234), self-generated CM, or in co-culture with ECs. Cells were allowed to grow for 4 DIV and then DFFDA retention by FACS was evaluated by assessing medium fluorescence intensity (MFI) and the percentage of DFFDA^{high} cells. These are slow-cycling cells that we defined as the 10% of the population with higher retention of the tracer in the culture (Belenguer, *et al.*, 2021a). Conversely, DFFDA^{low} population had higher proliferation rates and was defined as the 40% of the total cells with lower tracer intensity.

Alternatively, thymidine analogue EdU was also used to evaluate proliferation *in vitro*. EdU will be incorporated during DNA replication during S-phase of the cell cycle, allowing us to identify proliferating cells. Cells were seeded at 10,000 cell/cm² in growth media in uncoated or coated plates depending on the experiment. After 4 DIV, EdU (ThermoFisher, Ref. C10338) was added at 20 µM (2X) in the same volume as the cells were seeded, which will dilute it to a final concentration of 10 µM (1X). EdU was incubated for 1 h at 37 °C. NSC cultured attached, over Matrigel™, over control or BMP4-CM or in co-culture with ECs, Accutase® solution (Sigma, Ref. A6964) was directly added to the well after washing with PBS. Then, reaction was stopped by adding control media to the wells, cells were collected and pipetted up and down to assure single-cell suspensions. Cells were then centrifuged at 300g 10 min and incubated, when needed, with primary antibodies (*Table 1 Annex*) diluted with FACS buffer, 30 min on ice and protected from

light. Then, for EdU detection, cells were fixed and permeabilized by incubating with Cytotfix/Cytoperm (Fisher, Ref. BD 555028) for 20 min at 4°C protected from light. For the detection of the analogue, cells were incubated with Click-iT[®] reaction solution that contains a fluorescent azide that will bind to EdU, together with other components that will favor the reaction. All the components were supplied by Click-iT EdU Alexa Fluor™ 555 Imaging Kit (ThermoFisher, Ref. C10338) and performed following manufacturer's instructions. In brief, cells were incubated with Click-iT[®] reaction solution for 30 min at RT protected from light, washed, and resuspended in 500 µl FACS buffer for the analysis. Finally, cells were filtered (40 µm), counterstained with DAPI (1 µg/ml) only when live unfixed cells were used, and analyzed with a LSR-Fortessa cytometer (Becton Dickinson). For evaluating proliferation with EdU, the percentage of EdU+ cells was assessed. For the rest of the markers, median fluorescence intensity (MFI) was evaluated.

4.7 Immunocytochemistry

For adhered NSCs, cells were washed with PBS and fixed with prewarmed 2% PFA for 15 min at RT. When NSC were adhered over control or BMP4-CM, as cells were easily detached, warm 4% PFA (2X) was directly added to the wells without removing the existing media, to the final concentration of 2% PFA. Non-specific antigen binding was reduced by treating the cells with blocking solution containing 10% normal horse serum and 0.1 % Triton X-100 in PBS for 1 h at RT. Then, primary antibodies (*Table 1 Annex*) diluted in blocking solution were added and incubated overnight at 4°C using an orbital shaker. After washing thoroughly with PBS, cells were incubated with fluorescence-conjugated secondary antibodies (*Table 2 Annex*) for 1 h at RT protected from light. Finally, after washing, nuclei were counterstained with DAPI (1 µg/ml) diluted in distilled water and coverslips were mounted for its visualization and correct long-term maintenance using the fluorescence protectant Fluoromount-G™ Mounting Medium (Electron Microscopy Sciences, Ref. num. 17984- 25). Images were acquired with an Olympus FV10i confocal microscope (405, 458, 488 and 633 nm lasers; Olympus) and a Nikon ECLIPSE Ni-U microscope (Nikon) with a Zyla 4.2 sCMOS camera (Andor).

4.8 NSC nucleofections

To evaluate the mechanisms of NSC adhesion and quiescence induction over self-assembled ECM, we nucleofected NSCs with diverse plasmids to disturb specific proteins and assess its behavior in response. To confirm the effect observed after ROCK pharmacological inhibition, we used the ROCK1 WT and the dominant negative ROCK1

Material and Methods

$\Delta 5$ constructs supplied by Enric Poch from Universidad CEU Cardenal Herrera (*Figure 1 Annex*). In addition, for evaluating YAP function in NSCs, we used the following plasmids, kindly supplied by Jorge Oliver from the Institute for Bioengineering of Catalonia (*Figure 2 Annex*): pBabe-YAP-5SA, a constitutively active form of YAP which has 5 serine-to-alanine substitutions that do not allow the inactivation of YAP by phosphorylation, pBabe-YAP-5SA/S94A, that has an additional mutation in serin 94 that does not allow the interaction of YAP with the transcription factor TEAD and an empty pBabe used as a negative control. To assess YAP-TEAD activity, we used pLL3.7 FLAG-YAP1-TEAD-P-H2B-mCherry from Yutaka Hata (Addgene, 128327) (*Figure 3 Annex*). This plasmid encodes for GFP under a constitutive promoter CMV and expresses mCherry fused to histone 2B (H2B) when YAP1-TEAD is active.

For plasmid amplification, single colonies were picked and seeded in 200 ml of liquid LB with the proper antibiotic in an Erlenmeyer flask. They were incubated at 37°C with agitation overnight. Bacterial pellets were collected after centrifugation (3,500g, 15 min, 4 °C) and plasmids were purified using the Genopure Plasmid Maxi Kit (Roche, Ref. 3143422001) following the instructions provided by the manufacturer. Plasmid concentration and quality was estimated with a Nanodrop. Before nucleofection, plasmids were checked by digestion with restriction enzymes (pROCK1WT and pROCK1 $\Delta 5$ with EcoRI; pBabe, pBabe-YAP-5SA and pBabe-YAP-5SA/S94A with EcoRI and XbaI; and pLL3.7 FLAG-YAP1-TEAD-P-H2B-mCherry with NotI and BamHI). Once confirmed, purified plasmids were stored at -20 °C until use. For the transfections, the nucleofection kit (Lonza, Ref. vpg-1004) was used. 5-10 million of primary NSCs (n=3 or 4) were resuspended in 90 μ l of nucleofection buffer containing 4 μ g of the plasmid of interest. The mixes were placed in aluminum cuvettes and nucleofections were carried out with a Nucleofector 2b device (Lonza, Ref. AAB-1001) using program G013. Cells were seeded in growth medium to which we added supplement B27 (Gibco, Ref. 17504044) and were allowed to recover for 24 h (*Table 7 Annex*). The following day, cells were disaggregated with Accutase® solution (Sigma, Ref. num. A6964), washed with Debris Removal Solution (Miltenyi, Ref. 130-109-398), counted and seeded in a growth medium without B27 in the different conditions to be tested. For YAP reporter, fluorescence was evaluated by FACS 48 h after the seeding over Matrigel™ or over control and BMP4-CM. For YAP constructs, NSCs were seeded with or without BMP4 (50 ng/ml) in uncoated p48 wells to test the effect of BMP4 treatment in adhesion. In addition, cells were seeded in p24 uncoated, or coated (control and BMP4-CM) wells to evaluate proliferation. Analysis was performed 24 h after the seeding, when cells were imaged to assess adhesion, and also 1 h EdU pulses were performed to evaluate proliferation by FACS (see section 4.6).

5. EC culture methods

5.1 Primary EC isolation with CD31⁺ magnetic beads

Primary ECs were isolated from the cortex or the SEZ of 2 month-old C57BL/6J mice. The meninges from each of the hemispheres were carefully pulled out by gently rolling them on filtering paper, and the regions of interest were dissected and minced in sterile PBS. For SEZ ECs, at least 2 animals (4 SEZs) were pooled to obtain a higher number of cells in the isolation. As a basis, cortex ECs were used in our cell culture experiments, and SEZ EC isolation was performed punctually for NSC-EC co-isolation studies.

The dissociation protocol is very similar to the one explained before for the *in vivo* FACS strategy (see 2.2), but in this case, Neural Tissue Dissociation kit (P) (Miltenyi, Ref. 130-093-231) was used. One of the differences is the proportion of the enzyme mix (1) recommended by the supplier, that in this case is 50 µl of papain (component P) in 1,900 µl of buffer X. For the SEZ, due to the reduced number of cells, 1:10 papain dilution was used (1,945 µl of buffer X + 5 µl of papain). The other main difference is the buffer used, in this case the isolation buffer (*Table 4 Annex*) contains Ca²⁺ and Mg²⁺ and does not have EDTA, to favor cell adhesion in culture. For the cortex samples, myelin was removed by using the Debris Removal Solution (Miltenyi, Ref. 130-109-398). Once myelin-free single-cell suspensions were obtained, samples were centrifuged (300g for 10 min) and resuspended with 1:10 CD31 microbeads (Miltenyi, Ref. 130-097-418) in 90 µl of isolation buffer and incubated for 15 min at 4 °C protected from light. After that, cells were washed, resuspended in 500 µl of isolation buffer, and passed through previously equilibrated MS columns (Miltenyi, Ref. 130-042-201) placed in a strong magnetic field to retain CD31⁺ fraction. After, 500 µl of blocking buffer was passed through the columns to wash the retained fraction (x3 times) and then columns were removed from the magnetic field and placed in Falcon tubes to elute the samples. For EC cultures, supplemented EC medium (Endothelial Growth Medium-2, Promocell PromoCell (Ref. C-39211)) (*Table 6 Annex*) was used. Then, cells were counted and a minimum density of 25,000 cells/cm² were seeded over fibronectin-coated wells (3 µg/cm²) to allow EC adhesion. Once confluency was reached, usually after 5-7 DIV, cells were fixed for ICC or used in NSC co-culture experiments. When EC co-isolated cells wanted to be evaluated by FACS, cells were resuspended in FACS buffer (*Table 3 Annex*), which do not contain Ca²⁺ and Mg²⁺ and do contain EDTA. The use of this buffer, together with further disaggregation with the pipette, enables the detachment those cells that have been co-isolated due to strong ECs binding, and favor single cell suspensions that can be characterized by FACS (section 2.2).

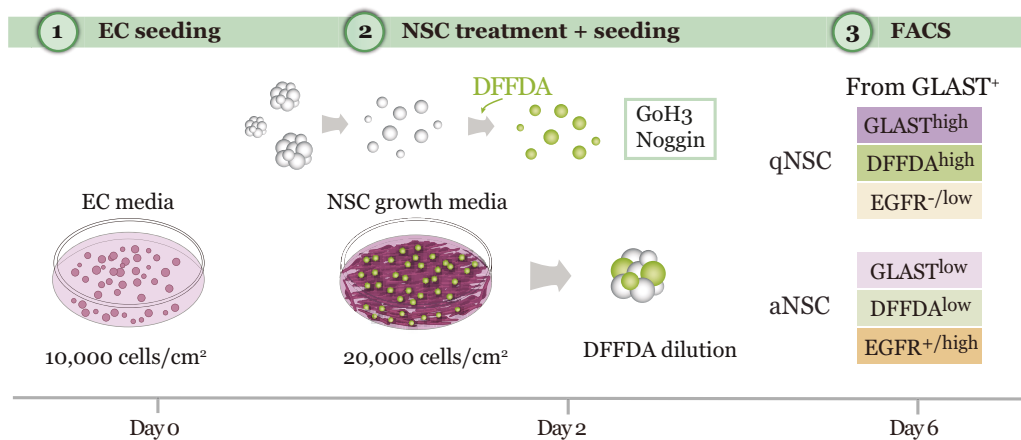
Material and Methods

5.2 Endothelial cell line maintenance

Human umbilical vein EC cells (HUVECs) were purchased from Merck (Ref. SCCE001) and cultured in supplemented EndoGro LS medium (Millipore, Ref. SCME-001) (*Table 5 Annex*). They were passaged and used up to passage 7 as recommended. When confluency was reached, cells were washed with PBS and 1 ml trypsin/EDTA (Life Technologies, Ref. 25200-056) was added to the plates for cell detachment. Reaction was stopped with 5 ml of medium and cells were collected, centrifuged (300g, 5 min) and resuspended in supplemented media for cell counting and plating. For long-lasting maintenance, cells were snap-frozen in liquid nitrogen in their media with 10% DMSO.

5.3 Direct NSC-EC co-culture and treatments

For NSC-EC direct co-culture experiments, HUVECs, or primary EC were used (10,000 cells/cm²). Once EC confluency was reached, usually after 24-48 h for HUVECs and 5-7 days for primary ECs, cells were washed with NSC medium to remove serum that could induce differentiation and NSCs were seeded overlaying ECs. To evaluate proliferation changes, NSCs were loaded with DFFDA prior to its seeding in co-culture at 20,000 cell/cm² in NSC growth medium (**Graphical Method 5**).



Graphical Method 5. NSC-EC co-cultures. (1) Primary brain ECs or HUVEC cells are seeded in EC culture media. (2) when confluent, EC medium is washed and NSCs are disaggregated, loaded with DFFDA, and seeded over EC monolayers in NSC growth media. Before seeding, cells were pretreated with GoH3 blocking antibodies or BMP4-antagonist Noggin. (3) Cells dilute the DFFDA tracer in each division. After 4DIV cells are detached with Accutase and analyzed by FACS. NSCs are identified as GLAST⁺ cells and intensity of DFFDA, GLAST and EGFR is evaluated.

In parallel, NSCs were usually cultured at the same density in suspension or in wells coated overnight with Matrigel™ as a control of adhered cells. After 4 DIV, cells were analyzed by FACS or fixed for ICC.

To study the contribution of BMP signaling in co-culture, Noggin (0.4 µg/ml) or its vehicle (DMSO) were added to the growth media when seeding NSCs over ECs monolayers. With the aim of blocking integrin α6-mediated adhesion, single-cell suspensions of NSCs previously charged with DFFDA were centrifuged and resuspended in 200 µl of FACS buffer with GoH3 antibody (Sigma, Ref. MAB1378) diluted to a final concentration of 40 µg/ml, as recommended by the supplier for function blocking experiments. An isotype-matching antibody was used as a control at the same concentration. Samples were incubated for 30 min on ice and protected from light and then washed and seeded in growth media over EC monolayers.

6. Molecular methods

6.1 RNA extraction and qPCR

Ribonucleic acid (RNA) was extracted with the RNeasy Micro or Mini kit (Quiagen, Ref. 74.134) depending on the number of cells, as they enabled a maximum of 45 or 100 µg of RNA, respectively. This system consist of sequential steps that use spin columns with short centrifuge times to extract RNA after removing genomic DNA, and cleaning the sample with multiple buffers as recommended by the supplier. After the extraction, RNA was eluted in RNase-free water and was quantified using the Qubit™ RNA HS Assay Kit (Thermo Fisher, Ref. 32852) in a Qubit™ Fluorometer (Thermo Fisher). Reverse transcription of 0.5–1 µg of messenger RNA (mRNA) was performed using the PrimeScript RT reagent kit (Takara, Ref. num. RR037A) to a final volume of 20 µl with the presence of both 50 pmol random hexamers and 25 pmol oligo-dT primers.

For gene expression analysis, reverse transcription quantitative polymerase chain reaction (qPCR) was performed using 5-15 ng of complementary DNA (cDNA) and predesigned TaqMan™ probes (*Table 11 Annex*). Following standard protocols, Premix Ex Taq™ Kit (Takara, Ref. RR390) was mixed with the probes and cDNA for amplification in a Step One Plus detection system (Applied Biosystems). A standard 40 cycle program with annealing and extension steps at 60 °C was used. Relative expression levels were calculated using the 2^{-ΔΔCt} method to calculate the relative gene expression compared to the endogenous expression of *Gapdh* and *18S*.

6.2 Laminin immunoprecipitation and western blot

To assess the presence of LM in NSC control and BMP4-CM, we immunoprecipitated (IP) the potential protein present in the media prior to its detection by western blot (WB), as the high concentration of BSA hindered the direct identification of the protein. To do so, we used 1 ml of CM obtained as in section 4.3 (n=4 cultures) and incubated it overnight with 5 µg of LM antibody (Novus Biotechnne, Ref. num. NB300-14) or a matching isotype control in an orbital shaker at 4 °C. Then, samples were incubated with 50 µl of magnetic Protein G Dynabeads (Invitrogen, Ref. num. 10003D) for 1 h at RT on a wheel. After 4 washes with 1 ml of PBS to remove the excess of antibody using a magnet to retain the Dynabeads (DynaMag, Ref. num. 12321D), the IP proteins were released by adding 50 µl of Laemmli buffer (*Table 12 Annex*) to the beads and incubating at 95 °C for 5 min. Finally, once the Dynabeads had been removed with the magnet, the samples were loaded into a 7% polyacrylamide electrophoresis gel and resolved by sodium dodecyl sulfate polyacrylamide gel electrophoresis. After that, proteins were transferred to a nitrocellulose membrane using the Mini Trans-Blot® Cell (Biorad) with transfer buffer (*Table 13 Annex*). Potential nonspecific interactions were minimized by blocking the membrane with 5% skimmed milk in tris buffer saline with tween (TBS-T) (*Table 14 Annex*) during 1 h at RT before incubation with LM antibody (2 µg/ml, 1:500) in TBS-T with 5% BSA overnight at 4 °C on agitation. Although the same antibody was used for the IP and the detection, we could identify LM from the light and heavy chains of the antibody by size. The membrane was washed several times with TBS-T before incubation with a horseradish peroxidase-conjugated secondary antibody (1:800) (*Table 2 Annex*) 1 h at RT. After washing again with TBS-T, the signal was detected with SuperSignal™ West Femto Maximum Sensitivity Substrate (Thermo Scientific, Ref. num. 34095) and images were acquired with a Mini HD 9 chemiluminescence imaging system (Uvitec).

6.3. Proteomics of BMP4-treated NSCs

6.3.1 Sample processing and digestion

NSC cultures (n=4) at passage 4 were treated with BMP4 (50 ng/ml) or its vehicle for 4 DIV. Then, cells were collected by centrifugation (400g, 10 min), and given to the proteomics facility of Servei Central de Suport a la Investigació Experimental at Universitat de València, where they prepared the samples and performed the proteomic analyses. Briefly, cell pellets were lysed with 100 µl of lysis solution from EasyPep™ MS Sample Prep Kits (Thermo Scientific, Ref. A40006) according to manufacturer instructions and were quantified with Qubit (ThermoFisher). 20 µg of each sample was digested and further processed with EasyPep™ MS to generate mass-spectrometry (MS)-compatible

peptide samples. Once samples were cleaned, they were dried with a rotatory evaporator, and dissolved in 50 μ l of 2% acetonitrile (ACN) 0.1% trifluoroacetic acid (TFA). With these samples we performed quantitative proteomics, Sequential Windowed Acquisition of All Theoretical Fragment Ion Mass Spectra (SWATH), a variant of data independent acquisition (DIA) method. To perform this differential proteomics, we first generated a spectral library by a *shotgun* mode and then used it to compare the samples.

6.3.2 LC-MS/MS in differential proteomics

Using a liquid chromatography system (Ekspert nanoLC 425, from Eksigent), 1.2 μ g of pooled peptide mixture was loaded onto a trap column (3 μ m C18-CL, 350 μ m x 0.5mm) (SCIEX, Ref. 5016752) and desalted with 0.1% TFA at 5 μ l/min during 3 min. The peptides were then loaded onto an analytical column (3 μ m C18-CL 120 Å, 0.075 x 150 mm) equilibrated in 7% ACN and 0.1% formic acid (FA). Elution was carried out with a linear gradient of solvents A (0.1% FA in water) and B (0.1% FA in ACN) from 7% to 37% of solvent B in A at a flow rate of 300 nl/min for 120 min in LC-MS/MS. Peptides were analyzed in a mass spectrometer nanoESI qTOF (6600plus TripleTOF, ABSCIEX). Sample was ionized in an Optiflow < 1 μ l Nano applying 3.0 kV to the spray emitter at 200°C. Analysis was carried out in a data-dependent mode. Survey MS1 scans were acquired from 350–1400 m/z for 250 ms. The quadrupole resolution was set to 'LOW' for MS2 experiments, which were acquired 100–1500 m/z for 25 ms in 'high sensitivity' mode. Following switch criteria were used: charge: 2+ to 4+; minimum intensity; 250 counts per second (cps). Up to 100 ions were selected for fragmentation after each survey scan. Dynamic exclusion was set to 15 s. The rolling collision energies equations were for all ions as for +2, according to the following equation: $|CE|=(0.049)\times(m/z)+(2)$. For LC-MS/MS-DIA analysis, 3 μ l of every peptide mixture were loaded to the same trap and analytical columns. Then, peptide elution was performed with the same protocol in this case for 60 min. This time, the tripleTOF was operated in SWATH mode, in which a 0.050-s TOF MS scan from 350–1250 m/z was performed. After, 0.080-s product ion scans in 100 variable windows from 400 to 1250 m/z were acquired throughout the experiment. The total cycle time was 2.79 secs. The individual SWATH injections were randomized to avoid bias in the analysis.

6.3.3 Protein identification and quantification

For protein identification, ProteinPilot default parameters were used to generate peak lists directly from 6600 plus TripleTof.wiff files. The Paragon algorithm (Shilov *et*

Material and Methods

al., 2007) of ProteinPilot v 5.0 (ABSciex) was used to search the Uniprot Mammalia Mouse database (210806, 87624 proteins). The parameters used were: *trypsin specificity*, *cys-alkylation*, *taxonomy restricted to mouse* and the search effort set to “rapid with FDR analysis”. The protein grouping was done by the Pro Group™ algorithm. A protein group in a Pro Group Report is a set of proteins that share some physical evidence. Unlike sequence alignment analyses where full length theoretical sequences are compared, the formation of protein groups in Pro Group™ is guided entirely by observed peptides only. Since the observed peptides are determined from experimentally acquired spectra, the grouping can be guided by usage of spectra. Then, unobserved regions of protein sequence play no role in explaining the data. Differential protein expression analysis between BMP4-treated and control samples was performed with the DESeq2 (2.11.40.7) package, using the DIA-NN derived protein expression quantification matrix as input and with default parameters, which include filtering of outliers and low-count proteins.

7. Bioinformatic analyses

The DIA-NN output was inspected at three levels: i) principal component analysis (PCA, Figure 2A) was used to evaluate the similarity of the biological replicates; ii) MA plot (Figure 2B) was used to visualize the relationship between mean protein expression and change bin expression between the two conditions for all proteins after filtering and size factor calculations performed by DESeq2; iii) the list of proteins with a False Discovery Rate (FDR) value <0.05 for the differential test conducted by DESeq2 were considered differentially expressed in BMP4-treated samples compared to control samples. The lists of up- and down-regulated proteins were used as inputs for gene set enrichment analysis. The analyses were based on the use of the *compareCluster* function as implemented in the *clusterProfiler* R package. The *compareCluster* function ran with the following parameters: `fun = “enrichGO”, OrgDb = “org.Mm.eg.db”, ont=“BP”, keyType=“SYMBOL”`. Enriched GO term redundancy was minimized by using the *simplify* function of the same package, applying the following parameters: `cutoff = 0.5, by = “p.adjust”, select_fun = min, measure = “Wang”, semData = NULL`. All heatmaps were generated using both the *ComplexHeatmap* (v1.10.2) and *ggplot2* (v3.0.0) packages in R. For expression heatmaps, the Spearman rank correlation distance was used as the base for the hierarchical grouping and clustering of genes, unless otherwise stated (literature-defined groups in Figure 7A). The overlap between two lists of genes was represented as a Venn Diagram (Figure 3C) and analyzed at two levels: 1) the representation factor, and 2) the probability of finding the overlap. The representation factor is the number of overlapping genes divided by the expected number of overlapping genes drawn from two independent lists. A representation factor > 1 indicates

more overlap than expected of two independent lists, a representation factor < 1 indicates less overlap than expected, and a representation factor of 1 indicates that the two lists share the number of genes expected for independent lists. The probability is then calculated as the exact hypergeometric probability as $C(D, x) * C(N-D, n-x) / C(N, n)$, being: $x = \#$ of genes in common, $n = \#$ of genes in list 1, $D = \#$ of genes in list 2, $N =$ total genes, $C(a, b)$ is the number of combinations of a things taken b at a time, the representation factor = $x /$ expected $\#$ of genes, expected $\#$ of genes = $(n * D) / N$. Density scatterplot (Figure 3B) was generated with the *geom_pointdensity* function from the R package *ggpointdensity*, whereas the Spearman correlation values were obtained by using the *stat_cor* function from the *ggpubr* R package. The *GOcircle* function from the *GOplot* R package was used to generate circular plots of representative GO terms (Figure 4C).

8. Image analyses

For quantification of nuclear YAP fluorescence, NSCs from 4 independent cultures were seeded at 10,000 cells/cm² over Matrigel™ or BMP4-CM matrix for 4 DIV in growth media. Then, pre-warmed PFA 4% was added to the well without removing the existing media to avoid cell detachment. After YAP ICC, Phalloidin-Texas red (ThermoFisher, Ref. T7471) was used to stain the cell cytoskeleton and DAPI to counterstain the nuclei. Cells were photographed with a confocal microscope (Olympus FV10i) at 60X. DAPI channel was used to generate a binary mask that was used to select the nuclei and quantify the mean fluorescence intensity from each analyzed cell. Each cell analyzed from the different cultures ($n=4$) was represented together and used for the statistical t-test analysis between Matrigel™ and BMP4-CM.

For the evaluation of morphological parameters of NSCs cultured over NSC-derived ECM, cells were cultured over control and BMP4-CM matrices at 10,000 cells/cm² after blocking or not integrin $\alpha 6$ with GoH3 (40 μ g/ml) or an isotype control. Cells were cultured for 4 DIV in growth media, and a minimum of 32 random fields were live-imaged with a 10x objective using an IN CELL Analyzer 2000 (GE Healthcare) keeping the plate at 37°C and under a constant inflow of humidified CO₂. Images corresponding to the same well were converted to a single stack and pre-processed by applying two sequential *Sharpen* filters plus a *Subtract Background* operation set with a *sliding paraboloid 5 pixel radius rolling ball*. Next, objects-of-interest were converted into binary masks by *Thresholding* with the Yen algorithm using the stack histogram for calculations. Binary images were then post-processed with one *Erosion* (neighbor pixel count = 6), four *Close* (neighbor pixel count = 2) and one *Fill Holes* operations. Finally, objects smaller than 100 pixel² were discarded and Area fraction and Shape descriptors were obtained from the remaining masks.

9. Statistical analyses

All statistical tests were performed using the GraphPad Prism Software, version 9.0.1 for Mac (<http://www.graphpad.com>). Analyses of significant differences between means were assessed using the unpaired or paired two-tailed Student t-test or one-way ANOVA with Tukey post-hoc test when appropriate. When comparisons were carried out with relative values (normalized values and percentages), data were first normalized by using a log or arcsin transformation, respectively. p-values lower than 0.05 were considered as statistically different and referred as * $p < 0.05$, ** $p < 0.01$ and *** $p < 0.001$. Data are always presented as the mean \pm standard error of the mean (SEM). The number of experiments carried out with independent cultures/animals (n) is either shown as dots in the graphs or listed in the Figure Legends.

Results



1. BMP4 as a model of NSC quiescence *in vitro*

1.1 BMP4 response is EGF-dependent and favors NSC adhesion

In this thesis, we decided to address the specific mechanisms regulating qNSC maintenance in the SEZ niche, and the fact that no one has been able to culture *in vivo* sorted qNSCs, prompted us to use *in vitro* systems to model this state. As explained in the introduction, it has been established that culturing hippocampal NSCs with BMP4 combined with bFGF can induce a reversible *quiescent-like* state (Mira *et al.*, 2010). However, the fact that subependymal NSCs are exposed to both bFGF and EGF *in vivo*, made us raise the question of whether SEZ NSCs would behave differently under the exposure of both mitogens in response to BMP4.

To understand the experimental setup, I will refer to a strategy that has been recently reported by our laboratory to study NSC proliferation dynamics *in vitro* by using a fluorescent tracer, DFFDA (Belenguer *et al.*, 2021a) (section 4.6 from Material and Methods). DFFDA is diluted by half in each cell division, thus, loading single cells with the tracer and allowing them to generate neurospheres, identifies cells with different cycling dynamics according to their tracer dilution rates. In around 50 % of all grown neurospheres we could find some DFFDA-retaining (DFFDA^{high}) cells. This indicated that the cell that had initiated the neurosphere, divided a few times before changing to a slower mode of division. Yet, its cell derivatives continued dividing and diluting the tracer (DFFDA^{low}), accounting for the overall growth of the clone (Belenguer *et al.*, 2021a).

To evaluate quiescence induction in response to BMP4, we seeded DFFDA-loaded primary single neurosphere cells in the presence of bFGF or EGF alone, or in NSC growth media (with the combination of both EGF/bFGF) with or without BMP4 (50 ng/ml). Then, we evaluated tracer dilution by assessing DFFDA fluorescence intensity by FACS after 4 DIV. As expected, most cells had diluted the tracer (DFFDA^{low}) while they divided to give rise to neurospheres. The rate of dilution, however, varied depending on the mitogenic stimulation (**Figure 1A-C**). In NSC growth media we obtained maximal dilution of the tracer, whereas each mitogen alone induced lower proliferation rates (blue histograms in **Figure 1A-C**). Culturing with BMP4 in the presence of bFGF alone did not considerably change DFFDA fluorescence intensity, in agreement with the mild proliferation of NSCs cultured only with this mitogen (**Figure 1A**). However, BMP4 could clearly antagonize the mitogenic effects of EGF, both alone (**Figure 1B**) or when combined with bFGF (**Figure 1C**), in which DFFDA retention in response to BMP4 was even more pronounced (**Figure 1C**).

Results

Our data indicated that BMP4 acted as a cytostatic factor for SEZ NSCs when they were properly activated by EGF-containing media, justifying its use when modeling quiescence *in vitro* with BMP4.

To further characterize the effect in proliferation in this condition, we did a 1h EdU pulse to chase all proliferating cells after 4 DIV in the presence of BMP4 in growth media and observed that, while 35% of cells were found to incorporate the nucleoside analog in the control, only 10% of EdU⁺ cells were detected after BMP4 treatment (**Figure 1D**). Strikingly, we discovered that exposing cells to BMP4, caused cells to adhere to the bottom of the wells, arranging in an elongated bipolar morphology that completely differed from the control condition, in which NSCs grew as floating neurospheres (**Figure 1E**). We systematically assessed adhesion in response to BMP4 by using different BMP4 batches and following the effect in neurospheres at different culture passages (up to passage 7), and, although we found some variability in the degree of adhesion, the effect was highly reproducible.

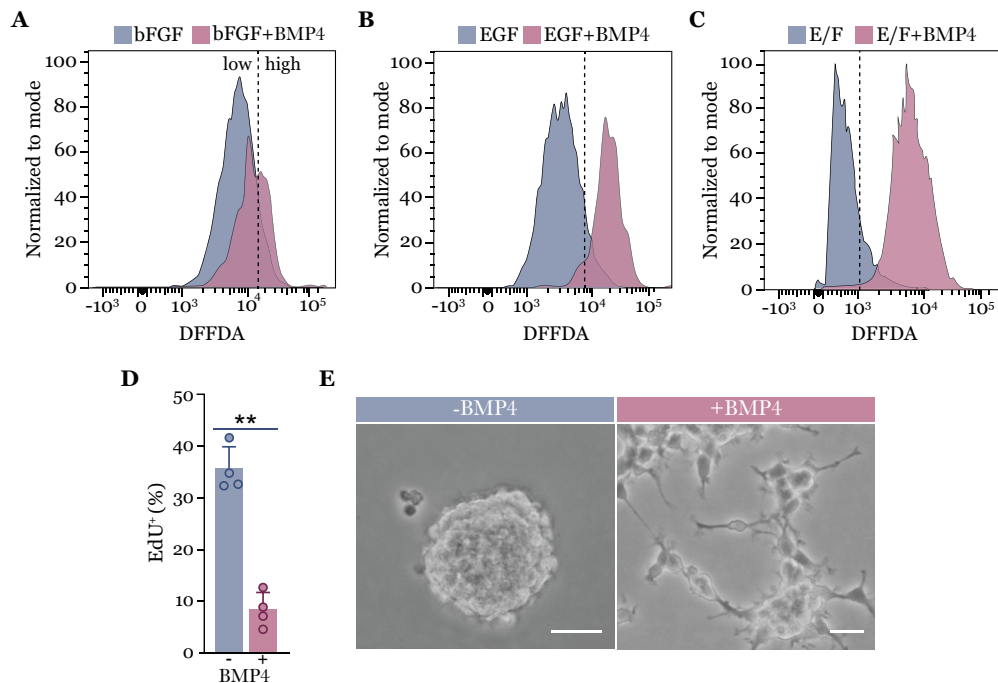


Figure 1. BMP4-induced quiescence depends on mitogenic stimulation and induces NSC adhesion. (A) Histogram showing normalized DFFDA intensity in primary NSCs after 4 DIV in bFGF (blue) or bFGF+BMP4 (magenta) supplemented media. Dotted line limits DFFDA^{low}/DFFDA^{high} populations. (B) DFFDA dilution in EGF (blue) and EGF+BMP4 (magenta). (C) DFFDA intensity with both mitogens (E/F) with or without BMP4. (D) Percentage of EdU⁺ cells (1h pulse) after 4 DIV under BMP4 stimulation in E/F supplemented media. (E) Phase contrast images showing NSCs morphology when adding BMP4 in growth media. Scale bars: 50 μ m.

This serendipitous observation made us hypothesize that some proteins may be secreted in response to BMP4 that could potentially favor NSC adhesion and spreading. To delve further into this idea, we decided to perform a proteomic analysis of BMP4-treated primary NSCs.

1.2 BMP4-treated NSCs resemble *in vivo* quiescent cells

Cells from short passage neurosphere cultures (n=4) were treated with BMP4 or its vehicle for 4 DIV in growth media. Then, cells were collected and given to the Proteomics facility (Universitat de València) where they were processed for SWATH differential proteomic analysis (see 6.3 in Material and Methods).

PCA clearly clustered control and BMP4-treated samples (**Figure 2A**) and as many as 5,076 proteins were detected in all samples. From them, 942 and 893 were significantly up and downregulated, respectively, in BMP4 compared to controls (**Figure 2B**). To gain new insights into the biological processes affected by quiescence induction after BMP4 treatment, we performed a GO enrichment analysis and found distinguished categories up and downregulated in BMP4 versus (*vs.*) control (**Figure 2C**). Among the top GO terms enriched in BMP4 samples we found *protein secretion, positive regulation of cell projection*

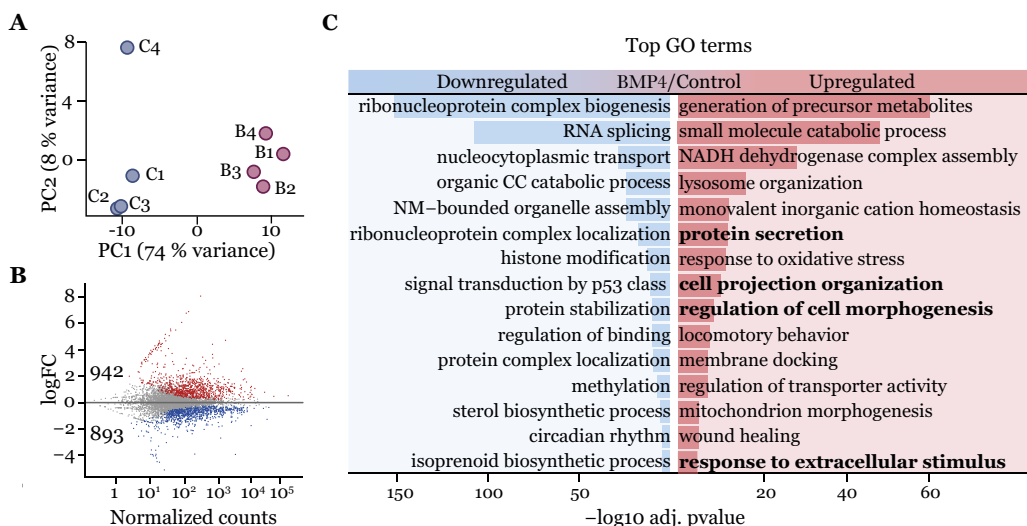


Figure 2. Proteomic analysis of BMP4-treated NSCs. (A) PCA of control (blue) and BMP4-treated (magenta) samples. (B) MA plot with upregulated (red) and downregulated (blue) proteins in BMP4/control samples. (C) List of top GO terms from BMP4 upregulated proteins. Bars show the adjusted $-\log_{10}$ p-value of each GO category. PCA: principal component analysis; FC: fold change; NM: non-membrane; CC: cyclic compound.

Results

organization, cell morphogenesis or response to extracellular stimulus, which supports the idea of BMP4 priming for cell spreading *in vitro*.

To better characterize the state induced by BMP4 treatment, we decided to align our proteome datasets with our already characterized *in vitro* transcriptomes from DFFDA^{high}/DFFDA^{low} populations (Belenguer *et al.*, 2021a). When we described these populations, we showed that DFFDA^{high} cells displayed a molecular signature that resembled that of the pNSCs *in vivo*, while highly proliferative DFFDA^{low} cells were transcriptionally similar to aNSC (Belenguer *et al.*, 2021a). Remarkably, we found that most BMP4/control upregulated proteins were found enriched at the transcriptional level in DFFDA^{high} and downregulated in DFFDA^{low} cells (**Figure 3A**), which rendered a positive correlation when aligning both datasets ($R = 0.53$, $p < 2.2e-16$) (**Figure 3B**). If we selected the common genes/proteins from both datasets, we found that among the changed proteins in BMP4 *vs.* control (grey), 61,5% (1,077) of them were also differentially expressed (DE) in DFFDA^{high} *vs.* DFFDA^{low} (**Figure 3C**), which suggests that these protein changes could be transcriptionally regulated. Interestingly, this overlap was found to be 4.8 times higher than the one expected by chance, indicating a high degree of similarity between the molecular phenotypes observed in the two experimental conditions.

The fact that BMP4 treatment mimicked DFFDA^{high}/DFFDA^{low} changes suggested that BMP4 treated cells were not differentiating, as they resembled untreated cultured slow-cycling NSCs. Furthermore, it proposed that BMP4 treatment was shifting NSC

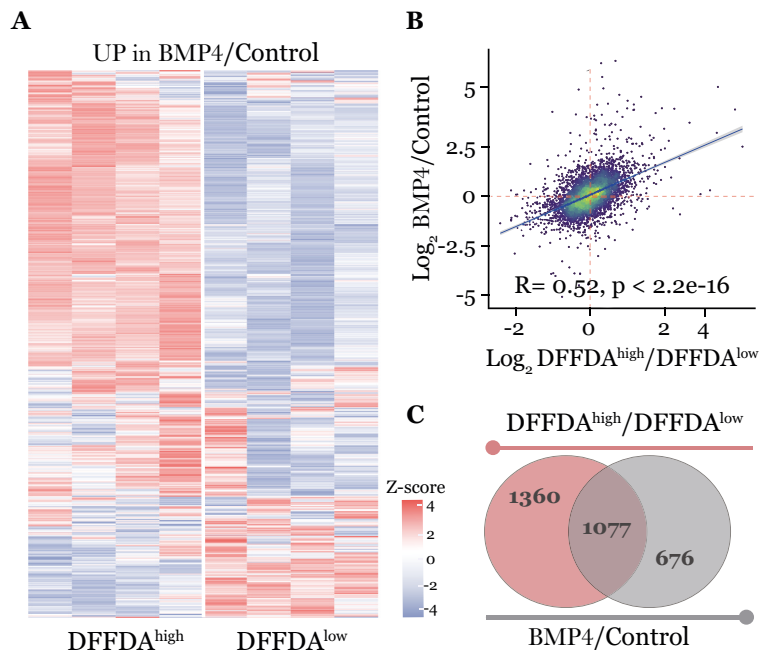


Figure 3. BMP4-treated NSCs resemble DFFDA^{high} cells. (A) Heatmap with relative expression levels of BMP4/control upregulated proteins in DFFDA^{high} and DFFDA^{low}. Raw Z-scores are represented. (B) Scatter plot colored by density aligning BMP4/control and DFFDA^{high}/DFFDA^{low}. The Spearman correlation coefficient (R) and p-value (p) are shown. (C) Venn diagram illustrating the overlap between datasets.

transcriptional profile from a state of activation to a state closer to quiescence.

In this context, we assessed the expression of BMP4 upregulated proteins in the different populations *in vivo* and observed that they were highly upregulated at the transcriptional level in qNSCs and pNSCs and downregulated in aNSCs (**Figure 4A**). For a more quantitative evaluation, we compared the mean mRNA normalized expression levels of BMP4 upregulated proteins in the different populations and found significant differences between qNSCs (which displayed the highest expression), compared to pNSCs and aNSCs, the latter expressing the lowest levels (**Figure 4B**). Besides, we found that literature-reported GO categories associated to qNSC, as *lipid catabolism*, *lysosome organization*, *cell-cell communication* or *glucose metabolism* were enriched in BMP4-treated

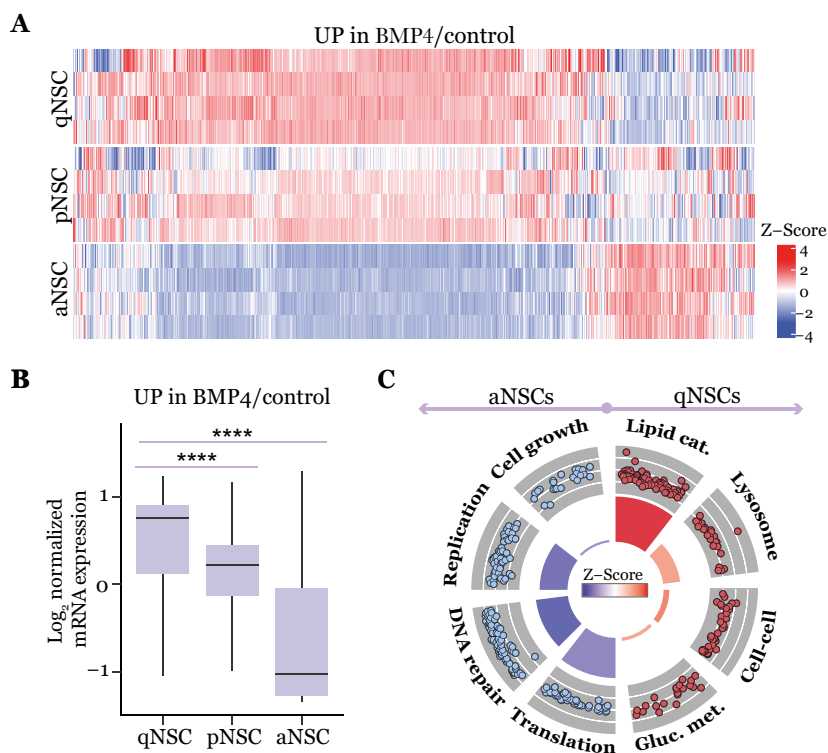


Figure 4. BMP4 mimics the molecular profile of *in vivo* qNSCs (A) Heatmap showing the relative expression levels of BMP4/control upregulated proteins in NSC populations. Column Z-scores are represented. (B) Box plot illustrating the normalized mean mRNA expression of BMP4/control upregulated proteins in NSC populations. (C) Circular diagram representing four representative GO categories of *in vivo* qNSC (right) and aNSC (left). Each dot illustrates a BMP4 upregulated (red) or downregulated (blue) protein associated to the categories. The outer circle shows the log₂ fold change (FC), the height of the inner bar plot indicates the significance level of the GO term ($-\log_{10}(\text{FDR})$), and the color represents the Z scores. Cat: catabolism; gluc. met: glucose metabolism.

Results

cells (**Figure 4C**). Instead, aNSC-associated categories as *translation*, *DNA repair*, *DNA replication* or *cell growth* were only found in control samples. All in all, this data supported the idea of BMP4 treatment inducing a state that resembled the deeply quiescent NSC state *in vivo*. (**Figure 4C**).

2. BMP4 in ECM secretion

2.1 BMP4 proteomics reveal changes in ECM components

Looking deeper into the idea of BMP4-induced NSC spreading *in vitro*, GO enrichment analysis revealed many adhesion-related categories only represented in BMP4 proteomes and not present in control samples. For example, *actin filament organization*, *small GTPase mediated transduction* or *cell-substrate adhesion* were among the most represented categories in BMP4 samples (**Figure 5A**), pointing to the potential role of actin cytoskeleton on BMP4-induced adhesion. Among the upregulated proteins associated to these categories, we could find specific ECM constituents, supporting the idea of BMP4

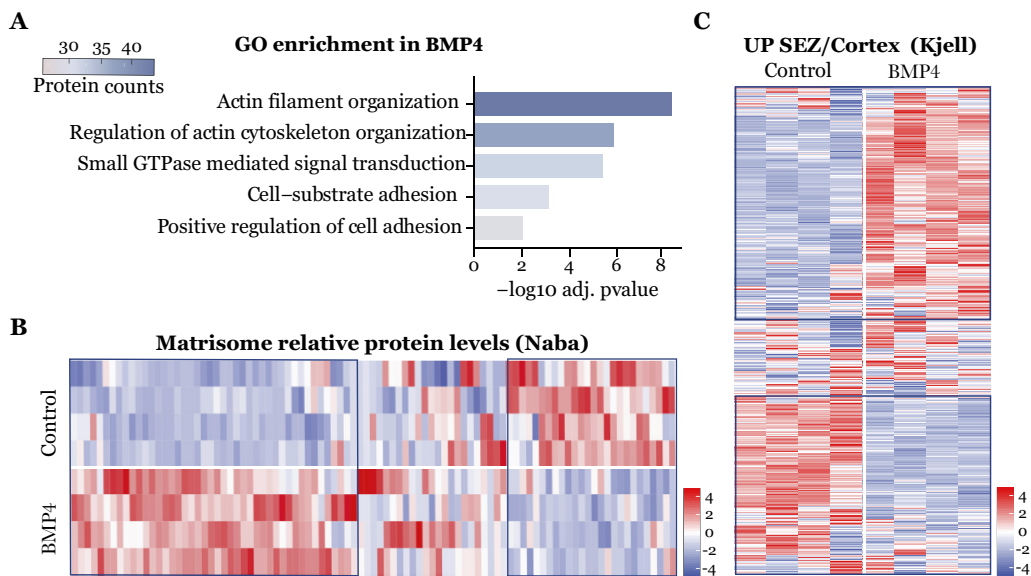


Figure 5. Matrisome-associated and SEZ-specific proteomes are affected after BMP4 treatment. (A) GO analysis showing enriched adhesion-related categories in BMP4 samples. $-\log_{10}$ of adjusted p-values are indicated for each category, and protein counts are represented with the color code. (B) Heatmap illustrating relative protein levels of published matrisome genes (Naba *et al.*, 2012) in BMP4 and control proteomes. Column Z-scores are represented. (C) Heatmap representing relative protein abundance in BMP4 and control samples of enriched SEZ *vs.* cortex proteins (Kjell *et al.*, 2020). Raw Z-scores are illustrated.

not only affecting cell responses to the ECM, but, as hypothesized, also modulating the matrix composition *per se*.

To assess the specific changes in ECM-related proteins, we decided to take advantage of the matrisome published by Naba and colleagues (Naba *et al.*, 2012). It is compilation of *in silico* and *in vivo* data that defines a set of genes encoding for ECM proteins, named as the *core matrisome* (collagens, GPs and PGs), and for ECM-associated proteins (categorized as ECM-regulators, ECM-affiliated, and secreted factors). When we checked for matrisome genes in our proteomic data, we identified two differentiated clusters of proteins up and downregulated after BMP4 treatment (**Figure 5B**), revealing a potential BMP4-induced ECM remodeling during aNSC-qNSC transitions mediated by the morphogen. Besides, we found a cluster of proteins upregulated in BMP4 that had been reported to be specifically enriched in the SEZ compared to the cortex (Kjell *et al.*, 2020), suggesting that BMP4 may have a role in defining the specialized SEZ proteome (**Figure 5C**). Indeed, BMP4 treatment induced very specific ECM changes (**Figure 6**).

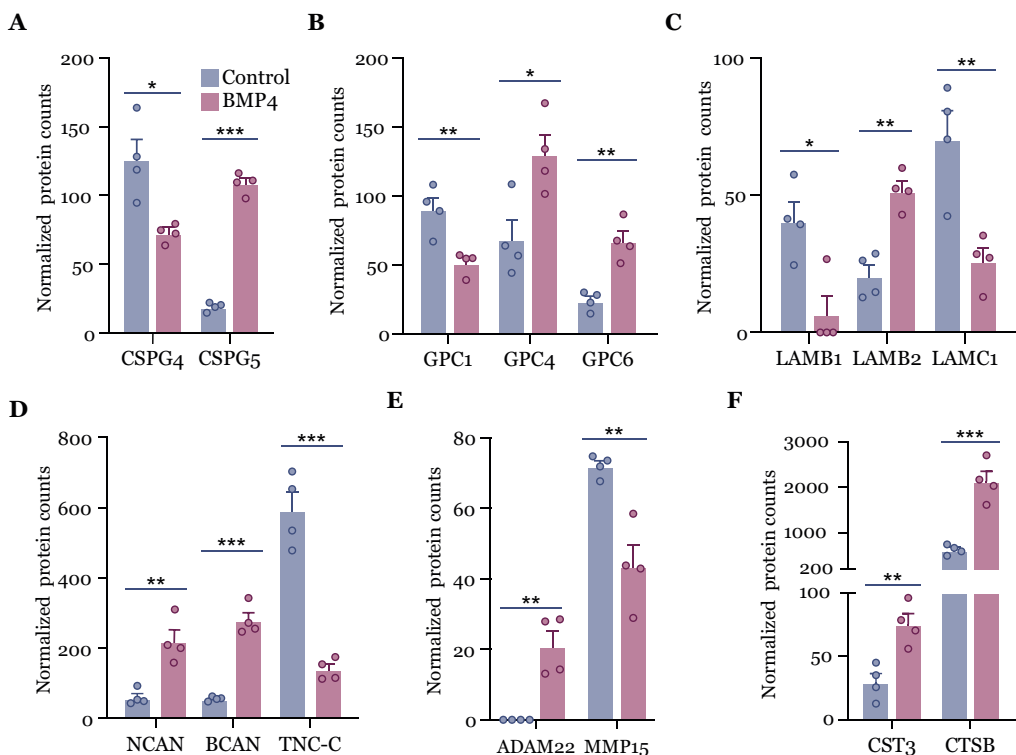


Figure 6. BMP4 tightly regulates ECM protein levels. (A) Normalized protein counts of chondroitin sulfate proteoglycans, CSPG4 and CSPG5, after BMP4 treatment. (B) Glypican family (GPC1, GPC4 and GPC6) regulation with BMP4. (C) Laminin isoforms (LAMB1, LAMB2,

Results

LAMC1) affected by the treatment. **(D)** Normalized counts in different components of perineural nets: neurocan (NCAN), brevican (BCAN) and tenascin-c (TNC-C). **(E)** Matrix metallopeptidases (ADAM22 and MMP15) changes after BMP4 treatment. **(F)** Cathepsin b (CTSB) and cystatin 3 (CST3) induction with BMP4.

We found different isoforms from the same family of ECM proteins up and downregulated after the treatment (**Figure 6A-F**). For example, while chondroitin sulfate PG 5 (CSPG5), glypican 4 (GLP4) and 6 (GLP6) or LM β 2 (LAMB2) were found upregulated with BMP4, CSPG4, GLP1 or LAMB1 and LAMC1 were downregulated (**Figure 6A-C**). Further, BMP4 also favored changes in proteins that compose perineural nets, as it increased GP neurocan (NCAN) and brevican (BCAN) while drastically reducing tenascin-c (TNC-C) (**Figure 6D**). Interestingly, apart from ECM components, our proteome revealed an enrichment in enzymes related to ECM remodeling. For example, we showed increased levels of a desintegrin and metalloproteinase domain-containing protein 22 (ADAM22) and decreased metalloproteinase 15 (MMP15) (**Figure 6E**). Also, BMP4 induced diverse lysosomal enzymes which participate in extracellular ECM remodeling, as cathepsin b (CTSB) (Vidak *et al.*, 2019) or extracellular protease inhibitors, as cystatin 3 (CST3) (**Figure 6F**). This opened the possibility of a potential BMP4-induced remodeling of the matrix not only through changes in ECM components, but also through regulating protease function.

2.2 Quiescent NSCs display a shared ECM-related signature

Taking into consideration the ECM protein changes observed after BMP4-induced quiescence, we wondered whether qNSC *in vivo* also differentially expressed ECM-related genes. To assess this, we aligned Naba matrisome datasets (Naba *et al.*, 2012) with our RNA-seq transcriptomes from the different NSC populations (Belenguer *et al.*, 2021a) and discovered that qNSCs displayed a higher expression of matrisome genes regardless of the category evaluated (**Figure 7A**). In contrast, the expression was reduced in pNSCs and lowered in aNSCs and more committed NPCs and NB1s, to partially increase again in migrating NB2. Interestingly, when we evaluated the average expression of the genes related to each of the aforementioned categories in qNSCs, we found that ECM-regulators had the highest expression levels (**Figure 7B**). Furthermore, among the core matrisome, GPs were the family of proteins that were found more expressed in qNSCs (**Figure 7B**).

In order to check whether this changes in matrisome genes also occurred in DFFDA^{high}/DFFDA^{low}, we aligned both datasets and found a correlation between DE matrisome-related genes (Naba *et al.*, 2012) (highlighted in orange) (**Figure 7C**). In addition, we were surprised to discover that BMP4-induced ECM protein changes also partially recapitulated the changes observed for qNSCs/aNSCs *in vivo* at the transcriptional

level (**Figure 7D**). This is especially relevant when considering that we are comparing protein fold changes (FC) *in vitro* with gene expression changes *in vivo*. Overall, this pointed to the existence of a specific ECM signature in quiescent NSCs populations, which was reproduced with BMP4 treatment. As part of this signature, we found that qNSCs/aNSCs, DFFDA^{high}/DFFDA^{low} and BMP4/control shared the upregulation of calcium-binding annexin family (e.g ANXA2, ANXA5, ANXA6 and ANXA7), S100 proteins (S100b, S100a13), ECM components (GPC4 or LAMB2) or FGF ligands (FGF2), among others.

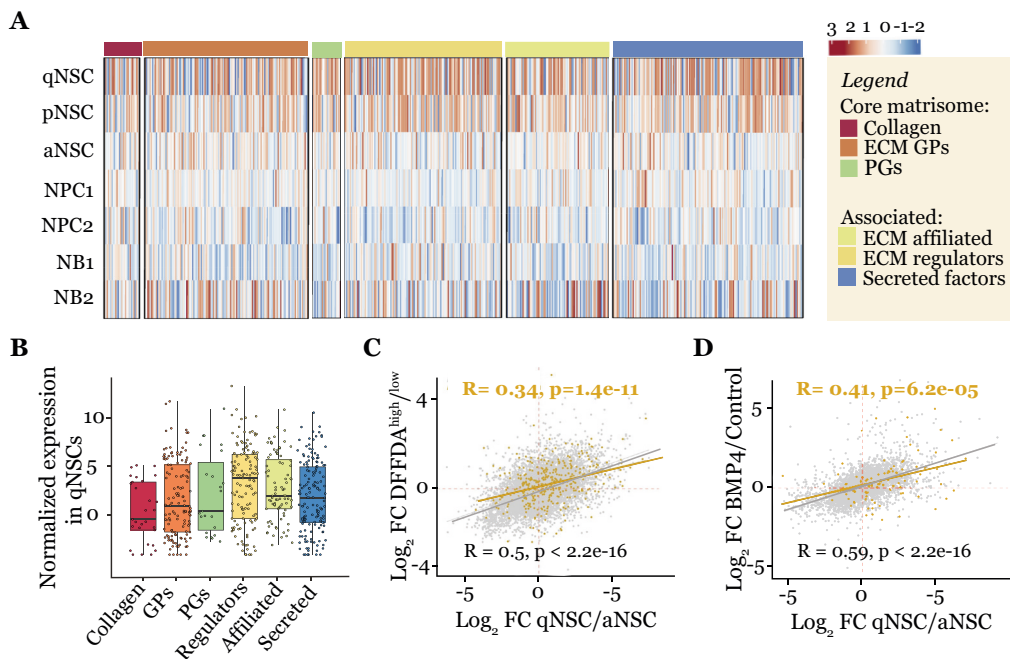


Figure 7. qNSCs have increased expression of matrisome genes. (A) Heatmap showing the expression of matrisome genes in the neurogenic lineage, organized by categories. Upper right panel shows the matrisome color code used. Column Z-scores are shown. (B) Box plots representing the normalized expression in qNSCs of the different genes (showed as colored dots) included in each category. (C) Scatter plot illustrating the correlation between DFFDA^{high}/DFFDA^{low} and qNSCs/aNSCs. Matrisome genes are highlighted in orange. Log₂ of the fold change (FC) is represented, and the Spearman correlation coefficient (R) and p-values are shown both for the global and the matrisome-specific correlation. (D) Scatter plot illustrating the similarities between BMP4/control protein changes and qNSC/aNSC expression changes.

Interestingly, annexins and S100 proteins were also described as part of the SEZ specific proteome (Kjell *et al.*, 2020), suggesting that BMP4 may have a role in defining this specific ECM niche *in vivo*.

Results

To test which receptors could be important for ECM interaction in qNSC, we assessed the expression of the genes associated with the GO category *extracellular matrix binding*. Interestingly, we found that the transitions from qNSCs to aNSCs came along with the downregulation and upregulation of multiple ECM-binding proteins (**Figure 8A**). Among the qNSC-upregulated genes, we could find different LM-binding receptors, such as *Itga7*, *Bcam* or *Dag1* (**Figure 8A**).

Due to their essential role in ECM binding and FA assembly and signaling (Kechagia *et al.*, 2019), we decided to deepen in the expression of integrin-coding genes and found that most of them were upregulated in qNSCs (**Figure 8B**). Remarkably, among the genes encoding for alpha subunits, the ones that had specificity for LM (pointed with arrowheads) were found upregulated in qNSCs compared to aNSCs (**Figure 8B**). Besides, when we checked whether this changes were reproduced at the protein level after BMP4 treatment, we found significant differences in three heterodimers (**Figure 8C**): ITGA6, which was found increased with the morphogen, upregulated vitronectin-binding ITGAV,

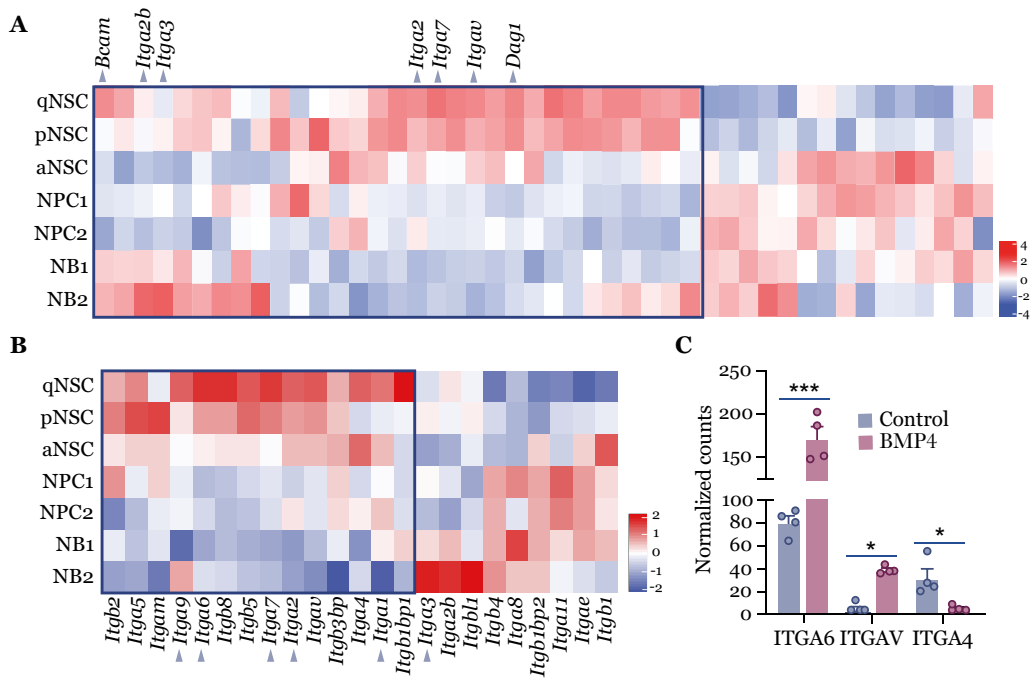


Figure 8. LM receptors are enriched in qNSCs. (A) Heatmap showing the relative expression of the genes associated to the GO term *Extracellular matrix binding* in the neurogenic lineage. A cluster of genes upregulated in qNSCs is highlighted, with different examples of upregulated LM receptors. Column Z-scores are represented. (B) Heatmap illustrating the relative expression of integrin genes. Arrowheads point LM binding α subunits. Column Z-scores are shown. (C) Normalized protein counts of integrin receptors after BMP4 treatment.

and downregulated fibronectin-binding ITGA4. All in all, this data suggested that qNSCs, in addition to remodeling the environment, may have a specialized interaction with it, especially considering LM-integrin-mediated signaling.

2.3 BMP4 induces LM secretion

Taking into consideration the limitations of a proteomic analysis, especially regarding insoluble and high molecular weight ECM components (Byron *et al.*, 2013), we decided to check for more sensitive LM gene expression changes to better characterize the ECM-related transcriptional signature in response to BMP4. In our RNA-seq dataset, we found specific LM isoforms (*Lama3*, *Lama5*, *Lama2*, *Lamb2*, *Lamb3*) upregulated in qNSCs (**Figure 9A**). Among them, some isoforms have been described in the literature as present only in vascular (V in figure) (*Lama2*) or speckled (S in figure) (*Lama3*) BMs, while the rest have been reported in both structures (S/V) (*Lama5*, *Lamb2*) (Sato *et al.*, 2019) (**Figure 9A**).

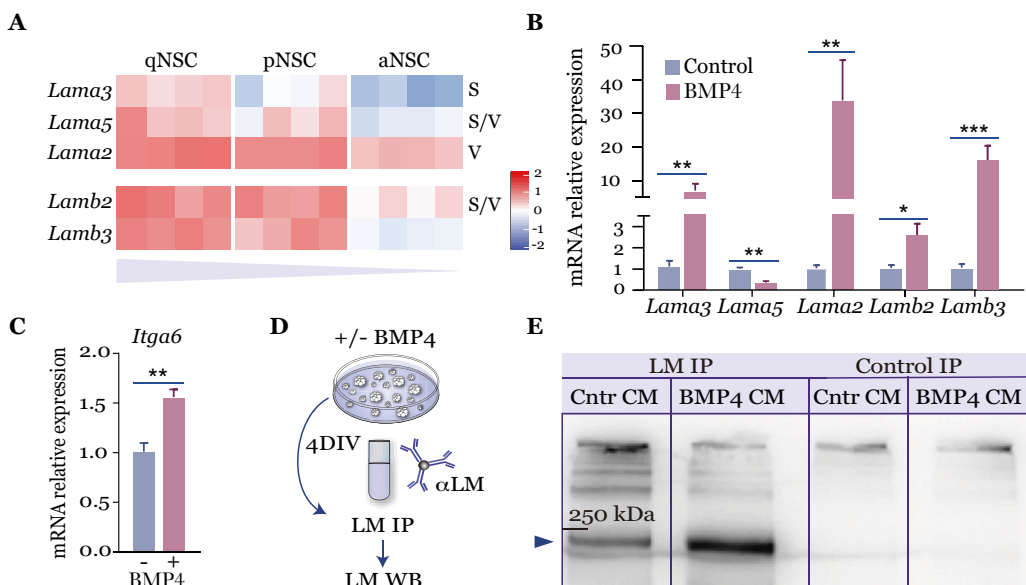


Figure 9. BMP4 regulates LM transcription and protein secretion. (A) Heatmap showing the relative expression of LM isoforms upregulated in qNSC populations. Column Z-scores are represented. (B) mRNA relative expression to control samples of the different LM genes in neurospheres after BMP4 treatment for 4DIV. (C) *Itga6* expression in BMP4 relative to control. (D) Experimental setup for LM detection in CM by immunoprecipitation. (E) LM WB from the IP fraction using LM or a non-related (control) antibody in BMP4 CM and control CM. S: speckled BM; V: vascular BM; cntr: control; IP: immunoprecipitation; WB: western blot.

Results

To evaluate whether BMP4 treatment reproduced these expression changes, we used neurospheres and assessed the relative expression of the aforementioned isoforms after 4DIV in the presence of the morphogen. Except for *Lama5*, which was shown to be downregulated, the rest of the isoforms tested (i.e. *Lama2*, *Lama3*, *Lamb2* and *Lamb3*) were found upregulated with BMP4 (**Figure 9B**). Considering the increase in ITGA6 protein levels after BMP4 treatment, we also checked for *Itga6* mRNA expression changes and found a BMP4-induced upregulation (**Figure 9C**).

Nevertheless, to test whether these LM transcriptional changes resulted in an increased LM secretion to the extracellular milieu by NSCs, we decided to assess the presence of LM in the CM of BMP4-treated neurospheres (BMP4-CM). As we found that the presence of BSA and other concentrated proteins in the media disturbed the results, we decided to immunoprecipitate the potential LM in the media for its detection. To do so, we used an antibody recognizing all LM isoforms or an unrelated antibody as a control and assessed the presence of the protein in the immunoprecipitated fraction, enabling a more clear and reliable detection (**Figure 9D**). Remarkably, we could indeed find LM (250 kDa) in both control and BMP4-CM, the latter showing, in addition, higher levels of protein (**Figure 9E**).

These results made us suggest that NSCs, and especially quiescent NSCs, secrete LM and contribute to their own ECM niche in response to the pro-quiescence factor BMP4. In addition, BMP4 can prime for cell interaction with the LM niche, as it increased the expression of LM-binding integrin receptors. However, this data also raised some of the main questions to be addressed in this thesis. In the first place, whether qNSCs differentially interact with its ECM niche *in vivo*, and secondly, by which mechanisms ECM secretion and adhesion may lead to NSC regulation. To elucidate this, we first swapped to *in vivo* analyses to evaluate NSC-ECM interactions and then went back to *in vitro* models to go deeper into the molecular mechanisms of ECM adhesion.

3. qNSC disposition in the SEZ niche

3.1 qNSC display heterogeneous apico-basal positions

Although we and others have developed strategies to identify different NSC populations by FACS using a combination of specific markers (GLAST/CD9/CD24/EGF) and their differences in fluorescence intensity (Belenguer *et al.*, 2021a, b), the histological detection of quiescent NSCs remains controversial. This topic has been in the spotlight for many decades, as the combination of long-chases of traceable nucleoside pulses with the staining for classical NSC markers, such as GFAP/Sox2, has been

shown to be limiting. Hence, very little is known about the disposition of qNSCs in the SEZ and their interaction with other niche elements, including the ECM.

Taking advantage of the fetal specification of adult NSCs and their persistence in a quiescent state from mid-gestation (Fuentelba *et al.*, 2015), we used IUE to specifically target and fluorescently detect qNSCs (**Figure 10**). IUE was performed to deliver episomal plasmids carrying the red or green fluorescent proteins (RFP/GFP) under the control of a β -actin synthetic promoter (CAG::mRFP) into the LV of mouse embryos (section 2.1 in Material and Methods), favoring the incorporation in the cells lining the LV. Through the different rounds of cell division, plasmids will be diluted and lost and only those cells that have remained quiescent since mid-gestation and into adulthood, will still retain the plasmids and will remain fluorescent in the adult brain (Ortiz-Álvarez *et al.*, 2019).

In line with this, IUE at E15.5 resulted two months later in the labeling of differentiated cells, as cortical neurons, derived from NSCs that have exited cell cycle and differentiated early in development (**Figure 10A**).

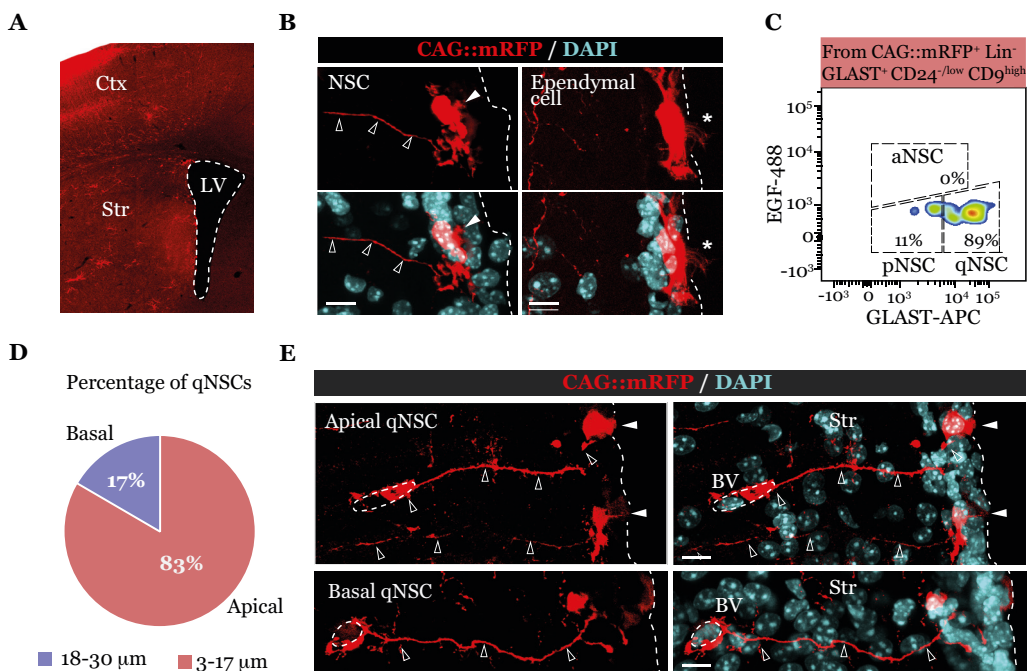


Figure 10. Apico-basal distribution of IUE-labelled qNSC. (A) Direct fluorescence of CAG::mRFP⁺ cells in a 2-month old mouse brain section. (B) Confocal images of NSCs and ependymal cells. White arrowheads indicate NSC primary cilia and empty arrowheads, NSCs basal projections. Ependymal cilia are indicated with an asterisk. (C) FACS plot with the percentages of the different populations from CAG::mRFP⁺ NSCs, distinguished by GLAST and EGF-488. FACS gating strategy is shown in the red header. (D) Pie chart illustrating the percentage of qNSC located

Results

at apical (3-17 μm) or basal (18-30 μm) positions. **(E)** Confocal image showing CAG::mRFP⁺ qNSCs with apical and basal locations, with projections directly terminating in blood vessels. Scale bars: 10 μm . Ctx: cortex; str: striatum; LV: lateral ventricle; BV: blood vessel.

Also, LV-lining ependymal cells, that become postmitotic also during gestation are easily distinguished by their cuboidal shape and their multiple cilia (Ortiz-Álvarez *et al.*, 2019) (**Figure 10B**). In addition, we could detect labeled cells with the distinctively NSC elongated morphology, presenting a unique primary cilium and long basal projections directed towards the striatum (**Figure 10B**).

Using our reported FACS cytometry strategy to characterize the neurogenic lineage (section 2.2 from Material and Methods), we showed that almost 90% of the plasmid-retaining cells corresponded to qNSCs, with a small fraction constituted by pNSCs (**Figure 10C**). As expected, aNSCs, NPCs and neuroblasts did not remain fluorescent, due to episomal plasmid dilution during consecutive divisions. Regarding the positioning of these quiescent (q/p) NSCs in the SEZ, we discovered that 80% of them were found in the first 17 μm from the ventricle (considering the apical side of ependymal cells as a reference), exhibiting ependymal contact with either access to the LV through a primary cilium or not. Another fraction of q/p NSCs with no ependymal nor CSF contact was found at further distances from the LV, ranging from 18 to 30 μm (**Figure 10D,E**), which may correspond to the reported basal NSCs (Baur *et al.*, 2022; Obernier *et al.*, 2018). Our observations suggested that the quiescent NSC population is heterogeneous regarding its apico-basal positioning, which makes cells susceptible to receiving diverse signals from the surrounding matrix of both domains.

3.2 qNSCs closely interact with LM-enriched BM structures

Although some groups have studied the positioning of neurogenic cells in relation to vascular or speckled BMs (Nascimento *et al.*, 2018; Sato *et al.*, 2019; Shen *et al.*, 2008; Tavazoie *et al.*, 2008), they used general GFAP immunostainings that do not consider NSC heterogeneity. In view of the potential role of qNSCs in ECM deposition, we decided to assess qNSC interaction with these ECM structures *in vivo*.

BMs are mainly composed of different LM isoforms, together with type IV and type VI collagens, and some PGs and GPs (Sato *et al.*, 2019). Hence, LM immunostainings allowed us to visualize vascular and speckled BM structures in the SEZ (**Figure 11A**). Speckles were mostly positioned in the apical side and displayed both rounded and tubular structures. Instead, the basal side was occupied by LM⁺ BVs running in parallel to the SEZ, with some LM⁺ speckles located alongside vasculature (**Figure 11A**).

To evaluate whether this high expression of LM in BVs was specific to this neurogenic niche, we analyzed LM intensity in CD31⁺ cells by FACS, showing that SEZ BVs are especially enriched in LM compared to cortical BVs, in line with its role in this germinal region (**Figure 11B**). Further, our immunostainings showed that quiescent NSCs were interestingly located alongside BVs, directly leaning on them or creating pocket-like structures that surrounded vasculature in both apical and basal sides (**Figure 11C**).

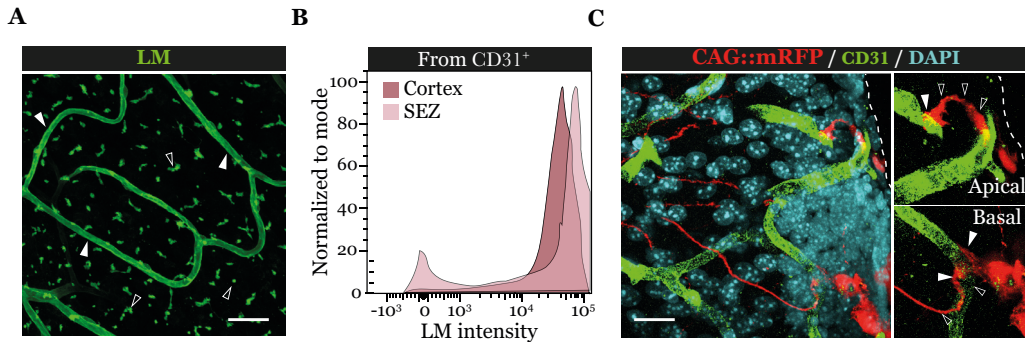


Figure 11. qNSC contact LM⁺ BVs. (A) IHC of LM in a SEZ wholemount preparation. White arrowheads indicate vascular BM and empty arrowheads, speckled BM. Scale bar: 20 μ m. (B) FACS histogram showing LM intensity in endothelial cells (CD31⁺) obtained from the cortex and the SEZ. (C) IHC of CD31 to stain BVs in sections with IUE-stained quiescent NSC (CAG::mRFP⁺). Empty arrowheads point end-feet projections in apical and basal NSCs. White arrowheads indicate sites of qNSC-BV contacts. Scale bar: 10 μ m. LM: laminin.

To study contacts with speckles finely, we decided, on the one hand, to clarify wholemount preparations (section 3.2 in Material and Methods) to obtain higher imaging depth to study both apical and basal interactions and, on the other, to use expansion microscopy (Asano *et al.*, 2018) (section 3.3 in Material and Methods). This latter technique accomplishes 3-dimensional expansion by 4.5-fold, which enables nanoscale-resolution imaging. Fluorescence images from both clarified (**Figure 12A**) and expanded wholemount preparations (**Figure 12B**) showed that quiescent NSCs closely interact with multiple speckles both through their cell bodies and projections, in a way that speckles resembled a scaffold to which q/p NSC anchored.

In parallel, to analyze these contacts at the ultrastructural level, we stained the specific fluorescent proteins coded by the IUE-injected episomal plasmids with an antibody conjugated to gold particles, that enabled its visualization by TEM (section 3.4 in Material and Methods). These analyses confirmed the direct interaction already suggested by the confocal images. We could detect qNSCs directly contacting speckles, that were easily distinguishable due to their electron-dense fractal structures (**Figure 12C**).

Results

Although fractones were mostly localized in the apical side, beneath endymal cells, some of them were also found at further distances from the endymal layer, in line with the positioning of the quiescent pool (**Figure 12D**). In addition to speckle binding, direct interaction with BV BM was also confirmed by TEM (**Figure 12D**).

This made us conclude that quiescent NSCs are closely associated with BM structures *in vivo*, albeit raising the question on whether this interaction is specific to this cell state and a differential interaction with the ECM niche occurs between q/pNSCs and aNSCs.

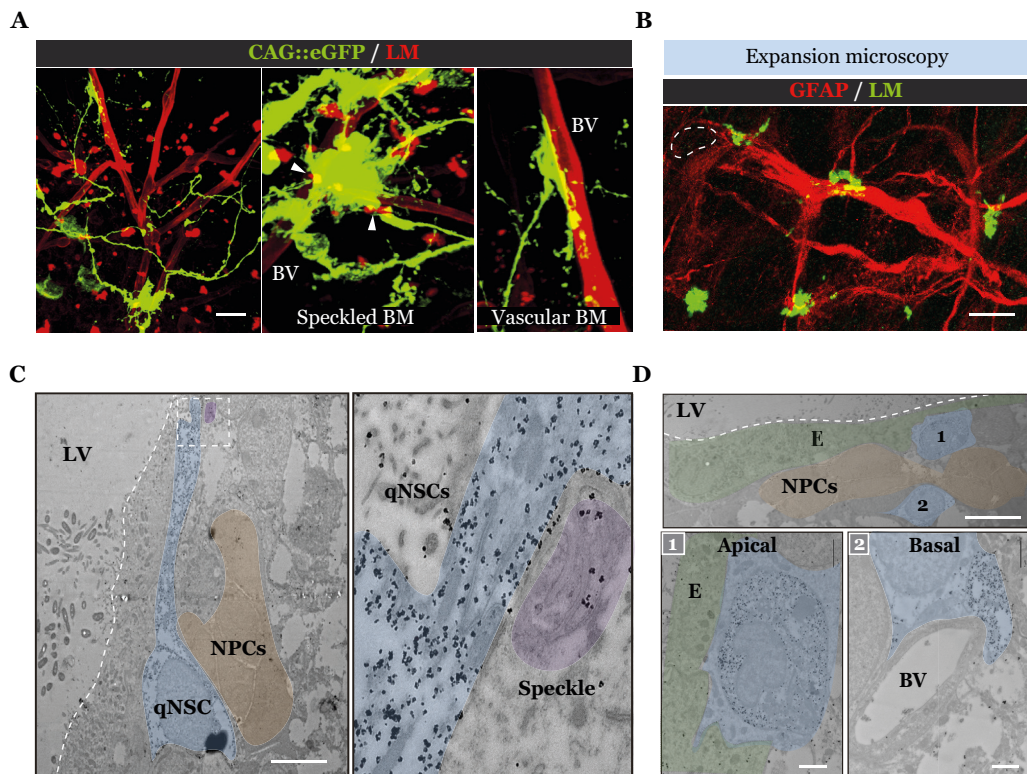


Figure 12. qNSC interaction with vascular and speckled BM. (A) IHC of LM (red) in clarified SEZ wholemount preparations with qNSCs labelled as CAG::eGFP⁺ cells. White arrowheads point qNSC contacts with speckles. Scale bar: 20 μ m (B) IHC of GFAP (red) and LM (green) in expanded SEZ wholemount preparations. Dotted line limits cell nucleus. Scale bar: 20 μ m (C) TEM images showing a coronal view of the SEZ with a qNSC (blue) stained with gold-conjugated α GFP antibody contacting a speckle (purple). NPCs are highlighted in orange. Right side panel shows a zoomed view of the dotted box. Scale bar: 4 μ m (D) TEM images of the SEZ, with endyma (E) shown in green, and an apical and basal qNSC (1 and 2, respectively) highlighted in blue. Scale bar: 4 μ m. Zoomed views of qNSCs are shown in the lower panels, with image 2 illustrating a qNSC directly contacting vascular BM. Scale bars: 1 μ m. BM: basement membrane; BV: blood vessel; LV: lateal ventricle; E: endymal cell.

4. Quiescent NSC are preferentially adhered to LM⁺ BMs

4.1 *In vivo* quiescent NSCs are differentially surrounded by LM

To study the potential differential adhesion of NSCs with specific states of activation to BMs, we decided to use our reported strategy to identify NSC populations (Belenguer *et al.*, 2021b) and combine it with LM stainings by FACS. We expected that, if NSCs expressed and potentially secreted ECM molecules, as suggested by our BMP4 *in vitro* observations and our proteomic analysis, we might be able to detect this protein extracellularly surrounding the cells. In this context, we found that not only we could detect LM on the surface of NSCs, but also we identified differences in LM intensity among the populations (**Figure 13A**). In line with our hypothesis, we observed that qNSCs were especially enriched in LM, followed by pNSCs and aNSCs that had intermediate and low levels, respectively (**Figure 13A**). When analyzing LM by IHC, we realized that among mRFP⁺ quiescent NSCs, we could identify cells with higher intensities (LM^{high}, red arrowhead), and others with lower LM levels (LM^{low}, pink arrowheads). It is tempting to speculate, that coherently with our FACS data, this populations could correspond to qNSCs and pNSCs, respectively. Instead, cells that had mostly diluted the plasmid (mRFP^{low}), potentially aNSCs, did not display any LM staining (grey arrowhead) (**Figure 13B**).

These significant differences between quiescent NSCs and more active states suggested that a differential interaction with the local ECM niche may have a biological significance regarding the maintenance of the quiescent phenotype.

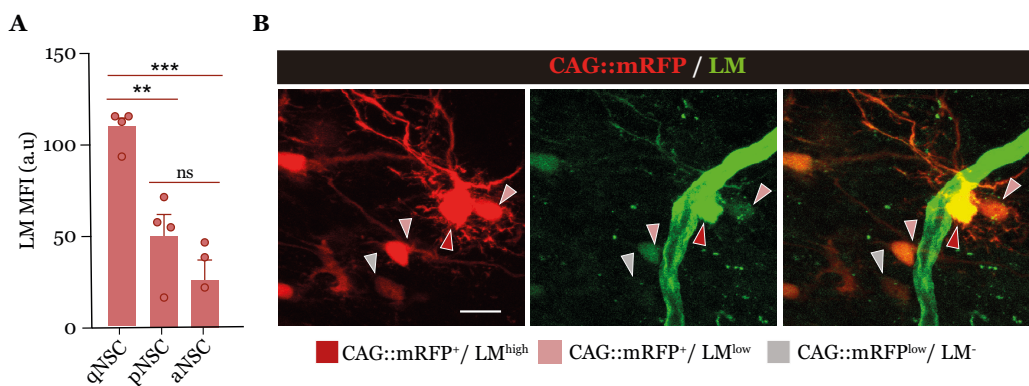


Figure 13. qNSCs display higher levels of LM. (A) LM MFI intensity in q/p/a NSC populations analyzed by FACS. (B) IHC of LM (green) in SEZ wholemount preparations from adult mice, with quiescent NSCs identified as IUE CAG::mRFP-retaining cells. Red and pink arrowheads indicate CAG::mRFP⁺ NSCs displaying, respectively, high and low LM levels. Grey arrowhead points to a CAG::mRFP^{low} cell with no LM staining. Scale bar: 10µm. LM: laminin; MFI: median fluorescence intensity.

Results

4.2 qNSCs are differentially co-isolated with BVs

To specifically assess the differential adhesion to BV BMs, we hypothesized that, if cells were indeed adhered to vasculature, the isolation of microvessels after gentle dissociation of the tissue may be able to co-isolate other cells firmly attached. To test this, cerebral cortices and SEZs (n=5 each) were gently dissociated with diluted papain, and cells were incubated with EC-specific CD31 antibodies conjugated to magnetic beads, using a Ca^{2+} and Mg^{2+} chelator-free buffer to favor cell adhesion. Then, samples were passed through magnetic columns and the retained CD31⁺ fractions were eluted to either analyze them by FACS or to seed them over fibronectin-coated culture plates in EC medium (**Figure 14A**) (5.1 in Material and Methods).

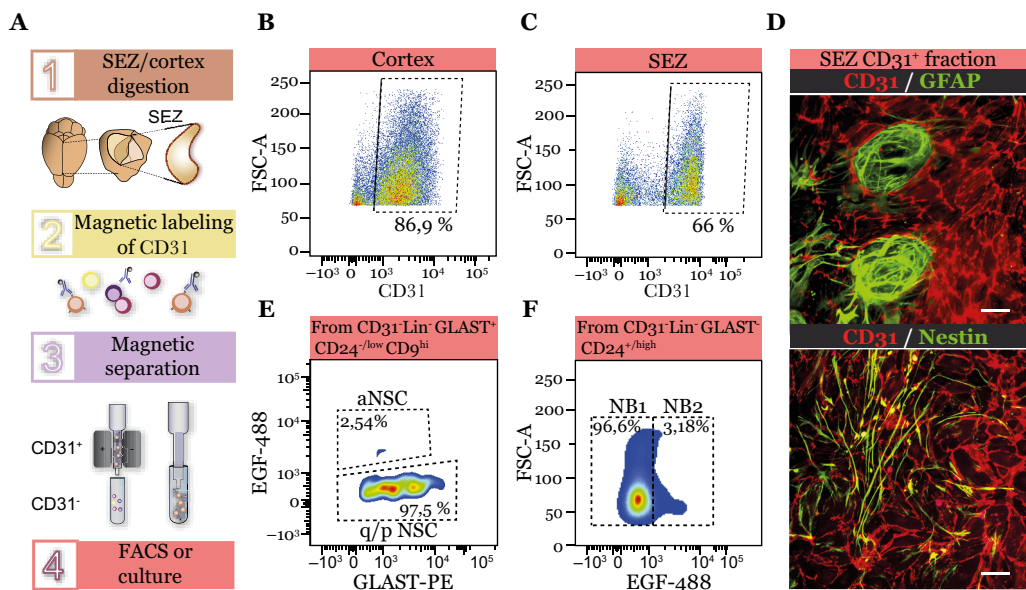


Figure 14. qNSCs are co-isolated with ECs. (A) Schematic diagram of the isolation strategy. (B) FACS dot plot showing the percentage of CD31⁺ cells after EC magnetic isolation from the cortex. (C) CD31⁺ population after isolation from the SEZ. (D) ICC of CD31 (red) combined with GFAP or Nestin (green) in SEZ CD31⁺ fraction after 5DIV. (E) Percentage of co-isolated quiescent (q/p) and aNSCs from the CD31⁺ fraction. The gating strategy used is indicated in the header. (F) NB1 and NB2 percentages in the CD31⁺ eluted fraction. Scale bars: 50 μm .

FACS analysis of the eluates revealed that isolation of cortical ECs was highly homogeneous, containing over 90% of CD31⁺ cells (**Figure 14B**). When cultured, ECs formed monolayers, with some co-isolated pericytes overlaying them (not shown). In contrast, SEZ eluates contained only around 66% of CD31⁺ cells (**Figure 14C**) that, instead of forming monolayers, exhibited a more irregular disposition in culture. We could

find, apart from pericytes, some GFAP⁺ and Nestin⁺ cells overlaying ECs and forming nest-shaped structures (**Figure 14D**).

This proposed that EC isolation also pulled down cells from the astrocytic and neural lineage, suggesting a differential adhesion of these cells to BVs compared to the cortex. To identify the cells that were being co-isolated, we analyzed the eluates by FACS, in this case favoring single-cell suspensions by further disaggregation and incubation with the aforementioned panel of antibodies (**Graphical Method 2**) using an EDTA-containing buffer. Our analysis revealed that among the isolated CD31⁺ fraction, there was a group of cells that were CD31⁻ and expressed markers that identified them as NSCs (Lin⁻ GLAST⁺ CD24^{-/low} CD9^{hi}). More interestingly, among the co-isolated NSCs, we found that most of them were in a quiescent state (Lin⁻ GLAST⁺ CD24^{-/low} CD9^{hi} EGFR^{-/low}), suggesting a differential vascular binding of the quiescent NSC populations compared to the activated NSC pool (**Figure 14E**). A fraction of NB2 (Lin⁻ GLAST⁺ CD24⁺ EGFR^{low}) were also co-isolated with ECs (**Figure 14F**), in line with reports showing that BVs act as scaffolds for late NB migration (Whitman *et al.*, 2009). It is worth noting that the complexity of the strategy renders a considerable degree of variability. However, qNSC co-isolation was consistently reproduced with different pools of animals (n=3 experiments with a pool of n=4-5 animals per experiment).

To go further into the mechanism of NSC-vascular adhesion *in vivo*, we decided to check whether q/pNSCs-BV co-isolation was dependent on the interaction with vascular BM. As integrin $\alpha 6$ has been described to be essential for NSC-BV adhesion and was found significantly increased in our proteomic analysis after BMP4 quiescence induction, we decided to evaluate its role in q/pNSC-BV binding *in vivo* by using our co-isolation strategy. We hypothesized that, if adhesion was mediated through this receptor, blocking the protein prior to EC isolation, would cause cell detachment and avoid the pull down of quiescent NSCs. To test this, we obtained SEZ dissociates and first incubated them for 30 min with an integrin $\alpha 6$ blocking antibody (GoH3) or with an isotype-matching control, followed by the incubation with magnetically coupled CD31 antibody. Finally, we eluted CD31⁺ and CD31⁻ fractions and analyzed them by FACS (**Figure 15**). The retained CD31⁺ fraction clearly differed between the treatments: while the control condition recovered a considerable number of cells, mainly quiescent NSCs, pre-treating with GoH3 blocking resulted in the pull-down of a reduced number of cells, suggesting that they had unbound during the treatment (**Figure 15A**). Instead, CD31⁻ fraction showed normal NSC percentages for both conditions, suggesting that the treatment had not affected the populations *per se* (**Figure 15B**). Overall, our data provides, for the first time, direct evidence of a differential BV binding between different states of activation, largely by LM-integrin interactions.

Results

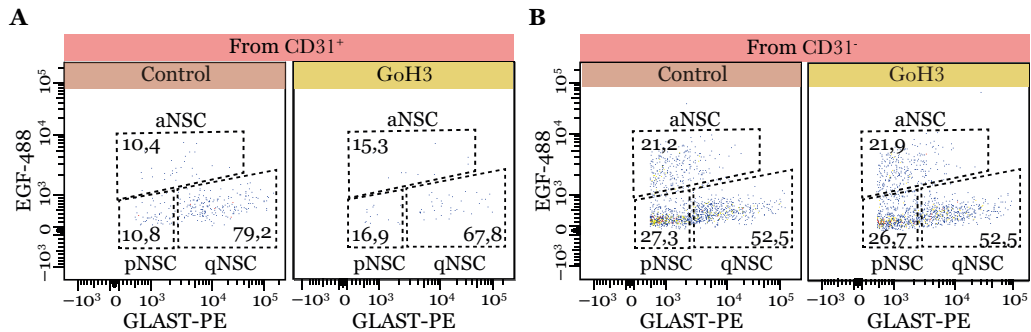


Figure 15. qNSC-EC binding is mediated by integrin $\alpha 6$. (A) Percentage of qNSCs, pNSCs and aNSCs evaluated by FACS in CD31⁺ fraction after treating with GoH3 or an unrelated antibody (control). (B) Same for the CD31⁻ fraction, which represents unrestrained NSCs.

5. Vascular regulation of NSCs

5.1 Direct co-culture with ECs induces NSC quiescence

Considering quiescent NSC-LM interaction *in vivo*, we decided to go deeper into its role in regulating NSC behavior. To do so, we took advantage of *in vitro* neurosphere cultures to test the effect of ECM-mediated adhesion, testing independently, in the first place, the role of vasculature and then, the potential role of NSC-derived ECM.

Different reports have shown antagonistic effects of vascular-derived signals (soluble and mediated by cell-cell or cell-ECM adhesion), some of which promote quiescence and others proliferation (Karakatsani *et al.*, 2019). To enable both soluble and adhesion-mediated signals simultaneously, we used a direct co-culture system in which NSCs were seeded over EC monolayers in NSC growth media for 4 DIV. After this time, we evaluated by FACS both NSC proliferation (using DFFDA dilution) and GLAST and EGFR protein levels, as they allow us to distinguish aNSCs (GLAST^{low}/EGFR^{high}) from qNSCs (GLAST^{high}/EGFR^{low}) *in vivo* (**Graphical method 5**). For handling ease, we mostly used HUVEC cells, and we further confirmed the results by using freshly isolated primary cortical ECs from adult mice. To evaluate proliferation changes, we loaded single neurosphere cells with DFFDA tracer in NSC growth media in non-adherent conditions, in which single NSCs will divide clonally to give rise to neurospheres, or in adherent conditions, both over commercial Matrigel™, used as a control of adhered cells, and over EC monolayers (**Figure 16A**). When seeding NSCs over ECs, NSCs adhered with a bipolar elongated morphology that differed from the morphology acquired when using Matrigel™ as a coating. Interestingly, NSCs in co-culture adhered over ECs and organized inside EC tubular structures enabling multiple contacts through their projections, suggesting a complex interaction also *in vitro* (**Figure 16A**).

To confirm that NSCs were not differentiating, we detached them after 4DIV and seeded them in fresh growth media to evaluate their ability to form neurospheres. We found that after co-culture, cells could still form neurospheres that, in addition, could be passaged normally (**Figure 16B**). Besides this, our FACS analyses after 4DIV showed that co-culturing with ECs promoted a switch to a non-proliferative, quiescent-like NSC phenotype *in vitro* (**Figure 16 C-F**).

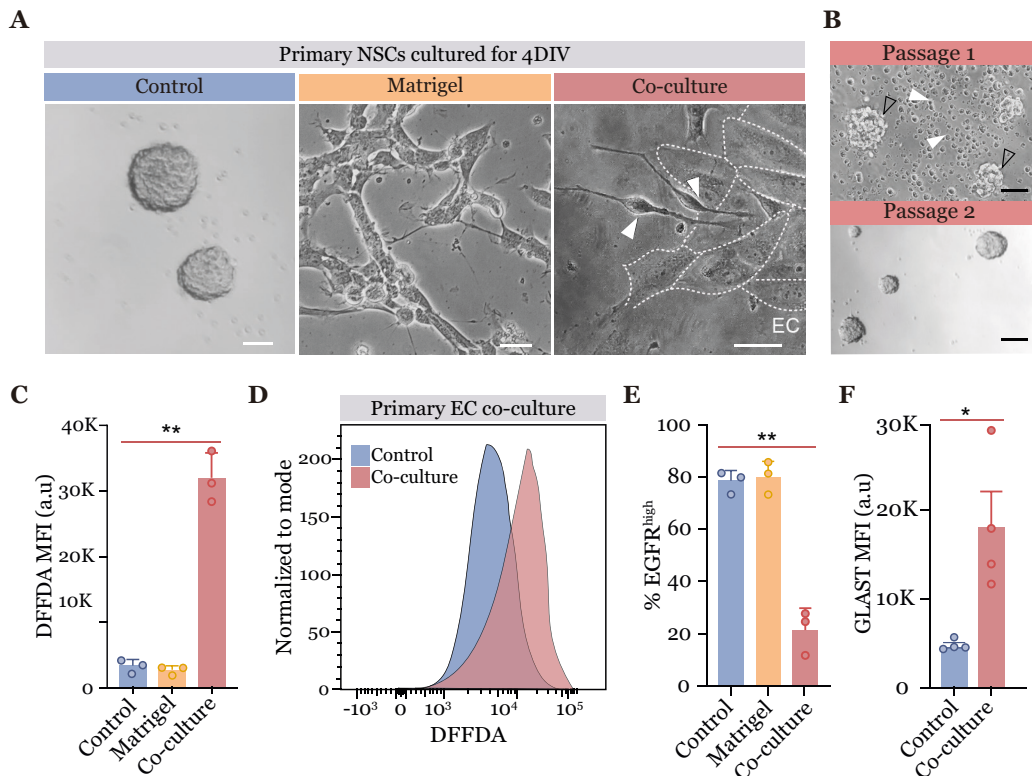


Figure 16. Direct EC co-culture induces NSC quiescence. (A) Phase contrast images showing NSC cultured in suspension (control), over MatrigelTM or over HUVECs for 4DIV. Dotted lines limit endothelial cells and white arrowheads point NSCs in co-culture. Scale bars: 50 μ m. (B) Phase contrast images of first and second NSCs passages after being co-cultured for 4DIV. White arrowheads point EC debris and empty arrowheads, neurospheres. Scale bars: 100 μ m (C) DFFDA MFI after 4DIV in the different conditions tested. (D) FACS histogram showing DFFDA intensity after co-culture with primary brain ECs for 4DIV. (E) Percentage of EGFR^{high} cells measured with fluorescently-labeled EGF-647 ligand. (F) GLAST MFI in co-culture compared to control. ECs: endothelial cells; MFI: median fluorescence intensity.

Indeed, while cells cultured over MatrigelTM clearly resembled NSC grown in suspension (control), direct contact with ECs resulted in a drastic reduction in DFFDA dilution rates, both when culturing with HUVEC cells (**Figure 16C**) and with primary

Results

mouse brain ECs (**Figure 16D**). Further, we also found a significant reduction in EGFR levels (**Figure 16E**) and an increased GLAST fluorescence intensity (**Figure 16F**) in co-culture compared to the control condition. These data suggested that ECs have an active role in regulating NSC quiescence, which may explain the observed enhanced qNSC-vascular interactions *in vivo*.

5.2 LM-integrin interactions are enhanced in co-culture

Considering our data showing integrin $\alpha 6$ -dependent interactions *in vivo*, we decided to test whether its expression was enhanced in NSCs as part of the EC-mediated quiescence induction process. We observed that direct co-culture with ECs for 4DIV increased integrin $\alpha 6$ (ITGA6) protein levels, compared to NSCs cultured over Matrigel™ or in suspension (**Figure 17A**). Strikingly, a significant increase was already observed when comparing adherent NSCs cultured over Matrigel™ with non-adherent cultures. This suggested that ITGA6 was being induced in NSCs through ECM binding, favoring a positive feed-back loop in which ECM interactions are enhanced. Interestingly, although both fast-cycling (DFFDA^{low}) and slow-cycling (DFFDA^{high}) cells in co-culture display integrin $\alpha 6$, a higher percentage of ITGA6⁺ cells was found among the DFFDA^{high} population (**Figure 17B**). This was coherent with our data showing *Itga6* upregulation in qNSC and its enhancement, at the protein level, after BMP4-induced quiescence. In order to check whether these interactions could be important for EC-mediated quiescence, we incubated single neurosphere cells with integrin $\alpha 6$ -blocking GoH3 prior to their seeding in co-culture. We found that this pre-treatment favored, after 4 DIV, an increase in NSC proliferation as shown by the decrease in the percentage of DFFDA^{high} cells (**Figure 17C**). These results suggested that LM-integrin $\alpha 6$ interactions are involved not only in quiescent NSC adhesion to vasculature *in vivo*, but also in mediating cell arrest in neurospheres.

Our previous experiments associated LM expression changes to quiescence induction, both among the different populations *in vivo* and after *in vitro* treatment with BMP4. As we had observed that co-culture induces quiescence, we decided to assess LM expression in this scenario. To do so, we cultured DFFDA-loaded neurosphere cells over HUVECs for 4 DIV and immunostained for LM. Culturing over Matrigel™, in which cells proliferate at the same extent as in suspension (shown in **Figure 16**), rendered a faint LM staining that displayed a dotted pattern in the cytoplasm of the cells. Nevertheless, EC co-culture increased LM intensity in NSCs, observed both in the cytoplasm and in cell projections at the interface with ECs (**Figure 17D**). We confirmed this result by FACS, showing that NSC (DFFDA⁺ GLAST⁺) displayed higher LM MFI after co-culture (**Figure 17E**).

Again, these results suggested that it is not adhesion *per se* that promoted LM protein deposition, but rather, it was specific to the quiescence-induction process after co-culture.

Taking advantage of the fact that HUVEC cells are of human origin, we decided to further assess the expression of different LM isoforms by qPCR using mouse-specific Taqman probes to target NSCs. Although we found highly variable samples, we observed a tendency to an upregulation of all LM genes tested in co-culture, together with a slight downregulation of *Lama5* (Figure 17F), and an increase in *Itga6* (not shown). This expression changes interestingly mimicked the gene expression changes observed after BMP4 treatment (see Figure 9), which made us wonder whether BMP4 could be secreted in co-culture.

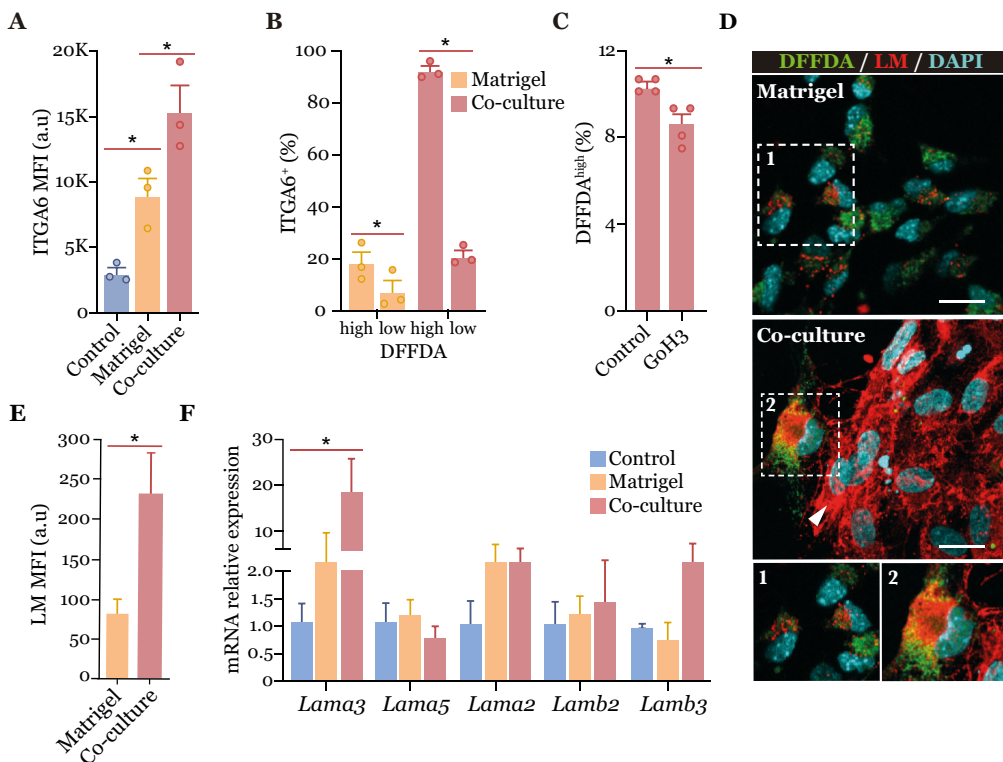


Figure 17. ITGA6-LM interactions in co-culture (A) ITGA6 MFI after 4DIV in the different culture conditions tested. (B) Percentage of ITGA⁺ cells in DFFDA^{high} and DFFDA^{low} cells over MatrigelTM or in co-culture. (C) Percentage of DFFDA^{high} population in cells pre-treated or not with ITGA6 blocking antibody (GoH3). (D) ICC of LM (red) in DFFDA-loaded NSCs (green) over MatrigelTM or in EC co-culture. White arrowhead point ECs. Bottom panels show zoomed views of the dotted regions. Scale bars: 10 μ m. (E) FACS analysis of LM MFI in NSCs after 4DIV in the culture conditions tested. (F) LM gene expression after 4DIV over MatrigelTM or in co-culture, relative to control (neurospheres).

Results

5.3 BMP4 participates in co-culture induced quiescence

Recent single-cell RNA-seq performed in the adult SEZ (Cebrian-Silla *et al.*, 2021), revealed that ECs and oligodendrocyte progenitors are the only SEZ cells expressing BMP4, supporting the idea of ECs acting as a source for this morphogen. To test this, we seeded DFFDA-loaded neurosphere cells in co-culture with HUVECs with or without BMP4 antagonist Noggin, a high-affinity BMP4 binding protein that antagonizes its bioactivity. We showed that in the presence of Noggin, NSCs proliferated at a higher extent, showing lower DFFDA retention (**Figure 18A**) together with reduced levels of GLAST (**Figure 18B**) and increased membrane EGFR (**Figure 18C**). This suggested that, as hypothesized, BMP4 was present in co-culture and that was, at least in part, responsible for the acquisition of the quiescent-like phenotype observed. In line with our data showing that BMP4 induces LM secretion, adding Noggin to co-cultures clearly reduced LM protein levels in NSCs (**Figure 18D**), suggesting that NSC LM deposition in co-culture is dependent on BMP4.

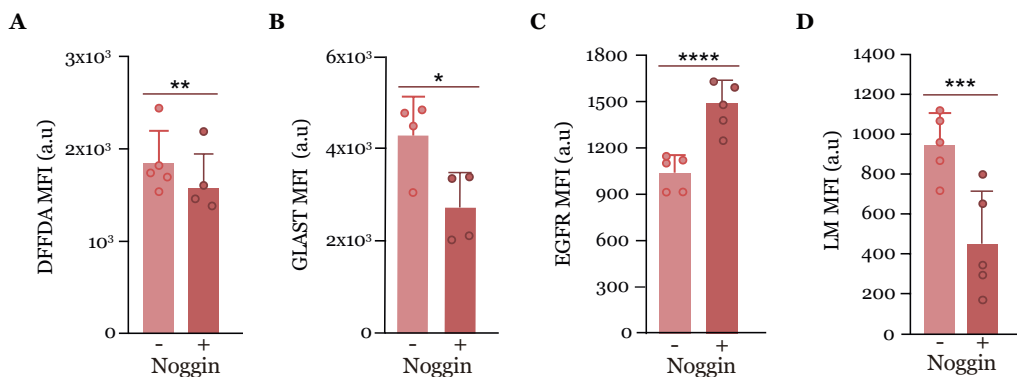


Figure 18. Noggin reverts co-culture induced quiescence and LM deposition. (A) DFFDA MFI in NSCs after co-culture with HUVECs in the presence of BMP4-antagonist Noggin for 4DIV. (B) GLAST MFI in the conditions tested. (C) EGFR levels measured by EGF-647 ligand intensity. (D) LM MFI from DFFDA⁺ GLAST⁺ NSCs.

6. Study of the role of NSC self-assembled ECM

6.1 BMP4-CM matrix favors a reversible cell cycle arrest

In order to distinguish between direct BMP4-induced quiescence and the effect of NSC-derived ECM secreted in response to BMP4, we decided to test the potential use of BMP4-CM as a coating. We hypothesized that NSC-derived ECM components might self-assemble and deposit in the bottom of cell culture wells, which could account for the observed BMP4-induced NSC adhesion.

To assess this idea, we treated neurosphere cultures with BMP4 or its vehicle and

allowed cells to grow and condition the media for 4 DIV. Then, we collected the CM, added Noggin to block the potential remaining BMP4, and used it to coat wells in cell culture plates overnight. The following day, coatings were removed and wells washed. Then, single neurosphere cells were seeded over the potential matrices and analyzed after 4 DIV (**Graphical Method 4**). We observed that, while NSCs cultured over control-CM matrix formed neurospheres, BMP4-CM matrix favored cell spreading (**Figure 19A**). Besides, NSCs adhesion was not dependent on BMP4, as similar morphologies were obtained with or without the addition of Noggin (**Figure 19A**). Interestingly, we found that adhesion over BMP4-CM matrix affected NSC proliferation also independently of BMP4: cells displayed higher DFFDA retention (**Figure 19B**) and reduced EdU incorporation (**Figure 19C**) over

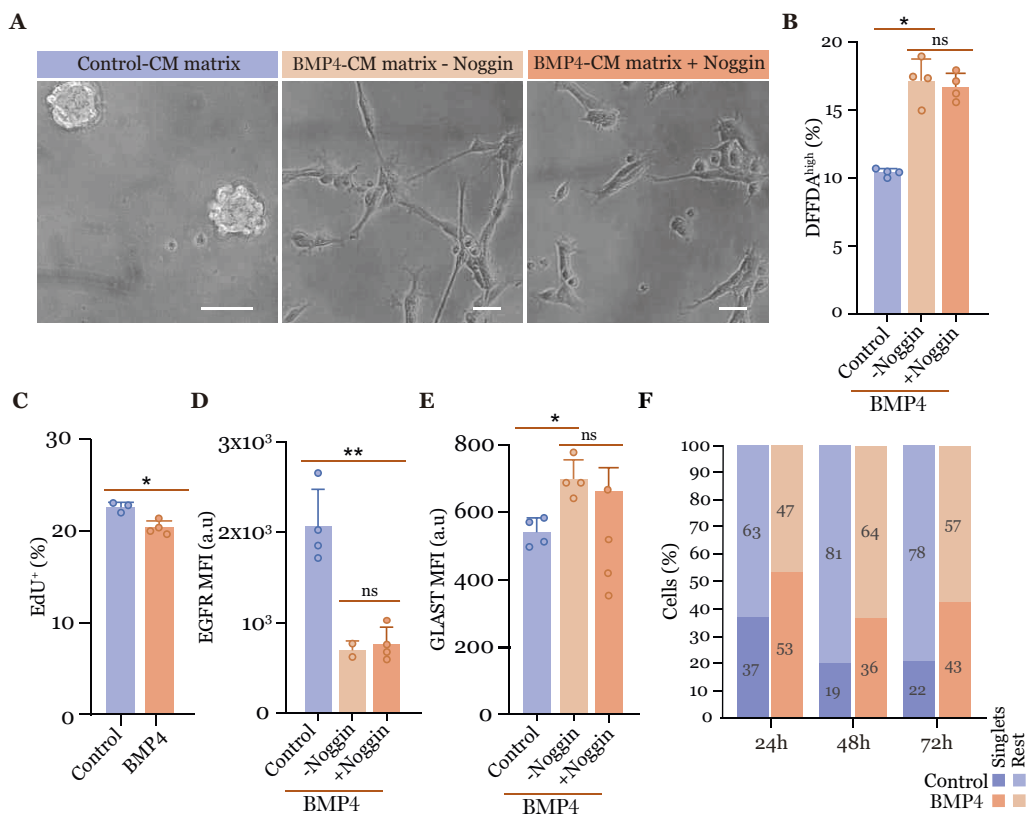


Figure 19. Culturing over BMP4-CM matrix favors NSC adhesion and quiescence. (A) Phase contrast images of NSC after 4DIV cultured over control-CM matrix (Scale bar: 100 μ m) or BMP4-CM matrix, with or without BMP4 antagonist Noggin (Scale bars: 10 μ m) (B) Percentage of DFFDA^{high} cells analyzed by FACS after 4DIV over the different matrices. (C) Percentage of EdU⁺ cells (1h pulse) after 4DIV. (D) EGFR MFI measured with EGF-647 ligand. (E) GLAST MFI in the conditions tested. (F) Sorted aNSCs cultured over the matrices. Bar graph shows the percentage of cells that remain as singlets in each condition (darker orange or blue) or that have divided at least one time (light orange or blue) after 24, 48 and 72h.

Results

BMP4-CM coatings. In addition, cells showed reduced EGFR levels (**Figure 19D**) and increased GLAST (**Figure 19E**), suggesting the acquisition of a quiescent-like phenotype.

To explore the effect of adhesion within a more homogeneous population closer to the *in vivo* state, we decided to sort aNSCs (n=300 cells) directly from the SEZ and seed them over control or BMP4-CM matrices to evaluate their cycling dynamics over 72h (**Figure 19F**). Although cells did proliferate when cultured over both matrices, 24h after the seeding we could already detect differences in cell division. Indeed, we found a higher percentage of cells remaining as singlets (53%) when cultured over BMP4-CM matrices, compared to control-CM matrices (37%). Although some of these cells started dividing after 48h, the cycling differences were maintained: we found that 36% of the cells were still singlets in BMP4-CM matrix with only a 19% found in the control. Finally, 72h after the seeding, the percentages remained unchanged and neurospheres only grew in diameter, indicating that new divisions were restricted to the first 48h.

To further characterize the effect, we cultured NSCs for 4 DIV over the matrices and then detached them with Accutase® solution to, on the one hand, perform cell cycle analysis at this time point and, on the other, seed them in suspension at a very low density to evaluate their ability to form neurospheres (**Figure 20A**).

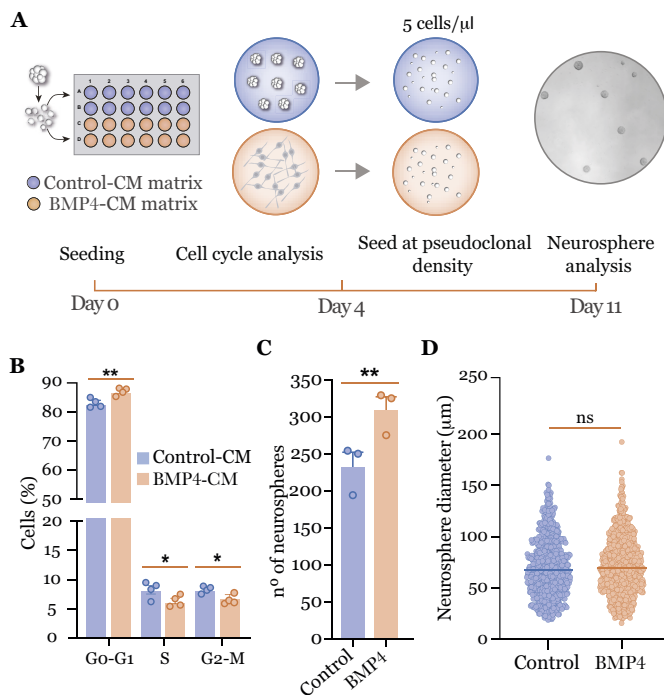


Figure 20. BMP4-CM matrix causes a reversible NSC cell cycle arrest. (A) Schematic representation of the experimental setup. NSCs are cultured over control or BMP4-CM matrices for 4 DIV and detached for 1) cell cycle analysis and 2) seeding single cells at low densities to perform a neurosphere formation assay. (B) Percentage of cells in the different cell cycle phases evaluated with DAPI after 4 DIV over control or BMP4-CM matrices. (C) Number of neurospheres formed after 7 DIV by cells that had been previously cultured over control-CM or BMP4-CM. (D) Diameter (µm) quantification of neurospheres after 7 DIV.

Cell cycle profile revealed a small increase in the percentage of cells in G0-G1 phase with a reduction in S and G2-M in cells cultured over BMP4-CM matrix compared to the control-CM matrix (**Figure 20B**), showing a partial cell cycle arrest. Regarding the neurosphere formation assay, cells were allowed to grow for another 5 DIV, when the number of neurospheres were counted and their diameters assessed. Our results showed that cells that had been adhered over BMP4-CM matrices could efficiently form normal neurospheres, suggesting that they remained undifferentiated. Besides, cells cultured in this condition could, in addition, form more neurospheres than the ones cultured over control-CM, suggesting that they have increased their ability to self-renew (**Figure 20C**), with unchanged neurosphere diameters (**Figure 20D**). All in all, our data showed that the response to NSC-derived ECM, named from now on as NSC self-assembled ECM, signals the cells in a way that prompts them to remain quiescent, changing the levels of qNSC-associated markers while slightly reducing proliferation in a reversible manner.

6.2 Integrin $\alpha 6$ conditions quiescence over self-assembled ECM

Following our results showing that quiescence-induction mediated by EC co-culture was dependent on integrin $\alpha 6$, we wondered whether this receptor could also participate in the interaction with NSC self-assembled matrix. To test this, we pre-treated DFFDA-loaded single-cell suspensions with blocking antibody GoH3 and seeded the cells in growth media over BMP4 or control-CM matrices. We observed that cells efficiently adhered over BMP4-CM matrix independently of the treatment (**Figure 21A**), which suggested that other receptors may be responsible for cell adhesion over self-assembled ECM. However, to test whether integrin $\alpha 6$ disturbance was affecting proliferation, we pre-treated NSCs with GoH3 and allowed DFFDA-loaded NSCs to grow for 4 DIV. Integrin disturbance favored, surprisingly, an increase in the percentage of DFFDA^{high} cells, suggesting a reduction in proliferation (**Figure 21B**).

Integrin $\alpha 6$ subunit can form heterodimers with both $\beta 1$ and $\beta 4$ to function as LM binding receptors (Takada *et al.*, 2007). As our transcriptome datasets showed that NSCs only expressed $\beta 1$ and not $\beta 4$ (not shown) (Belenguer *et al.*, 2021a, b), we decided to test if we could reproduce the proliferation effect observed by blocking $\beta 1$ subunit (CD29, Bioscience). Thus, we pre-treated with $\beta 1$ blocking antibody and with an unrelated antibody (control) and then cultured over control or BMP4 CM matrix for 4 DIV. After this time, we performed a 1h EdU pulse and observed a reduced incorporation of EdU in pre-treated cells compared to controls, which was coherent with the results obtained when blocking integrin $\alpha 6$ (**Figure 21C**).

Results

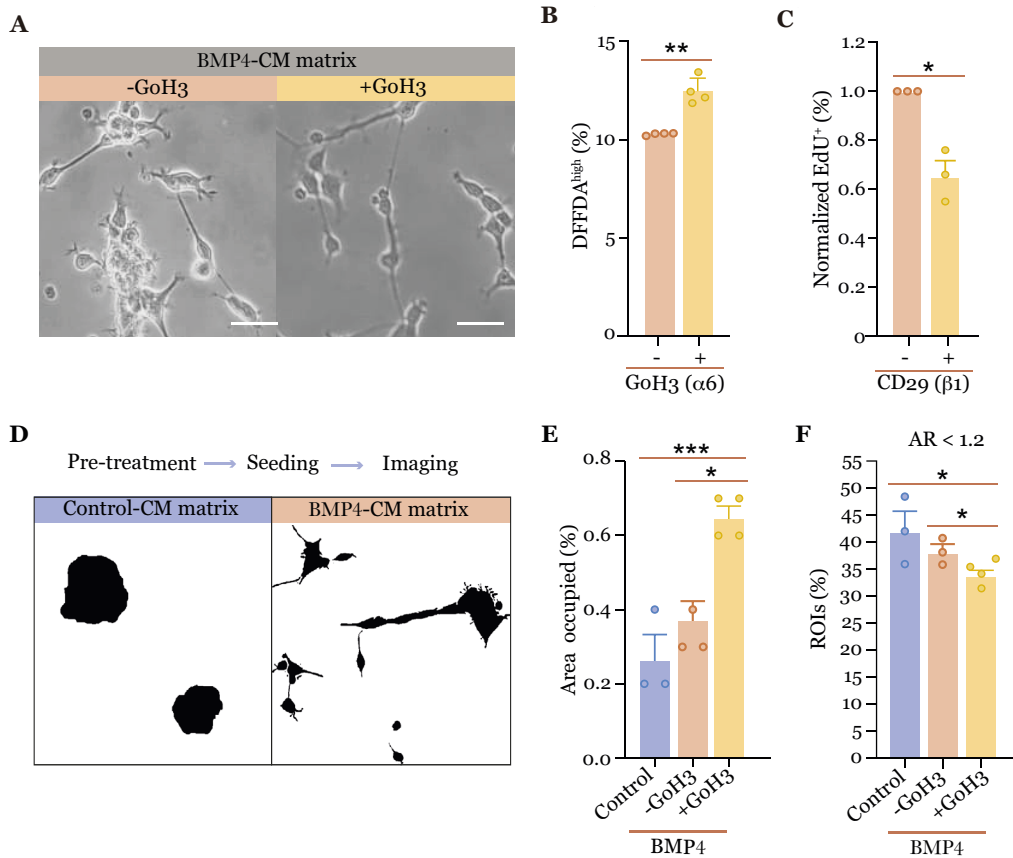


Figure 21. Integrin $\alpha 6$ conditions NSC proliferation and spreading over self-assembled matrix. (A) NSC cultured over BMP4-CM matrix after pre-treatment with integrin $\alpha 6$ blocking antibody (GoH3) or an unrelated antibody (control). Scale bars: 20 μ m. (B) DFFDA^{high} population after 4DIV over BMP4-CM matrix in NSC pre-treated with GoH3 or an unrelated antibody used as a control. (C) EdU⁺ population (percentages normalized to control) in NSCs pre-treated with integrin $\beta 1$ blocking antibody (CD29) after 4DIV cultured over BMP4-CM matrix. (D) Binarized images obtained with Fiji for the analysis of morphological parameters of NSCs cultured over both matrices. (E) Percentage of area occupied after 4DIV over control or BMP4-CM matrix in NSCs pre-treated with GoH3 or an unrelated antibody (control). (F) Percentage of registered objects of interest (ROIs) with an aspect ratio (AR) < 1.2 in the culture conditions tested.

This unexpected effect in proliferation in response to a punctual disturbance of integrin binding, made us hypothesize that subtle changes in cell morphology, spreading and interaction with the matrix could be mediating the observed effects. To go deeper into this idea, we pre-treated with GoH3 and cultured NSCs over CM-matrices and performed live-imaging of the cells after 4DIV. With this images, we deployed a custom fully automated image analysis workflow that could segment the regions-of-interest (ROIs), either neurospheres or individual/grouped spread cells (**Figure 21D**), and calculate

parameters related to their size and morphology (section 8 in Material and Methods). As an approximation for the evaluation of cell spreading, we measured the *Aspect ratio* (AR), which is the proportion of the maximum object width and height, and the *Area fraction*, the percentage of image area occupied by ROIs. Regarding the *Area fraction*, culturing over BMP4-CM matrix favored cell spreading, causing an increase in the percentage of area occupied compared to control-CM matrix (**Figure 21E**). While a small increase was observed in cells treated with an unrelated antibody (-GoH3) compared to control-CM, disturbing integrin $\alpha 6$ binding with GoH3 enhanced the response, showing a significant increase in the area occupied, suggesting higher spreading in this condition (**Figure 21E**). However, changes in *Area fraction* could be highly influenced by the number of cells in the well, therefore biased by different proliferation rates between experimental conditions. To circumvent this problem, we turned to AR which is only dependent on object shape. Using this metric, we showed that cells cultured over control-CM matrix, which grow as neurospheres, rendered AR values approaching 1 due to their roughly circular shape, while spread cells displayed more elongated configurations thus having higher ARs. After a first analysis comparing cells grown over control-CM *vs.* BMP4-CM matrices, we set $AR < 1.2$ as a threshold to identify circular/barely spread objects. Then, we calculated the percentage of ROIs with $AR < 1.2$ in each condition and found that the percentage of ROIs in this AR range was reduced in cells cultured over the BMP4-CM matrix, a consequence of their less circular morphologies due to cell spreading. In line with the result obtained with the *Area fraction*, blocking with GoH3 rendered a significant decrease in the percentage of circular objects (**Figure 21F**), suggesting higher spreading after integrin disturbance. These results are coherent with the changes in proliferation observed, as we have shown that NSC spreading over the matrix is related to quiescence-induction. Hence, more spreading could explain the reduction in proliferation observed. However, the mechanism regulating this process should be further evaluated, as potential compensatory mechanisms between ECM-binding receptors may occur.

7. Downstream mechanisms regulating adhesion to self-assembled ECM

7.1 NSC spreading and quiescence induction depends on ROCK

Our previous experiment highlighted the idea that NSC adhesion to self-assembled matrices is potentially regulated by multiple receptors which may cooperate. As it is very difficult to elucidate the specific proteins involved, especially considering the unknown composition of the matrix, we decided to directly target more downstream mechanisms regulating cell spreading. In order to have a wider view of the proteins involved, we decided to represent the interactions of all the proteins changed after BMP4 that were associated to

Results

adhesion-related GO categories (represented in **Figure 5A**) using the software STRING. By doing so, we found that BMP4-changed proteins constituted a unique cluster, which was, in addition, identified by the software as a biologically-associated group (Protein-protein interactions enrichment p value < 1.0e-16) (**Figure 22**). Within the cluster, most of the proteins were related to the GO *Actin filament-based process* (highlighted in red in the network), with a considerable group of proteins also related to *small GTPase signal transduction* (highlighted in blue) (**Figure 22**). For example, we could find RHOG, which is part of the Rho family of GTPases, upregulated. Besides, we could find some upregulated GEFs which participate in the activation of Rho GTPase activity by exchanging GDP to GTP, such as ARHGEF12 or ITSN1, suggesting a potential implication of this pathway in NSCs adhesion induced by BMP4.

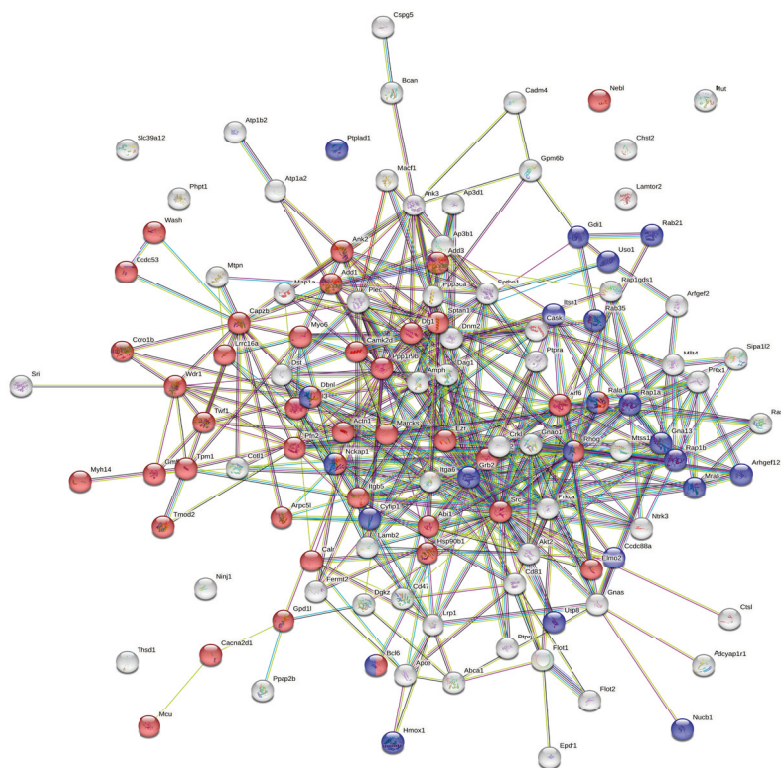


Figure 22. STRING analysis of BMP4 upregulated proteins from adhesion-related GO categories. Proteins associated to GO *Actin filament-based process* are shown in red and *Small GTPase-mediated signal transduction* proteins are highlighted in blue.

To analyze whether BMP4-induced NSC spreading is in fact dependent on Rho signaling, we decided to perturb its main effector, the kinase ROCK, which is needed for the formation and maturation of actin stress fibers. To test its role, we seeded single neurospheres over the BMP4-CM matrix in the presence or absence of ROCK inhibitor

Y27632 (25 μ M), which inhibits both ROCK1 and ROCK2 by competing with adenosine triphosphate for binding to the catalytic site. Morphological analysis after 4 DIV revealed that affecting ROCK disturbed normal adhesion to self-assembled matrix and cells formed, instead, neurospheres that resembled the control condition (**Figure 23A**). In addition to the defect in spreading, affecting ROCK reverted the adhesion-induced quiescent-like phenotype, causing an increase in proliferation, with a reduction in DFFDA^{high} population (**Figure 23B**) and a downregulation of GLAST towards control levels (**Figure 23C**). Furthermore, NSC nucleofection with an inactive form of mutant ROCK1 (Δ 5) (*Figure 1 in Annex*) reproduced the effect observed with the pharmacological inhibition, being mutant ROCK1 cells unable to adhere to BMP4-CM matrices (**Figure 23D**).

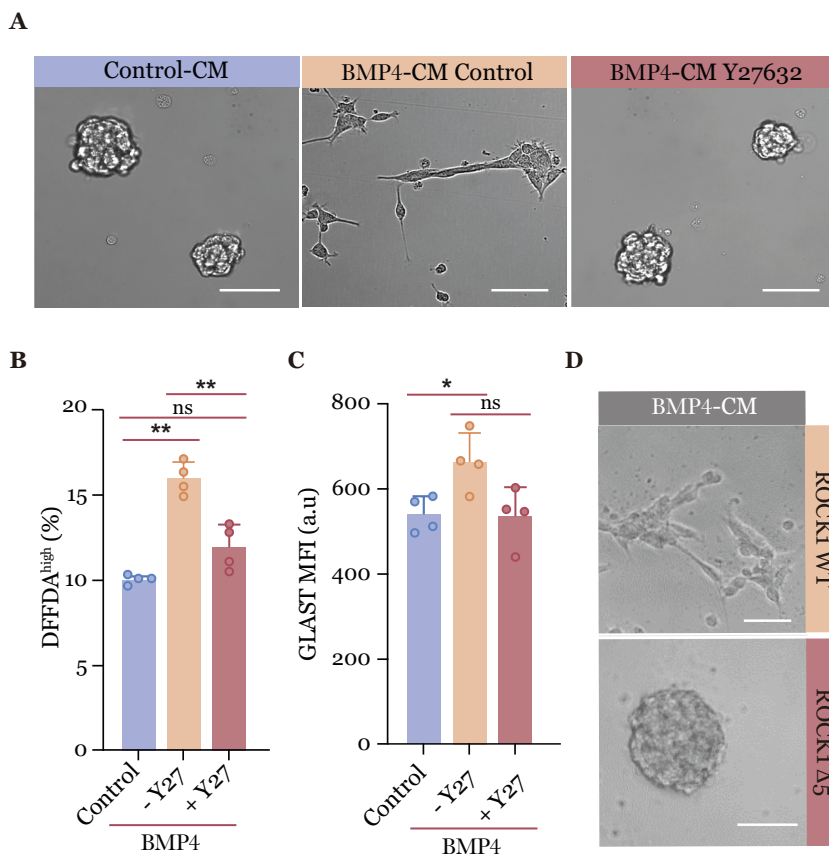


Figure 23. Adhesion to self-assembled matrix is dependent on ROCK activity. (A) Phase contrast images showing NSC cultured over control or BMP4-CM matrix in the presence or not of ROCK inhibitor Y27632 (25 μ M). Scale bars: 50 μ m. (B) Percentage of DFFDA^{high} cells in NSCs after 4DIV over BMP4-CM matrix with or without ROCK inhibitor (Y27), referred to control DFFDA^{high} population. (C) GLAST MFI of NSCs in the different conditions tested. (D) NSCs after nucleofection with ROCK1 WT and mutant (Δ 5) constructions over BMP4-CM matrix. Scale bars: 50 μ m

Results

7.2 YAP-TEAD activity is enhanced over self-assembled matrix

For NSCs to acquire a specific state of activation, they switch on particular transcriptional programs that will condition their cellular identity (Chaker *et al.*, 2016). RhoA/ROCK signaling and actin cytoskeleton can modulate transcription through YAP/TAZ (Nardone *et al.*, 2017; Vining & Mooney, 2017). They are the main effectors for sensing and transducing ECM responses, and function as co-activators of TEAD TFs in response to different mechanical signals. As we had shown ROCK activity to be essential for NSC adhesion over self-assembled ECM, we wondered whether YAP/TAZ-induced transcriptional activity could be responsible for the quiescence induction observed in this scenario. As a first approach to describe its potential role, we decided to check for *Yap1* and *Taz* expression in the different NSC populations using our *in vivo* RNA-seq datasets (Belenguer *et al.*, 2021a), and found that both regulators were significantly upregulated in qNSCs compared to pNSCs and aNSCs (Figure 24A,B).

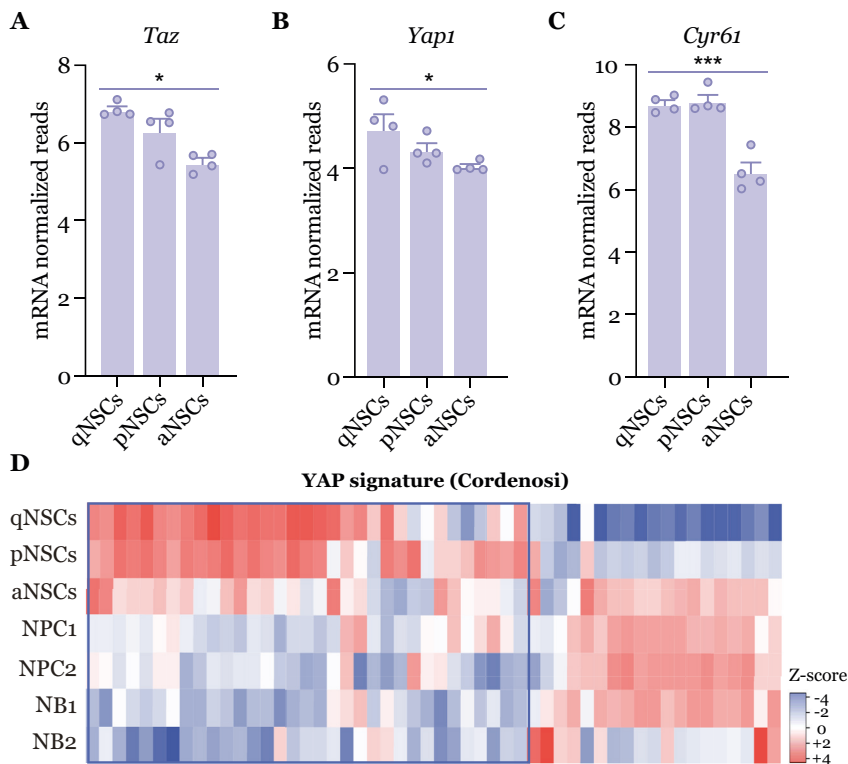


Figure 24. YAP signature in NSC populations. (A) *Yap1* normalized mRNA reads in qNSC, pNSCs and aNSCs from RNA-seq datasets (Belenguer *et al.*, 2021a). (B) *Taz* expression in NSC populations. (C) Normalized mRNA reads of YAP-regulated *Cyr61*. (D) Heatmap showing the relative expression of a conserved YAP gene signature reported in Cordenosi *et al.*, 2011 in the neurogenic lineage. Column Z-scores are shown.

YAP/TAZ activity, however, depends on its translocation to the nucleus, whereby its expression is not necessarily related to its function (Moya & Halder, 2019). Thus, to better assess YAP-dependent transcriptional activity, we evaluated the expression of YAP-targeted genes, as *Cyr61*, which is one of the most well-studied targets. In coherence with our hypothesis, *Cyr61* was found upregulated in q/p NSCs compared to aNSCs, suggesting higher transcriptional activity in the quiescent populations (**Figure 24C**). To assess this in a non-biased way, we evaluated the expression of a list of genes that is part of a conserved YAP transcriptional signature published by Cordenosi and colleagues (Cordenosi *et al.*, 2011). Among them, we found two clearly defined clusters of genes: one set commonly upregulated in q/pNSCs and drastically reduced with lineage progression, and another group downregulated in quiescent cells and upregulated in proliferating cells (aNSCs, NPCs and NB1) (**Figure 24D**). These results suggested that YAP might regulate different transcriptional programs with potential different functions in qNSCs and aNSCs.

To study YAP activity in response to self-assembled ECM, we quantified YAP nuclear fluorescence by ICC (**Figure 25A**). We evaluated it both over Matrigel™, in which proliferation levels are higher, and over BMP4-CM matrix, in which we had observed a partial cell arrest. Interestingly, YAP intensity in the nuclei was increased when cells were cultured over BMP4-CM matrix compared to Matrigel™ (**Figure 25A**). This suggested

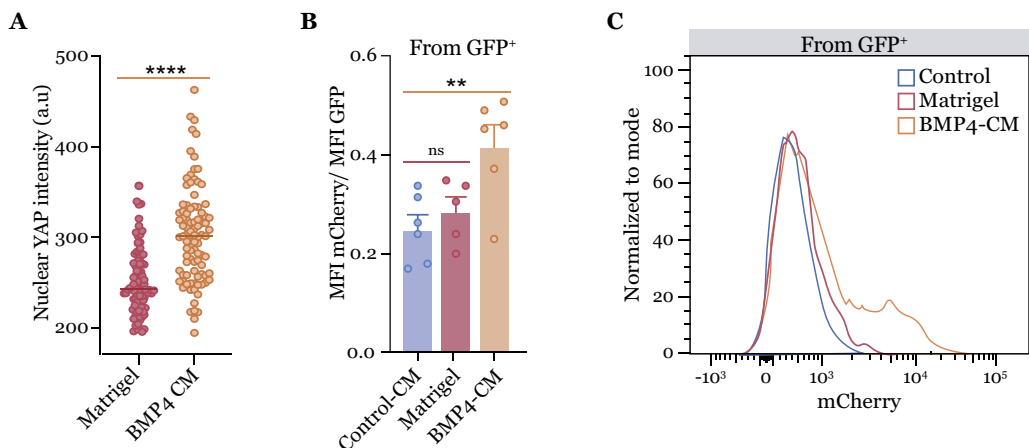


Figure 25. YAP/TEAD transcriptional activity is induced over BMP4-CM matrix. (A) YAP nuclear intensity detected by ICC, after 4DIV cultured over Matrigel™ or BMP4-CM matrix. Each dot corresponds to the measure from one specific cell. (B) Evaluation of the transcriptional YAP/TEAD activity using YAP reporter (FLAG-YAP1-TEAD-P-H2B-mCherry). From nucleofected GFP⁺ NSCs selected by FACS, MFI of mCherry normalized to GFP intensity is plotted. FACS analysis was performed after 24h cultured over control-CM matrix, Matrigel™ or BMP4-CM. An increase in the fluorescence ratio correlates with an increase in YAP/TEAD transcriptional activity. (C) Histograms showing mCherry normalized intensity over the different culture conditions tested. A representative sample is shown.

Results

that it is the specific composition and/or properties of the matrix deposited by NSCs, rather than adhesion itself, which specifically signals the cells in a way that favors YAP translocation to the nucleus. To better assess whether this nuclear localization was related to an increased YAP transcriptional activity when adhered over BMP4-CM, we used a reporter of YAP/TEAD-mediated gene transcription (pLL3.7 FLAG-YAP1-TEAD-P-H2B-mCherry, Addgene #128327) (*Figure 2 in Annex*). If YAP complexes with TEAD and binds to its promoter to activate transcription, mCherry will be expressed and translocated to the nucleus due to its fusion to H2B. This plasmid also contains GFP under the control of a constitutive cytomegalovirus (CMV) promoter, which will enable the fluorescent detection of nucleofected cells. We nucleofected neurosphere cultures (n=3/4 independent cultures in 2 independent replicates) and allowed them to recover for 24 h, to then seed them over Matrigel™, control-CM, or BMP4-CM matrices. After 24h in the different culture conditions, we selected nucleofected cells as GFP⁺ and evaluated YAP-TEAD transcriptional activity as mCherry MFI relative to GFP MFI by FACS. Interestingly, fluorescence ratios were significantly increased when NSCs were cultured over BMP4-CM compared to Matrigel™ or control-CM matrix (**Figure 25B,C**). This was in line with our ICC data and showed that YAP/TEAD transcriptional activity was specifically activated over BMP4-induced NSC self-assembled ECM.

7.3 Constitutive YAP activation induces NSC arrest

To assess if the activation of YAP/TEAD activity over BMP4-CM matrix is responsible for the quiescence induction observed in this context, we tested the effect of disturbing YAP function in NSCs cultures. To do so, we nucleofected, on the one hand, with a plasmid expressing a constitutively active form of YAP (pBabe-YAP-5SA), which has 5 mutated serines that avoid YAP inactivation by phosphorylation. On the other hand, we used a functionally inactive form of YAP (pBabe-YAP-5SA/S94A), which has an additional mutation in serine 94 which impedes its interaction with transcription factor TEAD (*Figure 3 in Annex*). After nucleofection, we waited for 24 h for cells to recover and then seed them in growth medium without any coating or over control or BMP4-CM matrices. We were surprised to discover that constitutively active YAP caused NSCs to adhere over uncoated wells (**Figure 26A**). This suggested a positive feedback loop in which YAP is activated by adhesion but its constitutive activation already favors cell adhesion and spreading. After 24h in culture, we performed a 1h EdU pulse to evaluate proliferation in the different conditions tested and showed that constitutively active YAP caused a surprising strong reduction in the incorporation of EdU that was recovered to the control levels with the functionally inactive construct (**Figure 26B**).

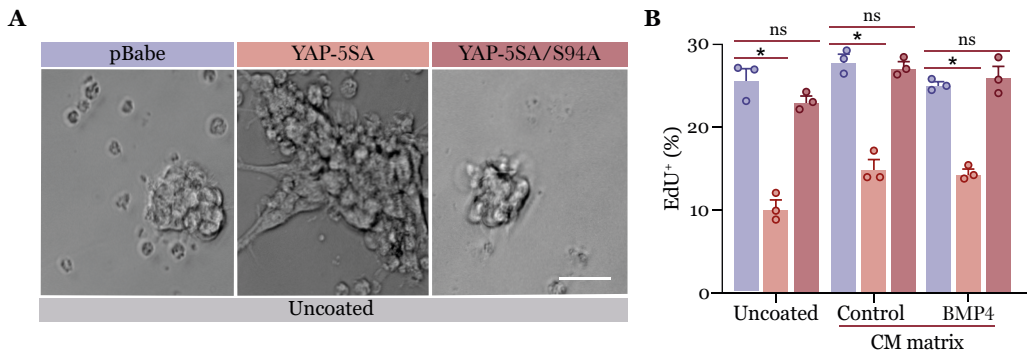


Figure 26. NSCs nucleofected with constitutively active YAP adhere over uncoated wells and reduce their proliferation. (A) Phase contrast images showing NSC cultured over uncoated wells 24h after nucleofection with constitutively active (5SA) or functionally inactive (5SA/S94A) YAP constructs. Empty vector (pBabe) was used as a control. Scale bar: 50 μ m. (B) Percentage of EdU⁺ cells in nucleofected NSCs, evaluated by FACS after 24h cultured over uncoated wells or wells previously coated with control or BMP4-CM matrices.

Considering the activation of YAP over BMP4-CM matrix and its effect in cell spreading and proliferation, we wondered whether BMP4-induced NSC adhesion could depend on the downstream activation of YAP. When we treated with BMP4, we were surprised to discover that YAP-5SA nucleofected NSCs displayed enhanced cell spreading when compared to control cells (pBabe) (Figure 27). Instead, when YAP interaction with TEAD was disturbed (YAP-5SA/S94A), cells did not adhere in response to BMP4 and resembled untreated cells that formed neurospheres (Figure 27). This experiment suggested that BMP4-induced NSC adhesion acts upstream YAP in regulating cell spreading, by still unknown mechanisms.

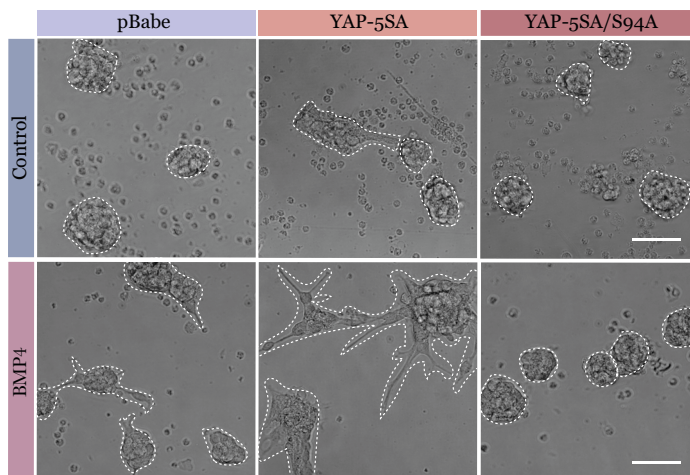


Figure 27. BMP4-induced NSC adhesion depends on YAP/TEAD activity.

Phase contrast images of NSC nucleofected with constitutively active (YAP-5SA) or functionally inactive (YAP-5SA/S94A) constructs after treating or not with BMP4 for 24h. Dotted lines are used to better distinguish NSC spreading in the different conditions tested. Scale bars: 50 μ m.

Discussion



The importance of unveiling the mechanisms regulating NSC quiescence is undeniable, as long-term maintenance of NSCs is key to sustain neurogenesis throughout life in homeostasis and/or after injury. This process, which is conditioned by both intrinsic and extrinsic signals from the environment, constitutes the first step in the generation of new functional neurons (Quaresmina *et al.*, 2022; Urban *et al.*, 2019). Thus, decoding its mechanisms could bring us closer to the development of new potential strategies to interfere with NSCs behavior *in vivo*, which is especially relevant in the context of a physiological (e.g. aging) or a pathological (e.g. tumorigenesis) NSC dysregulation. On this matter, it is worth noting that studying extrinsic signals instead of cell-intrinsic mechanisms makes this type of application more feasible, as we could more easily target specific regulatory components of the microenvironment that could directly or indirectly modify NSC behavior (Wang *et al.*, 2021).

Among the different extrinsic signals that regulate NSCs in the SEZ, the ECM is possibly one of the most challenging niche components to study. This is clearly evidenced by the fact that while many different soluble signals have been described over the years to have a role in NSC regulation (Karakatsani *et al.*, 2019; Quaresima *et al.*, 2022), studies related to cell-ECM adhesion have been published in dribs and drabs. One plausible explanation for this is that there are no straight-forward strategies or methodologies to evaluate adhesion *in vivo* beyond microscopy analyses. Indeed, while pioneer studies seeded the basis of NSC-ECM interactions more than a decade ago, when they discovered that NSCs bound to BV through integrins (Shen *et al.*, 2008; Tavazoie *et al.*, 2008), very little progress has been made regarding the study of NSC regulation through the ECM. The same happened for the interaction with speckles, structures that were first described by Mercier and colleagues in 2002 (Kerever *et al.*, 2007; Mercier *et al.*, 2002) and it was not until years later that the field started to unveil their composition and biological functions (Mercier *et al.*, 2014; Nascimiento *et al.*, 2018; Sato *et al.*, 2019).

Besides the technical difficulties, the field has, for years, confronted the great challenge of studying NSC heterogeneity. At the time the aforementioned studies were performed, besides classical immunostainings, they did not have the methodologies to approach the identification of specific NSC populations. Hence, they could not evaluate the potential different cellular responses to, for example, extrinsic signals. It has not been until more recent transcriptomic and single-cell analyses have been performed, that researchers have unveiled the molecular signatures of the three NSC populations that coexist in the niche: qNSCs, pNSCs and aNSCs (reviewed in Chaker *et al.*, 2016). Since then, different research groups have put a lot of effort in developing strategies to study these populations and the mechanisms regulating the acquisition and maintenance of the different cell states (Belenguer *et al.*, 2021a; Codega *et al.*, 2014; Leeman *et al.*, 2018; Llorens-Bobadilla *et*

Discussion

al., 2015). In this project, we have used our reported FACS strategy (Belenguer *et al.*, 2021b) to characterize the specific NSC states *in vivo*, which has given us the opportunity to study, for the first time, ECM interactions considering NSC heterogeneity. However, albeit quiescent NSCs can be studied by FACS, a second challenge has been driven by the fact that there are no defined markers to distinguish this population by histology, losing their spatial distribution in the niche. In this regard, we have used IUE to specifically target and fluorescently label deeply quiescent NSCs since their specification at embryonic stages, which has enabled us to study their disposition and interaction with the ECM *in vivo*, a topic that has remained largely unexplored until now. The combination of both IUE-based histology and FACS, has given us the perfect tools to study the differential interaction of NSC populations *in vivo* with the ECM in a quantitative manner, but using qualitative histological observations as a basis on which to build.

In brief, in this thesis we have studied, from a holistic and multi-level point of view, the role of the ECM in NSC regulation in the SEZ. Overall, the main contributions of our work have been the following: 1) we have studied the disposition and differential interaction of qNSCs with BM structures *in vivo* for the first time, 2) we have assessed the role of pro-quiescence inducer BMP4 in ECM remodeling and 3) we have evaluated of the effect of NSC-derived ECM and vascular ECM binding in regulating NSC state and the molecular mechanisms mediating these interactions. Having highlighted, at a glance, the main topics assessed in the project, I will go deeper into the relevance of our results, the methodologies used, and the applications that can be derived from our findings.

Our first proposed objective was to determine the contribution of NSCs to their ECM niche. Although it had been suggested that NSCs may participate in ECM remodeling (Kjell *et al.*, 2020; Nascimento *et al.*, 2018), neither direct evidence of this had been obtained, nor any molecular inducers had been studied so far. As already mentioned, *in vivo* sorted qNSCs cannot be maintained in culture and thus, we have used a BMP4 treatment to model NSC quiescence *in vitro* (Mira *et al.*, 2010). By this means, we serendipitously identified that BMP4 treatment could induce NSC adhesion and spreading over uncoated wells, an effect that occurred in parallel with quiescence induction. Some of the research papers that have used BMP4 as pro-quiescence inducer, have directly treated NSCs cultured in adherent conditions without further justification (Ahmed *et al.*, 2022; Marqués-Torrejón *et al.*, 2021), which may explain why BMP4-induced NSC adhesion had never been reported so far. In this work, we have also unveiled that SEZ-derived NSCs do not behave the same way when cultured in the presence of EGF, bFGF or both mitogenic stimuli. Until now, no one has ever used EGF ligand when inducing quiescence with BMP4 due to the antagonistic expected effects, albeit the fact that *in vivo* NSCs are exposed to both factors (Weickert *et al.*, 2000). However, instead of covering up the effect, we showed

that quiescence-induction was enhanced when NSCs were exposed to EGF, being more effective when both mitogens were added to the media. This may be explained by the fact that EGF and bFGF pathways interact with BMP signaling through different mechanisms (Sun *et al.*, 2011, 2020), which can render the cells with different susceptibility to BMP4 responses. One of the first BMP/EGFR interactions was reported in breast cancer cells, showing that BMP6 could be induced downstream EGF/EGFR signaling (Clement *et al.*, 1999). This crosstalk can also be mediated through EGF-activated proteins, as Erk, which has been shown to upregulate SMAD3 in smooth muscle cells (Ross *et al.*, 2007). All in all, our results have given new insights in the study of SEZ NSC responses to BMP4 *in vitro*, which are of great value as it brings us closer to the identification of the specific culture conditions to better mimic qNSC behavior in culture.

Interestingly, our BMP4 proteomic analysis showed that this pro-quiescence factor could modify the protein levels of multiple matrisome components (Naba *et al.*, 2012) in NSCs, some of which were found to be part of the SEZ-specific proteome (Kjell *et al.*, 2020). This suggested that BMP4 could have a role in defining the specific properties of the ECM in this germinal region, topic that should be further assessed *in vivo*. Interestingly, we have determined that quiescence is associated to the acquisition of a specific ECM-related signature, which is recapitulated at the protein level by BMP4 treatment. However, to better characterize BMP4-induced signature, we should also perform transcriptional studies that could complement our proteomic analyses. Besides, whether this ECM-related transcriptional and protein changes are a cause or a consequence of the acquisition of a quiescent phenotype, is still to be elucidated.

It is noteworthy that regarding the mechanisms of ECM adhesion, we have paid special attention to LM/integrin interactions. LM is indeed one of the most abundant components in BMs (Khalilgharibi & Mao, 2021) and is especially enriched in the SEZ (Kim *et al.*, 2021). Besides, it has been shown to have an undeniable role in NSC regulation (Kokovay *et al.*, 2010; Nascimento *et al.*, 2018; Sato *et al.*, 2019; Shen *et al.*, 2008). Interestingly, we have revealed that LMs genes are regulated and proteins secreted in response to BMP4, potentially modulating LM composition in vascular and speckled BM structures. In addition, we have shown that LM-binding integrins are enhanced in qNSCs and also display BMP4 responsiveness.

As far as we know, this is the first time that a factor has been shown to trigger ECM secretion by NSCs. However, the role of BMP4 in ECM remodeling should also be tested *in vivo*. This entails some additional difficulties, as it is challenging to distinguish between the direct effect of BMP4 in NSCs, and/or the indirect effect mediated by BMP4-induced ECM remodeling *per se*. Besides, BMP4 can be found as a soluble factor or bound

Discussion

to ECM structures (Mercier & Douet, 2014) which makes the pharmacological targeting of the protein less trivial. Moreover, the characterization of the ECM changes induced by BMP4 are also hard to evaluate, as we have shown that BMP4 treatment induces a very specific regulation, with different isoforms from the same family of proteins upregulated or downregulated after the treatment. This tight regulation may need a very detailed study for evaluating ECM remodeling *in vivo*, as using an antibody recognizing all isoforms can hide the effects of specific isoforms that can compensate for each other, rendering unaltered global levels. Considering that each LM isoform has a specific function (Barros *et al.*, 2020), we should study in more detail the subtype of LM secreted in response to BMP4 or present surrounding qNSCs *in vivo*, as it could give us new hints on the specific mechanisms mediating adhesion. In this regard, we are aware that ECM regulation is way more complex than the role of one of its specific constituents or a specific receptor. Indeed, other BM components have been shown to affect NSC behavior, as for example tenascin-c (reviewed in Faissner *et al.*, 2017) or growth factor binding PGs (reviewed in Kerever & Arikawa-Hirasawa, 2021), which we have also found to be upregulated after BMP4 treatment. Hence, we should keep in mind that we have evaluated a specific regulation which is part of a wider and more complex one, mediated by multiple different ECM components and receptors.

The fact that SEZ ECM composition is so unique, especially regarding BM structures, has attracted the attention of different research groups that have studied the role of BMs in NSC regulation (Kerever *et al.*, 2007; Mercier *et al.*, 2002; Nascimento *et al.*, 2018; Sato *et al.*, 2019). However, these studies have never considered the qNSCs pool, due to its challenging histological identification. Using IUE, we have showed that qNSCs have a heterogeneous apico-basal positioning in the niche and that they closely interact with both vascular and speckled BM structures *in vivo*. Although the distance to LV has been shown to be a determinant factor in conditioning neurogenesis (Kazanis *et al.*, 2010), very little is known regarding the mechanisms regulating apico-basal positioning and the consequences derived from it. The existence of a pool of cells with no contact with the ependyma was described many years ago (Doetsch *et al.*, 1997). However, it was not until more recent lineage-tracing analyses were performed, that the origin of these cells started to be unveiled (Obernier *et al.*, 2018). Specifically, they discovered that these cells are derived from a subpopulation of self-renewing apical NSCs (Obernier *et al.*, 2018), and they have specific traits that have been associated with q/a NSC transitions, as for example high density of free ribosomes (Dulken *et al.*, 2017; Llorens-Bobadilla *et al.*, 2015). This is coherent with the idea that basally-located NSCs in the adult mouse SEZ are responsible for the generation of most adult-born neurons in the OBs, as shown by a recent publication (Baur *et al.*, 2022). Our data suggests that although ~80% of qNSCs are positioned in

close contact with the ependyma, ~20 % are located basally, proportions that coincide with the percentage of plasmid retaining cells that are categorized as qNSCs and pNSCs, which makes us speculate, following also published observations, that these quiescent basal cells could correspond to defined states closer to activation. However, the identity of these cells and its regulation should be further evaluated, as it could allow us to gain new insights on how the differential interaction with the niche may affect the specific NSC states.

In addition to the histological detection, our reported FACS strategy (Belenguer *et al.*, 2021b) has enabled us to assess the potential differential adhesion of NSC populations to the local ECM niche *in vivo*. We have showed that qNSCs not only contact LM⁺ BM structures, but also have a stronger interaction than aNSCs. Specifically, we have found that qNSCs are remarkably more surrounded by extracellular LMs compared to pNSCs and aNSC, and that q/p NSCs are differentially bound to BV mostly through laminin-integrin interactions *in vivo*, suggesting differential adhesive responses with the ECM niche among different states of activation. For this purpose, we have developed unique strategies to evaluate adhesion *in vivo*, which will hopefully set precedent for this type of studies. In brief, they are based on the idea that under controlled enzymatic digestion conditions, we can detect ECM proteins extracellularly bound to cell membranes. We have only assessed this for LM, but it could be fine-tuned for other specific components, and could be implemented as a way of testing *in vivo* interactions with the local ECM niche. We have used this strategy also *in vitro*, and we have found it to be reproducible and consistent in both cases, allowing us to unveil small differences in extracellular LM levels. Regarding NSC-BV adhesion, we have discovered that when isolating ECs using CD31⁺ magnetic sorting, we can co-isolate adhered cells located in the perivascular region. Further, we found that this binding could be disturbed with integrin $\alpha 6$ blocking antibodies, hinting at the potential use of this methodology as a low-throughput screening technique to evaluate the role of specific molecules in vascular adhesion *in vivo*.

With the aim of studying the specific upstream and downstream mechanisms regulating NSC adhesion, we swapped to *in vitro* systems. By this, we could independently study the role of vascular ECM or BMP4-induced NSC-derived ECM. Of this last, we could, besides, separate the direct effect of BMP4 to the one derived from BMP4-induced secretome. Specifically, we have developed a strategy to study the role of BMP4-induced ECM deposition by using Noggin-blocked BMP4-CM as a coating in which to assay NSC adhesion-mediated responses. We have shown that NSCs can interact and spread over what we have named as *self-assembled* ECM, and that this interaction also affects NSC proliferative behavior. In line with our *in vivo* data showing qNSC differential interaction with vascular and speckled BMs, we have shown that culturing NSCs over ECs or over self-assembled ECM, favor the induction of a quiescent-like NSC state *in vitro*.

Discussion

Although both ECM structures, vascular and NSC-derived, have been tested independently, it is important to consider that their regulation is interconnected. On the whole, our data reveal different levels of vascular modulation of quiescence, that occur in parallel: 1) direct adhesion to vascular ECM binding through integrin $\alpha 6$, 2) BMP4 secretion that can directly affect quiescence induction and 3) ECM NSC deposition through BMP4, which also supports the quiescent phenotype. Interestingly, BMP4-induced LM gene expression changes in NSCs show an upregulation of *Lama2*, a LM isoform which has been described to be exclusively present in vascular BMs in the SEZ (Sato *et al.*, 2019), suggesting that NSCs could also participate in BV ECM remodeling, idea that should be tested *in vivo*. The observed closer interaction between qNSCs and BMs *in vivo* would, thus, make them more susceptible to receive these pro-quiescent signals. On the one hand, it will favor adhesion-mediated signaling while, on the other, it will enhance BMP4 accessibility, as BMP4 can be found bound to speckles (Mercier & Douet, 2014) and also secreted by ECs *in vivo* (Cebrian-Silla *et al.*, 2021; Mathieu *et al.*, 2008; Pineda *et al.*, 2013). This would favor a reciprocal positive feed-back loop in which pro-quiescence inducer BMP4 favors adhesion through ECM secretion while adhesion, *per se*, already favors cell arrest and transcriptional changes related to inducing a quiescent identity.

The fact that we have unveiled specific culture conditions in which we can induce a quiescent-like state *in vitro*, opens new possibilities regarding the study of qNSCs. BMP4-CM matrices or EC co-culture system may be used as models in which to study of the specific molecular mechanisms regulating the process of quiescence induction. Besides, if we could fine-tune these models for the maintenance of sorted *in vivo* qNSCs, it could allow us to study qNSCs in a more physiological state. Multiple studies have tried to decode the best matrices to mimic the *in vivo* microenvironment (Barros *et al.*, 2020), and we consider that, in this regard, the use of BMP4-CM matrix as a coating for NSC culture is a promising approach to be exploited. In addition, it may allow us to discover new mechanisms of NSC adhesion to its own ECM niche, as it enables a feasible system to assess the role of specific pathways with pharmacological or genetic approaches. Indeed, the use of this CM as a coating instead of commercial coatings renders a more physiological system to culture NSCs, and could be applied to more complex biodevices, as for example 3D cultures, or hydrogels with specific properties of stiffness that could better mimic the properties of the SEZ (Baker & Chen, 2012; Xu *et al.*, 2021). However, one of the main drawbacks of this system is that we have not been able to determine the composition of the media, since NSCs require BSA for their *in vitro* maintenance, which hinders the detection of less concentrated proteins. However, more innovative proteomic approaches or better pre-processing of the samples could be tested to cope with this problem (Byron *et al.*, 2013; Rozanova *et al.*, 2021). In this work, however, we have not focused on the composition,

but rather on the cell response to the matrix. Besides, even though we have had determined CM composition, we could never assure that the composition of the soluble media would be reproducing the components that are finally deposited and retained in the bottom of the wells.

The last part of the work has focused on the understanding of the upstream and downstream regulators affecting quiescence induction through ECM adhesion. Although integrin expression in NSCs is widely accepted, there is certain controversy regarding the specific NSC populations that express them and hence, its specific function in particular NSC states (Kokovay *et al.*, 2010; Rosa *et al.*, 2016; Zhu *et al.*, 2017). Our RNA-seq dataset revealed that qNSC have upregulated expression of this family of proteins, and specifically, integrin $\alpha 6$ is enhanced at the protein level after BMP4 treatment. Interestingly, we have shown that this receptor is enhanced by ECM adhesion. This reveals another feed-back loop in which adhesion incites to further qNSCs binding and signaling through the matrix due to the upregulation of integrin receptors. We have discovered that, although integrin $\alpha 6$ blocking disturbs ECM interactions and have an effect in proliferation, it is not enough for enabling a complete detachment. This partial effect can be explained by diverse reasons. In the first place, the redundancy in integrin binding affinities. For example, multiple integrins are shown to bind LM ($\alpha 1\beta 1$, $\alpha 2\beta 1$, $\alpha 3\beta 1$, $\alpha 6\beta 1$ and $\alpha 6\beta 4$) (Nirwane & Yao, 2018). Secondly, all *in vitro* functional blocking assays were performed by doing short 30-minute pre-treatments with the blocking antibodies, followed by cell washing prior to seeding for 4 DIV in the specific culture conditions. In this context, the fact that integrin $\alpha 6$ is upregulated after ECM binding could explain this cover up effect. Also, changing binding affinities by blocking a specific interaction may favor the binding of other receptors as a compensatory mechanism (Liddington & Ginsberg, 2002), that could be already expressed in the cell membrane or could be enhanced through favoring recycling trafficking pathways of other integrin partners (Moreno-Layseca *et al.*, 2019).

Surprisingly, we observed that integrin $\alpha 6$ disturbance had opposed effects when culturing NSCs over ECs or over self-assembled ECM. Over self-assembled ECM, integrin blocking induced a small but significant reduction in proliferation, suggesting that different mechanisms may be affecting NSCs adhesion in these two scenarios. This effect was concomitant with an increased cell spreading, suggesting the activation of a compensatory mechanism that enhances adhesion, which should be further assessed to understand the proteins and type of adhesions involved. The spreading and formation of mature adhesions will depend on multiple factors: the specific biochemical composition, growth factor availability, the forces to which cells are subjected, among others (Elosegui-Artola *et al.*, 2016; Morgan *et al.*, 2007). Similar effects have been observed in other cell types, as for example in keratinocytes and carcinoma cell lines, in which blocking integrin

Discussion

$\alpha6\beta4$ was shown to favor an increase in cell area and FA size (Wang *et al.*, 2020). In a different cellular context, blocking this specific integrin favored nuclear YAP responses that are usually associated with the activation of FA pathways (Kechagia *et al.*, 2022). With this, I want to highlight that integrin responses are dynamic and tightly and complexly regulated, and further research should be done to understand the role of the different receptors participating in NSCs interaction with self-assembled ECM.

For the correct development of FA downstream integrin activation, mature stress fibers have to be formed, for which Rho GTPases are known to be key regulators (Ohashi *et al.*, 2017; Vining & Mooney, 2017). Our BMP4 proteomics showed changes in proteins that were related to GO terms associated to actin cytoskeleton dynamics, making us hypothesize that it may participate in NSC adhesion. We found that NSC spreading over self-assembled ECM was indeed dependent on ROCK, as its pharmacological or genetic disturbance favored NSC detachment to form neurospheres, concomitant with an increased proliferation. Previous studies had suggested that changes in cell shape can regulate lineage-specific markers and even favor switches in lineage commitment and differentiation mediated by ROCK (McBeath *et al.*, 2004). However, we have shown that adhered NSCs can be detached and retain their self-renewing features, suggesting that we are not affecting differentiation programs. Rather, as suggested by our results, we may be affecting transcriptional programs to favor the acquisition of a quiescent-like state. Interestingly, some reports indicate that integrins regulate the deposition of LM by signaling to Rho GTPases (Hamelers *et al.*, 2005), which makes us wonder whether the effect observed is directly related to cytoskeletal tension, or also indirectly regulated through potential ECM deposition.

YAP/TAZ are the main transcriptional regulators in ECM mechanoresponses (Moya & Halder, 2019). Although recent reports have highlighted that YAP may have a role in regulating SGZ NSCs (Fan *et al.*, 2022), its function in the SEZ is completely unexplored. Hence, the discovery of YAP transcriptional activation when NSCs were specifically grown over BMP4-CM matrix, is particularly relevant. As we had shown that culturing over BMP4-CM matrix reduced NSC proliferation, the increase in YAP activity was an striking result, as its regulation is part of a conserved pathway that commonly regulates proliferation and organ growth in different systems (Panciera *et al.*, 2017). NSC expression of constitutively active YAP confirmed that its disturbance significantly reduced proliferation, effect that was dependent on its interaction with TEAD TFs. Differently from the SGZ, in which YAP transcriptional signature (Cordenonsi *et al.*, 2011) correlates with the aNSCs expression profile (Fan *et al.*, 2022), we have shown that in the SEZ, many YAP gene targets are upregulated in qNSCs and downregulated in aNSCs. All in all, we suggest that YAP/TAZ may have different functions in the two germinal regions of the brain.

Although it is tempting to speculate that YAP is acting downstream ROCK as it has been shown for diverse systems, we should evaluate the exact mechanism of action in NSCs. To shed some light in this regulation, we should undoubtedly set up to assess the role of YAP/TAZ *in vivo*, as we have only evaluated the effect of YAP disturbance in our *in vitro* system. Besides, it is known that YAP signaling interacts with other signaling pathways, which makes YAP responses highly context dependent and hence, should be evaluated in a more physiological context. For example, Li *et al* showed that Notch inhibition can be rescued by YAP (Li *et al.*, 2012). Further, stiffness can also regulate YAP activity (Aragona *et al.*, 2013; Dupont *et al.*, 2011), which should be accounted when studying the role of this proteins *in vivo*, especially since the SEZ displays stiffer ECM compared to non-neurogenic regions as the cortex (Kjell *et al.*, 2020). Interestingly, YAP also directly interacts with the BMP pathway. For example, YAP nuclear translocation is required for the stabilization of SMAD complexes, and can regulate BMP ligand expression, highlighting diverse crosstalk mechanisms between both pathways (reviewed in Heng *et al.*, 2020).

In this regard, our data shows that BMP4 and YAP may interact and coordinately regulate NSC adhesive responses, as some of our preliminary experiments show that BMP4-induced adhesion is dependent on YAP activation. However, the mechanisms are still unexplored and should be further assessed. One potential explanation is that the activation of non-canonical BMP pathways can induce RhoA/ROCK activity, which would condition adhesion upstream YAP (Derynck & Zhang, 2003). Specifically, it has been shown that BMPRII inhibit LIMK, the main downstream effector of ROCK, and BMP ligand binding release this inhibition favoring the formation of stress fibers (Toletta *et al.*, 2003). Moreover, we were surprised to discover that YAP constitutive activation was enough to favor untreated NSCs adhesion to uncoated wells. This may be explained by the fact that YAP, in other systems, has been shown to regulate the expression of genes coding for some integrins and ECM components, such as some isoforms of collagen and LM (Nardone *et al.*, 2017). Thus, our data suggests that YAP may not only be the downstream effector of the quiescence induction process in response to adhesion over self-assembled ECM, but may also act downstream BMP4 in the regulation of this response, hypothetically through affecting the expression of ECM-related genes. Whether BMP4-ECM deposition and induced spreading is dependent on YAP should be further evaluated, as well as the implication of the crosstalk of both pathways *in vivo* in the regulation of NSCs response.

As an overall sum up, and referring to this thesis title, in this project we have gained new insights that have brought us closer to unveiling quiescence in NSCs. Starting from the discovery of the novel role of pro-quiescence inducer BMP4 in ECM remodeling, we have revealed a bidirectional qNSC-ECM crosstalk that has shown to be key in regulating quiescence. While qNSC contribute to their ECM niche, ECM binding reciprocally

Discussion

participates in the maintenance of the quiescent state. The effect observed reminds us of the *chicken-egg* paradox, as BMP4 induces quiescence while favoring a specific ECM remodeling that, in turn, enhances this state even in the presence of mitogens. Truth be told, which of the signals comes first, remains elusive. What is clear is that the differential interaction of qNSCs with the vascular and speckled LM niche *in vivo* is of biological relevance, as we have demonstrated that NSC-ECM adhesion actively regulates NSC behavior. Regarding the regulatory mechanisms, we have learned that qNSCs are specially adhered to BV through integrin $\alpha 6$ *in vivo* and that both integrin $\alpha 6$ -mediated interactions and secreted BMP4 are mechanisms by which BVs induce quiescence. When it comes to the interaction with self-assembled ECM, we have shown that integrin $\alpha 6$ may have a different role in this context, as its blocking increased spreading and favored NSC quiescence. Although many questions remain unanswered, what we do know is that NSC adhesion to self-assembled ECM is dependent on cytoskeletal tension mediated by ROCK, and that downstream transcriptional activity of YAP/TEAD is activated in this scenario. As a way of closing this biological loop, we have shown that YAP/TEAD activity mediates both NSC adhesion and, more importantly, cell cycle arrest in response to self-assembled ECM.

Conclusions



1. The interaction with the ECM niche differs between NSC populations: qNSCs are highly surrounded by extracellular laminin and are differentially attached to the vascular basement membrane, making them especially susceptible to ECM-derived signals.
2. Endothelial cells induce a reversible quiescent state in NSCs through both BMP4 secretion and direct ECM binding.
3. BMP4 induces the acquisition of an ECM-related protein signature in NSCs *in vitro* that correlates, at the transcriptional level, to that of qNSCs *in vivo*.
4. BMP4-induced NSC quiescence depends on EGF stimulation and triggers the secretion and deposition of ECM proteins. NSC adhesion to this self-generated ECM favors a reversible cell cycle arrest.
5. NSC quiescence induced by adhesion to self-assembled ECM is regulated by integrin binding and dependent on actin cytoskeletal tension mediated by ROCK and YAP/TEAD transcriptional activity.

Resumen



Introducción

Las células madre somáticas (SCs, del inglés stem cells) tienen un papel esencial en el mantenimiento de la homeostasis de los tejidos en los que residen, ya que participan en el recambio celular y en la regeneración, tanto en condiciones basales como en un contexto de daño celular (Barker *et al.*, 2010; Simons & Clevers, 2011). Las SCs se caracterizan por ser auto-renovantes, es decir, dar lugar a células hijas que retienen su potencial replicativo, y por su capacidad de diferenciarse para formar uno o varios tipos celulares diferentes. Mantener un balance correcto entre la autorrenovación y diferenciación, y, por ende, entender los mecanismos que los regulan, son clave para evitar la reducción o depleción de las SCs con la edad (Goodell & Rando, 2015). Una consecuencia derivada de la longevidad de las SCs y del mantenimiento de su capacidad replicativa con el tiempo, es la potencial aparición de mutaciones que puedan favorecer la adquisición de ventajas replicativas que supongan un riesgo para la aparición de tumores (Blokzijl *et al.*, 2016; Ermolaeva *et al.*, 2018). Por ejemplo, se sabe que mutaciones en las células madre neurales (NSCs, del inglés neural stem cells) de la zona subependimaria (SEZ, del inglés subependymal zone) pueden originar uno de los tumores malignos más agresivos del cerebro, el glioblastoma (Lee *et al.*, 2018). Sin duda, el estudio de las SCs es de gran relevancia, ya que nos permite entender mejor su funcionamiento en homeostasis así como acercarnos a potenciales tratamientos terapéuticos enfocados en interferir en el envejecimiento de los tejidos o en potenciales procesos tumorigénicos. En esta tesis hemos estudiado específicamente las NSCs adultas de la SEZ en estado fisiológico, centrándonos en concreto en el estudio de los mecanismos que regulan su estado de activación.

Las NSCs son astrocitos multipotentes autorrenovables que, durante el desarrollo, tienen un papel esencial en la generación de neuronas y células gliales del cerebro y la médula espinal (Urbán *et al.*, 2019). Aunque de manera más limitada, las NSCs producen neuronas a lo largo de la toda la vida adulta (Altman, 1962; Altman & Das, 1965; Urbán & Guillemot, 2014), lo cual ocurre en nichos neurogénicos muy concretos que les proporcionan el microambiente idóneo para su mantenimiento: el giro dentado del hipocampo y la SEZ, situada en el revestimiento de los ventrículos laterales (LVs, del inglés lateral ventricles). La SEZ constituye el nicho germinal más grande y activo en la producción neuronal, proceso que se inicia cuando las NSCs se dividen para formar células progenitoras (NPCs, del inglés neural progenitor cells), que se dividirán 3-4 veces para dar lugar a neuroblastos (NB) tempranos más comprometidos hacia la diferenciación. Estos NB proliferantes aún pasarán por 1-2 rondas de división, para finalmente generar NB tardíos que migrarán formando la cadena rostral migratoria (RMS, del inglés rostral migratory stream) hasta alcanzar el bulbo olfatorio, donde se integrarán como interneuronas (Obernier *et al.*, 2018; Urbán *et al.*, 2019). En homeostasis, las NSCs coexisten en la SEZ en tres estados de activación:

Resumen

quiescentes (qNSCs), *primed* (pNSCs) y activadas (aNSCs) (Obernier & Alvarez-Buylla, 2019). Estudios transcriptómicos recientes han permitido definir la firma molecular de cada una de las poblaciones de NSCs (Belenguer *et al.*, 2021a, Codega *et al.*, 2014; Dulken *et al.*, 2017; Llorens-Bobadilla *et al.*, 2015), revelando las vías de señalización relevantes para el mantenimiento de su función. Por ejemplo, en el caso de las qNSCs, se ha visto que tienen un metabolismo dependiente de glicólisis y de ácidos grasos, que presentan una señalización activa por receptores acoplados a proteínas G (GPCR, del inglés G-protein coupled receptors), o mayores interacción a nivel célula-célula y célula-matriz (revisado en Chaker *et al.*, 2016). Por otro lado, las pNSCs representan un estado de quiescencia menos profunda, similar al estado descrito en las SC del músculo (G^{altr}) (Rodgers *et al.*, 2014). Las pNSCs expresan, por ejemplo, genes de ciclo, lo cual les hace más susceptibles a la activación (Llorens-Bobadilla *et al.*, 2015).

El estudio de la heterogeneidad de las NSCs ha obligado al campo a desarrollar sistemas que permitan distinguir de manera inequívoca a las diferentes poblaciones. En este contexto, nuestro laboratorio ha desarrollado una estrategia de citometría de flujo que nos permite, mediante el uso de una combinación de anticuerpos (GLAST/CD9/CD24/EGFR) y sus niveles intensidad relativa, estudiar todo el linaje neurogénico (Belenguer *et al.*, 2021a, b).

Tanto en el mantenimiento de un estado de activación concreto, como en su diferenciación progresiva en el linaje, las NSCs están sometidas a una regulación estrecha mediada en gran parte por factores extrínsecos derivados del microambiente en el que residen (Morante-Redolat & Porlan, 2019; Obernier & Alvarez-Buylla, 2019). Esta interacción, además, se ve favorecida por su disposición polarizada en el eje apico-basal, propiedad que mantienen de las células de glia radial de las que provienen (Doetsch *et al.*, 2003; Urbán & Guillemot, 2014; Yuzwa *et al.*, 2017). En su parte apical contactan con el líquido cefalorraquídeo a través de las células endoteliales, y en su parte basal, con los vasos sanguíneos (BVs, del inglés blood vessels), recibiendo de ambas partes múltiples señales que las regulan (Quaresima *et al.*, 2022; Zappaterra & Lehtinen, 2012). Es interesante remarcar, además, que algunas de las células o estructuras con las que coexisten, tienen características únicas; los BVs, por ejemplo, tienen una barrera hematoencefálica modificada que les confiere una mayor permeabilidad al paso de moléculas de la sangre (Shen *et al.*, 2008; Tavazoie *et al.*, 2008). El estudio de la regulación vascular ha llevado a descubrir a lo largo de los años, múltiples señales (tanto solubles como mediadas por adhesión) derivadas de la interacción estrecha que tienen con los mismos (revisado en Karakatsani *et al.*, 2019). Las respuestas celulares son muy variadas, por ejemplo, algunos factores angiocrinos, como el factor de crecimiento derivado del epitelio pigmentado (PEDF, del inglés pigmented epithelium derived growth factor), regulan la auto-renovación de las NSCs a través de

la activación de Notch (Andreu-Agulló *et al.*, 2009; Ramírez-Castillejo *et al.*, 2006). En cambio, otros como la neurotrofina-3 o la interacción célula-célula mediada por Jagged1/Notch, promueven la quiescencia celular (Delgado *et al.*, 2014; Ottone *et al.*, 2014). Aunque se ha estudiado menos, las NSCs también son reguladas por la interacción con la matriz extracelular (ECM, del inglés extracellular matrix) (Morante-Redolat & Porlan, 2019), tanto a nivel vascular mediado a través de integrina $\alpha 6$ (Shen *et al.*, 2008), como extravascular (Nascimento *et al.*, 2018; Sato *et al.* 2019). Mientras que algunos grupos sugieren que la integrina $\alpha 6$ está asociada a quiescencia (Shen *et al.*, 2008), otros apoyan que este receptor se asocia a aNSCs, revelando cierta controversia en cuanto a su función (Kazanis *et al.*, 2010; Rosa *et al.*, 2016).

La SEZ tiene una composición única en cuanto a sus estructuras de membrana basal (BM, del inglés basement membrane), un tipo de ECM que proporciona soporte a las células epiteliales y endoteliales, y actúa como una plataforma de interacción y señalización celular (Khalilgharibi & Mao, 2021a). Es interesante remarcar que la SEZ es la única región cerebral que presenta estructuras de BM independientes de la vascular, conocidas como *speckles* en inglés (Kerever *et al.*, 2007; Mercier *et al.*, 2002). Los *speckles* pueden regular a las NSCs a múltiples niveles: se ha descrito que las NSCs interactúan con estas estructuras a través de integrinas, lo cual condiciona tanto el comportamiento celular como la correcta formación de estas estructuras de BM (Nascimento *et al.*, 2018; Sato *et al.*, 2019). Por otro lado, también pueden actuar como reservorio de factores solubles, incluyendo el factor de crecimiento de fibroblastos (FGF, del inglés fibroblast growth factor) (Kerever *et al.*, 2014) o la proteína morfogenética del hueso (BMP, del inglés bone morphogenetic protein) (Mercier & Douet, 2014). Por último, estudios recientes sugieren que la ECM de la SEZ presenta unas propiedades únicas a nivel de rigidez (Kjell *et al.*, 2020), lo cual también podría ejercer una regulación a nivel de respuestas a estímulos mecánicos. En cuanto a su composición, se sabe que, aun siendo solapante con la vascular, presenta algunas diferencias, especialmente en cuanto a su composición de isoformas de lamininas (LMs) (Sato *et al.*, 2019). Empleando modelos genéticos, se ha determinado que tanto las NSCs como las endodermias podrían contribuir a la formación de los *speckles* (Nascimento *et al.*, 2018; Sato *et al.*, 2019). Sin embargo, el papel de las diferentes poblaciones de NSCs en la generación del nicho de ECM y los mecanismos de la interacción con la misma, son desconocidos.

Debido a que los mecanismos moleculares que regulan la quiescencia de las NSCs no se conocen con exactitud, las qNSCs nunca se han podido cultivar para su mantenimiento *in vitro*, lo cual limita considerablemente su estudio. En este trabajo hemos empleado el tratamiento con BMP4 para inducir quiescencia en cultivos de neuroesferas y generar un estado que se parezca al de las qNSCs *in vivo* (Mira *et al.*, 2010a). Este morfógeno se une a sus receptores (BMPR, del inglés BMP receptor) e inicia cascadas de señalización

Resumen

canónica (a través de SMADs) o no canónica, por ejemplo mediante la señalización por la kinasa c-Jun N-terminal (JNK, del inglés c-Jun N-terminal kinase) o el miembro A de la familia del homólogo de Ras (RhoA, del inglés Ras homolog family member A), regulando la transcripción y mediando múltiples procesos celulares (Derynck & Zhang, 2003; Le Dréau, 2022). *In vivo*, se sabe que las NSCs de la SEZ son susceptibles a la señalización por BMPs (Colak *et al.*, 2008; Lim *et al.*, 2000), y que diferentes ligandos y antagonistas son expresados por distintos elementos del nicho, incluyendo líquido cefalorraquídeo, vasos, o epéndimo (Lim *et al.*, 2000; Obernier & Alvarez-Buylla, 2019; Silva-Vargas *et al.*, 2016). La señalización por BMP tiene un papel clave en el mantenimiento de la quiescencia de las NSCs y en la regulación de transiciones entre quiescencia/activación (Llorens-Bobadilla *et al.*, 2015; Urbán *et al.*, 2019; Yousef *et al.*, 2015). Sin embargo, mientras que los mecanismos por los que actúa han sido considerablemente estudiados en hipocampo, la regulación en la SEZ, está todavía por explorar. En este proyecto, estudiaremos la potencial relación de BMP4 con la secreción de ECM, tema totalmente desconocido hasta el momento.

Para hablar de la respuesta celular a la ECM, es esencial comentar algunos principios básicos de mecanotransducción, proceso por el que una señal extracelular se transmite intracelularmente, a través del citoesqueleto, para generar una respuesta a nivel nuclear (Vining & Mooney, 2017). Tras un reconocimiento bioquímico y/o biomecánico de la matriz, la activación de integrinas promueve el reclutamiento citoplasmático de proteínas adaptadoras (e.j, talina, vinculina) y proteínas de señalización como la kinasa de adhesiones focales (FAK, del inglés focal adhesión kinase) (J. Z. Kechagia *et al.*, 2019). Las adhesiones focales conectan la matriz extracelular al citoesqueleto de actina, lo cual implica la generación de fuerzas que condicionarán el comportamiento celular a través de distintos mecanismos (Wagh *et al.*, 2021).

Para la correcta formación de las fibras de actina, se requiere la señalización a través de las GTPasas Rho, que son activadas por los factores intercambiadores de guaninas (GEFs, del inglés guanine exchange factors) y otras proteínas que finalmente determinarán el estado de activación de sus miembros (Lawson & Burrige, 2014). La activación de RhoA, en concreto, favorecerá la activación de su principal efector, la proteína kinasa asociada a Rho (ROCK, del inglés Rho-associated protein kinase), que participará activamente en la formación de las fibras de actina, al regular tanto la función de la miosina como la polimerización de la actina globular a filamentosa.

En respuesta a la vía de RhoA/ROCK y a la tensión del citoesqueleto, tiene lugar la activación de ciertos programas transcripcionales que condicionan procesos celulares como la proliferación, migración, o morfología (Ege *et al.*, 2018; Lachowski *et al.*, 2018). Esta respuesta está mediada principalmente por la proteína asociada a YES (YAP, del inglés

Yes-associated protein) y su parólogo TAZ, que constituyen los principales efectores de procesos de mecanotransducción (Moya & Halder, 2019). En concreto, actúan como co-activadores de factores de transcripción con dominios TEA (TEAD, del inglés TEA DNA-binding domains), entre otros, regulando la adquisición de programas génicos concretos (Heng *et al.*, 2020; Moya & Halder, 2019). Aunque estos factores se activan bajo diferentes señales como RhoA/ROCK o cambios en la morfología o la rigidez de matriz (Dupont *et al.*, 2011), su vía de activación principal es la vía de Hippo (Seo & Kim, 2018). Se trata de una vía conservada de kinasas que controla el estado de fosforilación y por ende, la activación de YAP/TAZ. Cuando la vía de Hippo está activa, YAP/TAZ se encontrará en su forma fosforilada e inactiva en el citoplasma. En cambio, con su inactivación, YAP/TAZ se activará y translocará al núcleo. A su vez, complicando aún más este escenario, otras vías de señalización, como la mediada por los receptores GPCR o BMPR, también pueden interactuar con la vía de RhoA/ROCK y de Hippo, convergiendo finalmente en la regulación de YAP/TAZ y condicionando en su conjunto las respuestas de adhesión a ECM (Moya *et al.*, 2018).

Objetivos

En este proyecto nos hemos propuesto evaluar los mecanismos moleculares que regulan el estado de activación de las NSCs, especialmente centrándonos en el mantenimiento de su estado quiescente. Este proceso está estrechamente regulado por señales extrínsecas que reciben del nicho especializado en el que residen. Entre ellos, las interacciones mediadas por la ECM son especialmente relevantes y todavía parcialmente desconocidas (Nascimeto *et al.*, 2018; Sato *et al.*, 2019). En este contexto, algunos estudios recientes han sugerido que las NSCs podrían contribuir a la generación de su propio nicho de ECM (Kjell *et al.*, 2020). Sin embargo, las evidencias en cuanto a los potenciales inductores de la deposición de matriz o las respuestas derivadas de la interacción con la misma, son limitadas.

Por ello, hemos propuesto los siguientes objetivos:

1. Analizar la potencial contribución de las NSCs a la ECM del nicho.
2. Estudiar la interacción diferencial de las NSCs con las estructuras de BM.
3. Evaluar el papel de la adhesión a la ECM vascular en la regulación de las NSCs.
4. Testar los mecanismos por los que la potencial matriz secretada por las NSCs modulan su comportamiento.

Material y métodos

Cepas de ratón y su mantenimiento: En este trabajo se han empleado ratones silvestres (wild-type en inglés) de fondo genético C57BL/6J adultos (entre 2-4 meses), comprados en Jackson Laboratory (stock no. 000664) y mantenidos en el estabulario de la Universidad de València (SCIE, Burjassot). Todos los procedimientos fueron aceptados previamente por un comité ético (CEEA: 2015/VSC/PEA/00132 y 00133).

Métodos *in vivo*:

Electroporación *in utero*: Para marcar qNSCs, se electroporaron plásmidos episomales que codifican para proteínas fluorescentes bajo promotores constitutivos (CAG::mRFP o GFP) (Mateos-White *et al.*, 2020). Fueron insertados en el LV del cerebro de embriones en día 15.5 del desarrollo, permitiendo el marcaje de todas las células limítrofes del ventrículo. El plásmido será diluido paulatinamente en las respectivas divisiones celulares y únicamente será retenido en el cerebro adulto en aquellas células que se hayan dividido ninguna o muy pocas veces desde la adquisición del plásmido. Es decir, células que se hayan diferenciado en divisiones tempranas, o las NSCs que se hayan mantenido quiescentes desde su especificación.

FACS para caracterizar el linaje neurogénico: Tras la disección fina de la SEZ, se obtuvieron suspensiones celulares empleando el sistema “gentleMACS” (Cat. 130-096-334) con el kit de disgregación “Neural Tissue Dissociation Kit” (Cat. 130-093-231). Después, se disgregó manualmente, y tras filtrar y centrifugar, los pellets se resuspendieron en 100 µl de tampón de bloqueo de FACS con la combinación de anticuerpos requerida para la estrategia de citometría (Belenguer *et al.*, 2021b) 30 min (*Tabla 1 Anexo*). Se analizó con un citómetro LSR-Fortessa (Benton Dickinson).

Perfusión: Tras anestesiarse a los ratones con ketamina/medetomidina (50-75 mg/kg) intraperitoneal, se perfundieron con NaCl (0.9%) seguido de PFA (4%) para la fijación. Después, se obtuvieron secciones coronales finas (40 µm) empleando un vibratomo VT1000 (Leica).

Inmunohistoquímica: Los cortes o, alternativamente, las preparaciones *in toto* de la SEZ fueron bloqueados durante 1h a temperatura ambiente (RT, del inglés room temperature) con suero de caballo (HS, del inglés horse serum) (10%) para evitar uniones inespecíficas y empleando Triton-X-100 (0.1-0.5 %) para la permeabilización del tejido. Después, se incubaron con los pertinentes anticuerpos primarios y secundarios para su posterior observación (*Tabla 1 Anexo*).

Microscopía: Las imágenes para tejido fijado se obtuvieron con un microscopio confocal

FV10i (Olympus) y un microscopio invertido ECLIPSE Ni-U (Nikon). Para fotografiar células vivas, se empleó un IN Cell Analyzer 2000 con sistema de temperatura y CO₂. Para el estudio de los contactos de qNSCs con la BM, realizamos el clareado de secciones de cerebro (300 µm) empleando el sistema X-Clarity™ (Logos Biosystems) siguiendo las instrucciones de los proveedores. También realizamos un protocolo de microscopía de expansión (Asano *et al.*, 2018), siguiendo el protocolo publicado. Finalmente, realizamos ensayos de microscopía electrónica empleando anticuerpos contra GFP (expresado en las qNSCs por electroporación), conjugados a oro coloidal (1:50, Ultrasmall, Aurion), y, para su observación, se convirtió a plata elemental electrodensa tras una serie de reacciones químicas.

Métodos *in vitro*:

Cultivos primarios de NSCs: Tras la disección de la SEZ, se disgregó con papaina (12 U/ml) (Worthington Biochemical Corporation, 24010-043) con L-cisteína y ácido etilendiaminotetraacético (EDTA, del inglés). Tras 20 min a 37 °C, también se disgregó mecánicamente hasta obtener una solución homogénea. Después, se centrifugó y los pellets se resuspendieron en 4 ml de medio de crecimiento suplementado con factores (*Tabla 8 Anexo*), que se distribuyeron en 8 pocillos de placas de 1 cm² y se cultivaron 7-10 días *in vitro* (DIV, del inglés *days in vitro*) hasta su pase.

Subcultivo de NSCs: Los cultivos se pasaron cada 5 días solo hasta pase 7 para evitar la senescencia celular (Ferrón *et al.*, 2004). Los pases se realizaron mediante disgregación enzimática de las neuroesferas con Acutasa (Sigma, A6964). Tras 10 min de digestión a RT, se terminó de disgregar mecánicamente y las células se lavaron, centrifugaron y resuspendieron en medio completo, para cultivarse a una densidad de 10,000 células/cm².

Tratamiento con BMP4 y cultivo sobre matrices: Para la inducción de quiescencia, se añadió BMP4 (RYD, Cat. 314-BP) a 50 ng/ml en el momento de la siembra de NSCs, y se mantuvieron durante 4 DIV con el tratamiento. El medio condicionado (CM, del inglés *conditioned media*) se recogió, centrifugó para eliminar restos y tras añadir el antagonista de BMP, Noggin (0.4 µg/ml), se empleó como recubrimiento y se mantuvo toda la noche en el incubador. Una vez lavados los recubrimientos, se sembraron las células. Para los ensayos de ROCK, se añadió Y27632 (25 µM) (Sigma, Ref. Y0503) en el momento de la siembra y se mantuvo durante 4 DIV. Para las integrinas, se pre-trató con los bloqueantes de α6 (GoH3 Sigma, 40 µg/ml) o β1-blocking (CD29, Bioscience) 30 min a 40 mg/ml y se lavó previo a la siembra. Las células se analizaron por citometría tras 4DIV.

Sorting aNSCs sobre matriz: Se seleccionaron aNSCs (300 células) de un pool de animales (n=2), empleando un sorter BD FACSAria™ Fusion Flow Cytometer con la estrategia de

Resumen

citometría (Belengue *et al.*, 2021b). Se cultivaron durante 4 DIV sobre las matrices de interés, contando manualmente las células que se dividían o se mantenían como singletes durante 72h.

Ensayo de formación de esferas: Las células se pasaron y se sembraron a muy baja densidad (5 cells/ μ l), para conseguir 1,000 células en 200 μ l y se sembró en pocillos de placas de 96, con 4 pocillos por condición. Tras 6-7 DIV se contó el número de esferas formadas y sus diámetros.

FACS de células *in vitro*: Para evaluar la proliferación de NSCs *in vitro* se empleó el trazador celular DFFDA (Belenguer *et al.*, 2021a). Un millón de células en suspensión de célula única se lavaron con PBS, y resuspendieron con el trazador (2 μ g/ml), manteniéndolas durante 7 min en un baño termostático en oscuridad. Después, se sembraron 20,000 células/cm² y se evaluó su dilución tras 4 DIV por citometría. También se emplearon pulsos de EdU (10 μ M) de 1h para evaluar proliferación, siguiendo las indicaciones del proveedor (Click-iT EdU AlexaFluor 555 Imaging Kit, Thermo Fisher).

Nucleofecciones: Tras la amplificación de los plásmidos empleados, se purificaron con Genopure Plasmid Maxi Kit (Roche, 3143422001) y se confirmaron empleando las enzimas de restricción pertinentes. Se nucleofectó 5-10 millones de NSCs con 4 μ g del plásmido de interés en 90 μ l de tampón (Lonza, vpg-1004), con el nucleofector 2b de Lonza. Las células se cultivaron en medio suplementado con B27 (*Tabla 7 Anexo*) y al día siguiente se lavaron (Debris Removal Solution, Miltenyi) y resembraron, manteniéndose durante 24-48h antes de su análisis por citometría.

Cultivos de endoteliales: Para el cultivo primario de células endoteliales (ECs, del inglés endothelial cells) o el análisis por citometría de las células adheridas *in vivo* a los vasos, se empleó un sistema de aislamiento magnético. La digestión celular se realizó con papaína diluida a 1:10 respecto a la recomendación del proveedor (Miltenyi, 130-093-231), y se emplearon anticuerpos CD31 conjugados a beads magnéticas para la selección magnética de las ECs. En cuanto a las líneas celulares, se emplearon las HUVECs (Merk, SCCE001), que se subcultivaron hasta pase 7 y se sembraron en co-cultivo directo con las NSCs durante 4 DIV. En este contexto, las NSCs se incubaron con el anticuerpo bloqueante de integrina α 6 (GoH3, Sigma, MAB1378) a 40 μ g/ml 30 min en hielo y se lavaron antes de su siembra en co-cultivo durante 4 DIV.

Métodos moleculares:

PCR cuantitativa: El RNA se extrajo con “RNeasy Micro or Mini kit” (Quiagen), se cuantificó con Qubit™ y se retrotranscribió con PrimeScript RT (Takara). Se emplearon sondas Taqman para la PCR (del inglés, polymerase chain reaction) (*Tabla 11 Anexo*).

IP: Se incubó el CM de n=4 cultivos tratados con BMP4 y sus controles con el anticuerpo de LM (5 µg, Novus, NB300-14). Después, se incubó con Dynabeads (Invitrogen, 10003D) y se precipitó la fracción positiva de LM, que se detectó empleando el mismo anticuerpo por WB.

Proteómica: Se realizó una proteómica diferencial de NSCs cultivadas 4 DIV con BMP4, llevada a cabo por el servicio de proteómica de la Universidad de València. Para obtener la librería espectral, las proteínas se eluyeron mediante cromatografía líquida, se analizaron en un espectrómetro de masas nanoESI qQTOD (5600 TripleTOF, ABSCIEX) (tándem masas/masas) en modo adquisición de datos dependiente (DDA, del inglés data dependent acquisition), y se identificaron los péptidos con ProteinPilot. Para la cuantificación, se empleó un software para proteómica con modo de adquisición de datos independiente (DIA, data independent acquisition), DIA-NN 1.8.

Análisis:

Análisis de imagen: Para evaluar la fluorescencia de YAP nuclear y cuantificar parámetros morfológicos en el contexto de la adhesión a matriz, empleamos el programa Fiji y desarrollamos nuestros propios códigos de programación para la cuantificación automatizada.

Análisis bioinformático: La proteómica se analizó a varios niveles: análisis de componentes principales, gráfico MA o análisis de enriquecimiento de *GO terms*. Para los heatmaps, se emplearon los paquetes de R *ComplexHeatmap* (v1.10.2) y *ggplot2* (v3.0.0) packages. Los gráficos de dispersión se generaron con la función *geom_pointdensity* del paquete de R *ggpointdensity*. Los valores de correlación *Spearman* se obtuvieron mediante la función *stat_cor* function del paquete de R *ggpubr*. La función *GOcircle* de R se empleó para generar el gráfico circular de GOs representativos.

Análisis estadístico: Las pruebas estadísticas se realizaron en el software GraphPad Prism (v 9.0.1) con pruebas t de Student o ANOVA de una vía seguida de test Tukey post-hoc.

Resultados

Entender los mecanismos que regulan la heterogeneidad de las NSCs constituye uno de los principales retos de la última década dentro del campo de la neurogénesis (Chaker *et al.*, 2016). En concreto, el estudio de la quiescencia de las NSCs resulta de especial interés, pues comprender los mecanismos que lo regulan activamente son clave para el mantenimiento de la neurogénesis a largo plazo en el nicho. En este trabajo, hemos hecho uso de un sistema de modelado *in vitro* de la quiescencia celular para estudiar este estado. En concreto, hemos tratado neuroesferas con el morfógeno BMP4 (Mira *et al.*, 2010) en diferentes condiciones de cultivo para evaluar la inducción de quiescencia en respuesta al

Resumen

mismo. Hemos determinado que la función de este factor pro-quiescente depende de la presencia de factores mitogénicos, ya que las células no frenan su proliferación de la misma manera cuando se cultivan en bFGF como en presencia del factor de crecimiento epitelial (EGF, del inglés epidermal growth factor). Nuestros datos demuestran que, mientras que con bFGF las NSCs proliferan poco y la inducción de quiescencia es muy sutil, las NSCs en presencia de EGF responden mucho más al tratamiento con BMP4. En concreto, añadir BMP4 en presencia de EGF/bFGF proporciona la mayor eficiencia en el proceso de inducción de quiescencia. Sin embargo, la observación más interesante de estos experimentos fue que en las condiciones de cultivo testadas, observamos que BMP4 favorecía la adhesión de las NSCs, que se disponían con una morfología elongada y emitían proyecciones sobre el fondo de los pocillos. Esta observación nos llevó a valorar la posibilidad de que BMP4, paralelamente a su papel inductor de quiescencia, estuviese participando en la secreción de componentes de la ECM.

Para testar esta hipótesis y estudiar la contribución de la qNSCs en el remodelado de matriz, caracterizamos a nivel proteómico los cambios producidos en las NSCs tratadas con BMP4 con respecto a sus controles (n=4). Así determinamos que BMP4 regulaba los niveles de múltiples proteínas de la ECM (e.j, proteoglicanos, LMs) y proteínas asociadas (e.j, enzimas relacionadas con el remodelado de la ECM), previamente descritos como componentes del *matrisoma*. Se trata de una recopilación de datos con los que han definido un conjunto de genes que codifican para componentes de ECM o asociados a la misma (Naba *et al.*, 2012). Un dato relevante es que, además, parte de estos cambios se asociaban a proteínas específicas del proteoma de la SEZ (Kjell *et al.*, 2020), sugiriendo un papel de BMP4 en definir las propiedades de ECM específicas de este nicho. Estos cambios, además, también los pudimos observar a nivel de secreción al medio extracelular, tal y como confirmamos para la LM. Al valorar la expresión de las proteínas asociadas a la ECM en las poblaciones de NSCs empleando el RNA-seq que realizamos previamente en el laboratorio en el contexto de otro proyecto (Belenguer *et al.*, 2021a, b), observamos que las qNSCs eran sin duda las que presentaban una mayor expresión de genes del matrisoma. Así pues, el modelo de BMP4 estaba induciendo un estado que se parecía en de las qNSCs *in vivo*, donde además, existía una correlación clara entre los cambios producidos entre BMP/controles con qNSCs/aNSCs *in vivo* o DFFDA^{high/low} *in vitro* (Belenguer *et al.*, 2021a), sugiriendo la existencia de una firma molecular de genes relacionados con la ECM asociadas al estado de quiescencia.

Debido al potencial papel de las qNSCs en el remodelado de la ECM, decidimos evaluar cuál era su interacción con las estructuras de BM en la SEZ *in vivo*. Marcamos específicamente las qNSCs mediante la estrategia de electroporación *in utero*, y observamos que éstas tenían una distribución apico-basal heterogénea. Además, nuestros estudios de

microscopía electrónica y de fluorescencia, revelaron un contacto directo entre las qNSCs y las dos estructuras de BM de la SEZ: los speckles y los vasos sanguíneos. Además de por su abundancia en las BMs, nuestras observaciones de secreción de LM en respuesta a BMP4 y la expresión de receptores de LM en las qNSCs *in vivo*, nos hicieron prestar especial atención al estudio de esta familia de proteínas. Para evaluar si las qNSCs estaban especialmente adheridas a estas estructuras de LM en comparación con otros estados de activación, empleamos nuestra estrategia de citometría de flujo (Belenguer *et al.*, 2021a, b), que nos permitió por primera vez estudiar potencial interacción diferencial de las poblaciones de NSCs con las estructuras de BM. Con ello, observamos que las qNSCs estaban rodeadas por LM en mayor medida a nivel de su membrana plasmática en comparación con otras poblaciones de NSCs, lo cual era coherente con nuestros datos de secreción de LM en respuesta a las señales pro-quiescentes y con nuestros estudios de inmunohistoquímica. Además, en cuanto a la interacción con la matriz vascular, observamos que al aislar microvasos cerebrales empleando un sistema de aislamiento magnético de las células CD31⁺, las qNSCs eran arrastradas con las endoteliales, sugiriendo que éstas estaban adheridas a los mismos de forma más estrecha que en otras poblaciones. Esta interacción resultó ser dependiente de integrina $\alpha 6$, uno de los principales receptores de LM, que además, encontramos sobreexpresado en qNSCs *in vivo* e inducido tras el tratamiento *in vitro* con BMP4.

En los siguientes apartados, empleamos ensayos *in vitro* para estudiar paralelamente el efecto regulador de la ECM de los vasos y la ECM secretada por las propias NSCs en respuesta a BMP4. Este tipo de ensayos es muy útil ya que nos permite discernir entre el efecto directo del BMP4 y el efecto indirecto de la ECM secretada en respuesta a BMP4, a la vez que permite testar funcionalmente los mecanismos que condicionan la adhesión y los fenotipos asociados a ella. Determinamos que cultivar las NSCs provenientes de neuroesferas en co-cultivo con células endoteliales o emplear el CM derivado del tratamiento con BMP4 como recubrimiento, frena la proliferación de las NSCs, además de favorecer la adquisición de marcadores asociados con la inducción de un estado de quiescencia (aumento de GLAST y reducción de EGFR). Tanto en un sistema como en el otro, las células se pudieron despegar y sub-cultivar, recuperando el estado proliferativo y volviendo a formar neuroesferas, sugiriendo que las células no estaban diferenciadas. Un detalle relevante del co-cultivo es que la inducción de quiescencia ocurre en dos niveles. En primer lugar, ocurre a través de la interacción directa con la ECM mediada por integrina $\alpha 6$, ya que observamos que su bloqueo inducía proliferación y, por otro lado, a través de BMP4. Detectamos que al añadir Noggin al co-cultivo, el efecto citostático se reducía, lo cual ocurría en paralelo con la reducción en la LM extracelular en las NSCs. La adhesión de las NSCs a la matriz secretada por ellas mismas también participa en la inducción de quiescencia, activándose así

Resumen

un proceso de retroalimentación positiva a través de BMP4.

Por último, nos hemos centrado en estudiar los mecanismos por los que las NSCs interaccionan con la ECM secretada por ellas mismas, y la respuesta celular derivada. Siguiendo con los datos obtenidos para la interacción con la ECM en co-cultivo, bloqueamos la señalización por integrina $\alpha 6$, y observamos que en el caso de adhesión a matriz secretada por las NSCs, el efecto obtenido fue el opuesto al del co-cultivo. Sorprendentemente, el bloqueo estimuló la parada de las NSCs en respuesta a la adhesión. Observamos, además, que este efecto tenía lugar en paralelo a una mayor extensión o esparcimiento de las células sobre la matriz, lo cual es coherente con nuestra idea de la adhesión como factor inductor de la quiescencia. Sin embargo, habría que realizar experimentos adicionales para determinar por qué ocurre este efecto y qué otros receptores están implicados en el proceso.

Debido a que nuestros datos de proteómica señalaban a que algunas de las categorías más representadas en cuanto a las proteínas reguladas por BMP4 eran aquellas relacionadas con el citoesqueleto de actina y la regulación a través de GTPasas Rho, decidimos centrarnos directamente en esta regulación del citoesqueleto aguas-debajo de la interacción con matriz. En este contexto, identificamos que la adhesión de las NSCs a la matriz secretada por ellas era, sin duda, dependiente de la formación de fibras de estrés del citoesqueleto de actina. Observamos que, al bloquear farmacológica o genéticamente el principal efector de la vía de GTPasas, ROCK, afectamos directamente a la adhesión de las NSCs, que volvían a proliferar y formar neuroesferas. En última instancia, la adquisición y mantenimiento de un estado celular concreto, como es el caso de la quiescencia en las NSCs, requiere de la activación de programas transcripcionales que le permitan adquirir su identidad molecular. Por ello, la última parte de la tesis doctoral la hemos centrado en estudiar el potencial papel de los reguladores de la transcripción, YAP/TAZ, que son los principal efectores en las vías de mecanotransducción en respuesta a interacción con matriz (Cai *et al.*, 2021). Aunque no hemos podido determinar si su función en este escenario ocurre aguas-debajo de la activación de ROCK, nuestros experimentos sugieren que cultivar las NSCs sobre la matriz generada por ellas mismas induce la actividad transcripcional de YAP mediada por el factor de transcripción TEAD. Además, hemos realizado ensayos de función en los que hemos determinado que la activación constitutiva de YAP/TAZ favorece, a través de su interacción con TEAD, tanto la adhesión de las NSCs, como la reducción en la proliferación celular. Esto sugiere otro bucle de retroalimentación en el que el potencial efector del proceso de inducción de quiescencia también participa en el proceso de adhesión, amplificando la respuesta a través de mecanismos todavía desconocidos.

Conclusiones

1. La interacción con el nicho de ECM es diferente entre poblaciones de NSCs: las qNSCs están rodeadas de mayores niveles de laminina extracelular y están diferencialmente adheridas a la membrana basal vascular, haciéndolas más susceptibles a señales asociadas a la ECM.
2. Las ECs inducen un estado de quiescencia reversible en las NSCs través de la secreción de BMP4 y de su interacción directa con la ECM.
3. BMP4 induce la adquisición de una firma molecular de proteínas de matriz que correlaciona, a nivel transcripcional, con la firma de las qNSCs *in vivo*.
4. La inducción de quiescencia mediada por BMP4 depende de la estimulación con EGF e induce la secreción y deposición de proteínas de matriz. La adhesión de las NSCs a esta ECM generada por ellas mismas, favorece una parada reversible en el ciclo celular.
5. La quiescencia inducida por la adhesión a la matriz secretada por las NSCs está mediada por integrinas, y es dependiente de la tensión del citoesqueleto de actina regulada a través de ROCK y YAP/TEAD.

Bibliography



- Ahmed, A. K. M. A., Nakagawa, H., Isaksen, T. J., & Yamashita, T. (2022). The effects of Bone Morphogenetic Protein 4 on adult neural stem cell proliferation, differentiation and survival in an in vitro model of ischemic stroke. *Neuroscience Research*, *183*, 17–29. <https://doi.org/10.1016/J.NEURES.2022.07.004>
- Alarcón, C., Zaromytidou, A. I., Xi, Q., Gao, S., Yu, J., Fujisawa, S., Barlas, A., Miller, A. N., Manova-Todorova, K., Macias, M. J., Sapkota, G., Pan, D., & Massagué, J. (2009). Nuclear CDKs drive Smad transcriptional activation and turnover in BMP and TGF-beta pathways. *Cell*, *139*(4), 757–769. <https://doi.org/10.1016/J.CELL.2009.09.035>
- Alcantara Llaguno, S., Chen, J., Kwon, C. H., Jackson, E. L., Li, Y., Burns, D. K., Alvarez-Buylla, A., & Parada, L. F. (2009). Malignant Astrocytomas Originate from Neural Stem/Progenitor Cells in a Somatic Tumor Suppressor Mouse Model. *Cancer Cell*, *15*(1), 45–56. <https://doi.org/10.1016/j.ccr.2008.12.006>
- Alcantara Llaguno, S. R., Xie, X., & Parada, L. F. (2016). Cell of Origin and Cancer Stem Cells in Tumor Suppressor Mouse Models of Glioblastoma. *Cold Spring Harbor Symposia on Quantitative Biology*, *81*(1), 31–36. <https://doi.org/10.1101/SQB.2016.81.030973>
- Altman, J. (1962). Are new neurons formed in the brains of adult mammals? *Science (New York, N.Y.)*, *135*(3509), 1127–1128. <https://doi.org/10.1126/SCIENCE.135.3509.1127>
- Altman, J., & Das, G. D. (1965). Autoradiographic and histological evidence of postnatal hippocampal neurogenesis in rats. *The Journal of Comparative Neurology*, *124*(3), 319–335. <https://doi.org/10.1002/CNE.901240303>
- Andreu-Agulló, C., Morante-Redolat, J. M., Delgado, A. C., & Fariñas, I. (2009). Vascular niche factor PEDF modulates Notch-dependent stemness in the adult subependymal zone. *Nature Neuroscience*, *12*(12), 1514–1523. <https://doi.org/10.1038/NN.2437>
- Aragona, M., Panciera, T., Manfrin, A., Giulitti, S., Michielin, F., Elvassore, N., Dupont, S., & Piccolo, S. (2013). A mechanical checkpoint controls multicellular growth through YAP/TAZ regulation by actin-processing factors. *Cell*, *154*(5), 1047–1059. <https://doi.org/10.1016/j.cell.2013.07.042>
- Asano, S. M., Gao, R., Wassie, A. T., Tillberg, P. W., Chen, F., & Boyden, E. S. (2018). Expansion Microscopy: Protocols for Imaging Proteins and RNA in Cells and Tissues. *Current Protocols in Cell Biology*, *80*(1), 1–41. <https://doi.org/10.1002/cpcb.56>
- Aumailley, M., Bruckner-Tuderman, L., Carter, W. G., Deutzmann, R., Edgar, D., Ekblom, P., Engel, J., Engvall, E., Hohenester, E., Jones, J. C. R., Kleinman, H. K., Marinkovich, M. P., Martin, G. R., Mayer, U., Meneguzzi, G., Miner, J. H., Miyazaki, K., Patarroyo, M., Paulsson, M., ... Yurchenco, P. D. (2005). A simplified laminin nomenclature. *Matrix Biology*, *24*(5), 326–332. <https://doi.org/10.1016/j.matbio.2005.05.006>
- Baker, B. M., & Chen, C. S. (2012). Deconstructing the third dimension-how 3D culture microenvironments alter cellular cues. *Journal of Cell Science*, *125*(13), 3015–3024. <https://doi.org/10.1242/JCS.079509/258092/AM/DECONSTRUCTING-THE-THIRD-DIMENSION-HOW-3D-CULTURE>

Bibliography

- Barker, N., Bartfeld, S., & Clevers, H. (2010). Tissue-resident adult stem cell populations of rapidly self-renewing organs. *Cell Stem Cell*, 7(6), 656–670. <https://doi.org/10.1016/j.stem.2010.11.016>
- Barros, D., Amaral, I. F., & Pêgo, A. P. (2020). Laminin-Inspired Cell-Instructive Microenvironments for Neural Stem Cells. *Biomacromolecules*, 21(2), 276–293. <https://doi.org/10.1021/acs.biomac.9b01319>
- Basak, O., Krieger, T. G., Muraro, M. J., Wiebrands, K., Stange, D. E., Frias-Aldeguer, J., Rivron, N. C., van de Wetering, M., van Es, J. H., van Oudenaarden, A., Simons, B. D., & Clevers, H. (2018). Troy+ brain stem cells cycle through quiescence and regulate their number by sensing niche occupancy. *Proceedings of the National Academy of Sciences of the United States of America*, 115(4), E610–E619. <https://doi.org/10.1073/PNAS.1715911114>
- Baur, K., Abdullah, Y., Mandl, C., Hölzl-Wenig, G., Shi, Y., Edelkraut, U., Khatri, P., Hagenston, A. M., Irmeler, M., Beckers, J., & Ciccolini, F. (2022). A novel stem cell type at the basal side of the subventricular zone maintains adult neurogenesis. *EMBO Reports*, 23(9). <https://doi.org/10.15252/EMBR.202154078>
- Belenguer, G., Domingo-Muelas, A., Ferrón, S. R., Morante-Redolat, J. M., & Fariñas, I. (2016). Isolation, culture and analysis of adult subependymal neural stem cells. *Differentiation; Research in Biological Diversity*, 91(4–5), 28–41. <https://doi.org/10.1016/J.DIFF.2016.01.005>
- Belenguer, G., Duart-Abadia, P., Jordán-Pla, A., Domingo-Muelas, A., Blasco-Chamarro, L., Ferrón, S. R., Morante-Redolat, J. M., & Fariñas, I. (2021a). Adult Neural Stem Cells Are Alerted by Systemic Inflammation through TNF- α Receptor Signaling. *Cell Stem Cell*, 28(2), 285–299.e9. <https://doi.org/10.1016/j.stem.2020.10.016>
- Belenguer, G., Duart-Abadia, P., Domingo-Muelas, A., Morante-Redolat, J. M., & Fariñas, I. (2021b). Cell population analysis of the adult murine subependymal neurogenic lineage by flow cytometry. *STAR Protocols*, 2(2). <https://doi.org/10.1016/J.XPRO.2021.100425>
- Berg, L. K., Larsson, M., Morland, C., & Gundersen, V. (2013). Pre- and postsynaptic localization of NMDA receptor subunits at hippocampal mossy fibre synapses. *Neuroscience*, 230, 139–150. <https://doi.org/10.1016/J.NEUROSCIENCE.2012.10.061>
- Bicker, F., Vasic, V., Horta, G., Ortega, F., Nolte, H., Kavyanifar, A., Keller, S., Stankovic, N. D., Harter, P. N., Benedito, R., Lutz, B., Bäuerle, T., Hartwig, J., Baumgart, J., Krüger, M., Radyushkin, K., Alberi, L., Berninger, B., & Schmidt, M. H. H. (2017). Neurovascular EGFL7 regulates adult neurogenesis in the subventricular zone and thereby affects olfactory perception. *Nature Communications*, 8. <https://doi.org/10.1038/NCOMMS15922>
- Blokzijl, F., De Ligt, J., Jager, M., Sasselli, V., Roerink, S., Sasaki, N., Huch, M., Boymans, S., Kuijk, E., Prins, P., Nijman, I. J., Martincorena, I., Mokry, M., Wiegnerinck, C. L., Middendorp, S., Sato, T., Schwank, G., Nieuwenhuis, E. E. S., Verstegen, M. M. A., ... Van Boxtel, R. (2016). Tissue-specific mutation accumulation in human adult stem cells during life. *Nature*, 538(7624), 260–264. <https://doi.org/10.1038/nature19768>

- Blomfield, I. M., Rocamonde, B., del Mar Masdeu, M., Mulugeta, E., Vaga, S., van den Berg, D. L. C., Huillard, E., Guillemot, F., & Urbán, N. (2019). Id4 promotes the elimination of the pro-activation factor *Ascl1* to maintain quiescence of adult hippocampal stem cells. *ELife*, 8. <https://doi.org/10.7554/ELIFE.48561>
- Bonaguidi, M. A., Peng, C. Y., McGuire, T., Falciglia, G., Gobeske, K. T., Czeisler, C., & Kessler, J. A. (2008). Noggin expands neural stem cells in the adult hippocampus. *The Journal of Neuroscience: The Official Journal of the Society for Neuroscience*, 28(37), 9194–9204. <https://doi.org/10.1523/JNEUROSCI.3314-07.2008>
- Bonaguidi, M. A., Wheeler, M. A., Shapiro, J. S., Stadel, R. P., Sun, G. J., Ming, G. L., & Song, H. (2011). In vivo clonal analysis reveals self-renewing and multipotent adult neural stem cell characteristics. *Cell*, 145(7), 1142–1155. <https://doi.org/10.1016/j.cell.2011.05.024>
- Bond, A. M., Peng, C. Y., Meyers, E. A., McGuire, T., Ewaleifoh, O., & Kessler, J. A. (2014). BMP signaling regulates the tempo of adult hippocampal progenitor maturation at multiple stages of the lineage. *Stem Cells (Dayton, Ohio)*, 32(8), 2201–2214. <https://doi.org/10.1002/STEM.1688>
- Bonnans, C., Chou, J., & Werb, Z. (2014). Remodelling the extracellular matrix in development and disease. *Nature Reviews Molecular Cell Biology*, 15(12), 786–801. <https://doi.org/10.1038/nrm3904>
- Böttcher, R. T., Veelders, M., Rombaut, P., Faix, J., Theodosiou, M., Stradal, T. E., Rottner, K., Zent, R., Herzog, F., & Fässler, R. (2017). Kindlin-2 recruits paxillin and Arp2/3 to promote membrane protrusions during initial cell spreading. *Journal of Cell Biology*, 216(11), 3785–3798. <https://doi.org/10.1083/jcb.201701176>
- Burd, G. D., & Nottebohm, F. (1985). Ultrastructural characterization of synaptic terminals formed on newly generated neurons in a song control nucleus of the adult canary forebrain. *The Journal of Comparative Neurology*, 240(2), 143–152. <https://doi.org/10.1002/CNE.902400204>
- Byron, A., Humphries, J. D., & Humphries, M. J. (2013). Defining the extracellular matrix using proteomics. *International Journal of Experimental Pathology*, 94(2), 75–92. <https://doi.org/10.1111/iep.12011>
- Cai, X., Wang, K. C., & Meng, Z. (2021). Mechanoregulation of YAP and TAZ in Cellular Homeostasis and Disease Progression. *Frontiers in Cell and Developmental Biology*, 9(May), 1–12. <https://doi.org/10.3389/fcell.2021.673599>
- Capela, A., & Temple, S. (2002). *LeX/ssea-1* is expressed by adult mouse CNS stem cells, identifying them as nonependymal. *Neuron*, 35(5), 865–875. [https://doi.org/10.1016/S0896-6273\(02\)00835-8](https://doi.org/10.1016/S0896-6273(02)00835-8)
- Case, L. B., & Waterman, C. M. (2015). Integration of actin dynamics and cell adhesion by a three-dimensional, mechanosensitive molecular clutch. *Nature Cell Biology*, 17(8), 955–963. <https://doi.org/10.1038/ncb3191>
- Cebrian-Silla, A., Nascimento, M. A., Redmond, S. A., Mansky, B., Wu, D., Obernier, K., Rodri-

Bibliography

guez, R. R., Gonzalez-Granero, S., Garcia-Verdugo, J. M., Lim, D. A., & Alvarez-Buylla, A. (2021). Single-cell analysis of the ventricular-subventricular zone reveals signatures of dorsal and ventral adult neurogenic lineages. *ELife*, *10*, 1–34. <https://doi.org/10.7554/eLife.67436>

Chaker, Z., Codega, P., & Doetsch, F. (2016). A mosaic world: puzzles revealed by adult neural stem cell heterogeneity. *Wiley Interdisciplinary Reviews. Developmental Biology*, *5*(6), 640–658. <https://doi.org/10.1002/WDEV.248>

Clement, J. H., Sanger, J., & Hoffken, K. (1999). Expression of bone morphogenetic protein 6 in normal mammary tissue and breast cancer cell lines and its regulation by epidermal growth factor. *International Journal of Cancer*, *80*(2), 250–256. [https://doi.org/10.1002/\(sici\)1097-0215\(19990118\)80:2<250::aid-ijc14>3.0.co;2-d](https://doi.org/10.1002/(sici)1097-0215(19990118)80:2<250::aid-ijc14>3.0.co;2-d)

Codega, P., Silva-Vargas, V., Paul, A., Maldonado-Soto, A. R., DeLeo, A. M., Pastrana, E., & Doetsch, F. (2014). Prospective identification and purification of quiescent adult neural stem cells from their in vivo niche. *Neuron*, *82*(3), 545–559. <https://doi.org/10.1016/J.NEURON.2014.02.039>

Colak, D., Mori, T., Brill, M. S., Pfeifer, A., Falk, S., Deng, C., Monteiro, R., Mummery, C., Sommer, L., & Gotz, M. (2008). Adult neurogenesis requires Smad4-mediated bone morphogenic protein signaling in stem cells. *The Journal of Neuroscience : The Official Journal of the Society for Neuroscience*, *28*(2), 434–446. <https://doi.org/10.1523/JNEUROSCI.4374-07.2008>

Cope, E. C., & Gould, E. (2019). Adult Neurogenesis, Glia, and the Extracellular Matrix. *Cell Stem Cell*, *24*(5), 690–705. <https://doi.org/10.1016/j.stem.2019.03.023>

Cordenonsi, M., Zanconato, F., Azzolin, L., Forcato, M., Rosato, A., Frasson, C., Inui, M., Montagner, M., Parenti, A. R., Poletti, A., Daidone, M. G., Dupont, S., Basso, G., Bicciato, S., & Piccolo, S. (2011). The hippo transducer TAZ confers cancer stem cell-related traits on breast cancer cells. *Cell*, *147*(4), 759–772. <https://doi.org/10.1016/j.cell.2011.09.048>

Crouch, E. E., Liu, C., Silva-Vargas, V., & Doetsch, F. (2015). Regional and stage-specific effects of prospectively purified vascular cells on the adult V-SVZ neural stem cell lineage. *The Journal of Neuroscience : The Official Journal of the Society for Neuroscience*, *35*(11), 4528–4539. <https://doi.org/10.1523/JNEUROSCI.1188-14.2015>

Culver, J. C., Vadakkan, T. J., & Dickinson, M. E. (2013). A specialized microvascular domain in the mouse neural stem cell niche. *PLoS One*, *8*(1). <https://doi.org/10.1371/JOURNAL.PONE.0053546>

Davies, S. P., Reddy, H., Caivano, M., & Cohen, P. (2000). Specificity and mechanism of action of some commonly used protein kinase inhibitors. *The Biochemical Journal*, *351*(Pt 1), 95–105. <https://doi.org/10.1042/0264-6021:3510095>

Daynac, M., Pineda, J. R., Chicheportiche, A., Gauthier, L. R., Morizur, L., Boussin, F. D., & Mouthon, M. A. (2014). TGF β lengthens the G1 phase of stem cells in aged mouse brain. *Stem Cells (Dayton, Ohio)*, *32*(12), 3257–3265. <https://doi.org/10.1002/STEM.1815>

Deepa, S. S., Carulli, D., Galtrey, C., Rhodes, K., Fukuda, J., Mikami, T., Sugahara, K., & Fawcett,

- J. W. (2006). Composition of perineuronal net extracellular matrix in rat brain: a different disaccharide composition for the net-associated proteoglycans. *The Journal of Biological Chemistry*, 281(26), 17789–17800. <https://doi.org/10.1074/JBC.M600544200>
- Delgado, A. C., Ferrón, S. R., Vicente, D., Porlan, E., Perez-Villalba, A., Trujillo, C. M., D'Ocón, P., & Fariñas, I. (2014). Endothelial NT-3 delivered by vasculature and CSF promotes quiescence of subependymal neural stem cells through nitric oxide induction. *Neuron*, 83(3), 572–585. <https://doi.org/10.1016/J.NEURON.2014.06.015>
- Derynck, R., & Zhang, Y. E. (2003). Smad-dependent and Smad-independent pathways in TGF-beta family signalling. *Nature*, 425(6958), 577–584. <https://doi.org/10.1038/NATURE02006>
- Dey, A., Varelas, X., & Guan, K. L. (2020). Targeting the Hippo pathway in cancer, fibrosis, wound healing and regenerative medicine. *Nature Reviews. Drug Discovery*, 19(7), 480–494. <https://doi.org/10.1038/S41573-020-0070-Z>
- Discher, D. E., Mooney, D. J., & Zandstra, P. W. (2009). Growth factors, matrices, and forces combine and control stem cells. *Science (New York, N.Y.)*, 324(5935), 1673–1677. <https://doi.org/10.1126/SCIENCE.1171643>
- Dityatev, A., & Rusakov, D. A. (2011). Molecular signals of plasticity at the tetrapartite synapse. *Current Opinion in Neurobiology*, 21(2), 353–359. <https://doi.org/10.1016/J.CONB.2010.12.006>
- Dityatev, A., Schachner, M., & Sonderegger, P. (2010). The dual role of the extracellular matrix in synaptic plasticity and homeostasis. *Nature Reviews Neuroscience*, 11(11), 735–746. <https://doi.org/10.1038/nrn2898>
- Doetsch, F., Caille, I., Lim, D. A., Garcia-Verdugo, J. M., & Alvarez-Buylla, A. (1999). Subventricular zone astrocytes are neural stem cells in the adult mammalian brain. *Cell*, 97(6), 703–716. [https://doi.org/10.1016/S0092-8674\(00\)80783-7](https://doi.org/10.1016/S0092-8674(00)80783-7)
- Doetsch, Fiona. (2003). The glial identity of neural stem cells. *Nature Neuroscience*, 6(11), 1127–1134. <https://doi.org/10.1038/NN1144>
- Doetsch, Fiona, García-Verdugo, J. M., & Alvarez-Buylla, A. (1997). Cellular composition and three-dimensional organization of the subventricular germinal zone in the adult mammalian brain. *The Journal of Neuroscience : The Official Journal of the Society for Neuroscience*, 17(13), 5046–5061. <https://doi.org/10.1523/JNEUROSCI.17-13-05046.1997>
- Domen, J., & Weissman, I. L. (2000). Hematopoietic stem cells need two signals to prevent apoptosis; BCL-2 can provide one of these, Kitl/c-Kit signaling the other. *Journal of Experimental Medicine*, 192(12), 1707–1718. <https://doi.org/10.1084/jem.192.12.1707>
- Douet, V., Arikawa-Hirasawa, E., & Mercier, F. (2012). Fractone-heparan sulfates mediate BMP-7 inhibition of cell proliferation in the adult subventricular zone. *Neuroscience Letters*, 528(2), 120–125. <https://doi.org/10.1016/j.neulet.2012.08.077>

Bibliography

- Dulken, B. W., Leeman, D. S., Boutet, S. C., Hebestreit, K., & Brunet, A. (2017). Single-Cell Transcriptomic Analysis Defines Heterogeneity and Transcriptional Dynamics in the Adult Neural Stem Cell Lineage. *Cell Reports*, *18*(3), 777–790. <https://doi.org/10.1016/J.CELREP.2016.12.060>
- Dupont, S., Morsut, L., Aragona, M., Enzo, E., Giulitti, S., Cordenonsi, M., Zanconato, F., Le Digabel, J., Forcato, M., Bicciato, S., Elvassore, N., & Piccolo, S. (2011). Role of YAP/TAZ in mechanotransduction. *Nature*, *474*(7350), 179–184. <https://doi.org/10.1038/nature10137>
- Ege, N., Dowbaj, A. M., Jiang, M., Howell, M., Hooper, S., Foster, C., Jenkins, R. P., & Sahai, E. (2018). Quantitative Analysis Reveals that Actin and Src-Family Kinases Regulate Nuclear YAP1 and Its Export. *Cell Systems*, *6*(6), 692–708.e13. <https://doi.org/10.1016/j.cels.2018.05.006>
- Elosegui-Artola, A., Bazellières, E., Allen, M. D., Andreu, I., Oria, R., Sunyer, R., Gomm, J. J., Marshall, J. F., Jones, J. L., Trepap, X., & Roca-Cusachs, P. (2014). Rigidity sensing and adaptation through regulation of integrin types. *Nature Materials*, *13*(6), 631–637. <https://doi.org/10.1038/nmat3960>
- Elosegui-Artola, A., Oria, R., Chen, Y., Kosmalska, A., Pérez-González, C., Castro, N., Zhu, C., Trepap, X., & Roca-Cusachs, P. (2016). Mechanical regulation of a molecular clutch defines force transmission and transduction in response to matrix rigidity. *Nature Cell Biology*, *18*(5), 540–548. <https://doi.org/10.1038/ncb3336>
- Engler, A. J., Sen, S., Sweeney, H. L., & Discher, D. E. (2006). Matrix Elasticity Directs Stem Cell Lineage Specification. *Cell*, *126*(4), 677–689. <https://doi.org/10.1016/j.cell.2006.06.044>
- Ermolaeva, M., Neri, F., Ori, A., & Rudolph, K. L. (2018). Cellular and epigenetic drivers of stem cell ageing. In *Nature Reviews Molecular Cell Biology* (Vol. 19, Issue 9, pp. 594–610). Nature Publishing Group. <https://doi.org/10.1038/s41580-018-0020-3>
- Faissner, A., Roll, L., & Theodoridis, U. (2017). Tenascin-C in the matrix of neural stem and progenitor cells. *Molecular and Cellular Neurosciences*, *81*, 22–31. <https://doi.org/10.1016/J.MCN.2016.11.003>
- Fan, W., Jurado-Arjona, J., Alanis-Lobato, G., Péron, S., Berger, C., Andrade-Navarro, M. A., Falk, S., & Berninger, B. (2022). Role of Yap1 in adult neural stem cell activation. *BioRxiv*, 2022.01.12.475985. [https://www.biorxiv.org/content/10.1101/2022.01.12.475985](https://www.biorxiv.org/content/10.1101/2022.01.12.475985v1%0Ahttps://www.biorxiv.org/content/10.1101/2022.01.12.475985v1.abstract). <https://www.biorxiv.org/content/10.1101/2022.01.12.475985v1.abstract>
- Ferrer-Ferrer, M., & Dityatev, A. (2018). Shaping Synapses by the Neural Extracellular Matrix. *Frontiers in Neuroanatomy*, *12*. <https://doi.org/10.3389/FNANA.2018.00040>
- Ferrón, S., Mira, H., Franco, S., Cano-Jimenez, M., Bellmunt, E., Ramírez, C., Fariñas, I., & Blasco, M. A. (2004). Telomere shortening and chromosomal instability abrogates proliferation of adult but not embryonic neural stem cells. *Development (Cambridge, England)*, *131*(16), 4059–4070. <https://doi.org/10.1242/DEV.01215>
- Foletta, V. C., Lim, M. A., Soosairajah, J., Kelly, A. P., Stanley, E. G., Shannon, M., He, W., Das,

- S., Massagué, J., & Bernard, O. (2003). Direct signaling by the BMP type II receptor via the cytoskeletal regulator LIMK1. *The Journal of Cell Biology*, *162*(6), 1089–1098. <https://doi.org/10.1083/JCB.200212060>
- Fuentealba, L. C., Rompani, S. B., Parraguez, J. I., Obernier, K., Romero, R., Cepko, C. L., & Alvarez-Buylla, A. (2015). Embryonic Origin of Postnatal Neural Stem Cells. *Cell*, *161*(7), 1644–1655. <https://doi.org/10.1016/J.CELL.2015.05.041>
- Gajera, C. R., Emich, H., Liubinski, O., Christ, A., Beckervordersandforth-Bonk, R., Yoshikawa, K., Bachmann, S., Christensen, E. I., Götz, M., Kempermann, G., Peterson, A. S., Willnow, T. E., & Hammes, A. (2010). LRP2 in ependymal cells regulates BMP signaling in the adult neurogenic niche. *Journal of Cell Science*, *123*(Pt 11), 1922–1930. <https://doi.org/10.1242/JCS.065912>
- Gilbert, P. M., Havenstrite, K. L., Magnusson, K. E. G., Sacco, A., Leonardi, N. A., Kraft, P., Nguyen, N. K., Thrun, S., Lutolf, M. P., & Blau, H. M. (2010). Substrate elasticity regulates skeletal muscle stem cell self-renewal in culture. *Science (New York, N.Y.)*, *329*(5995), 1078–1081. <https://doi.org/10.1126/SCIENCE.1191035>
- Gómez-Gaviro, M. V., Scott, C. E., Sesay, A. K., Matheu, A., Booth, S., Galichet, C., & Lovell-Badge, R. (2012). Betacellulin promotes cell proliferation in the neural stem cell niche and stimulates neurogenesis. *Proceedings of the National Academy of Sciences of the United States of America*, *109*(4), 1317–1322. <https://doi.org/10.1073/PNAS.1016199109/-/DCSUPPLEMENTAL/PNAS.201016199SI.PDF>
- Goodell, M. A., & Rando, T. A. (2015). Stem cells and healthy aging. *Science*, *350*(6265), 1199–1204. <https://doi.org/10.1126/science.aab3388>
- Hamelers, I. H. L., Olivo, C., Mertens, A. E. E., Michiel Pegtel, D., Van Der Kammen, R. A., Sonnenberg, A., & Collard, J. G. (2005). The Rac activator Tiam1 is required for (alpha)3(beta)1-mediated laminin-5 deposition, cell spreading, and cell migration. *The Journal of Cell Biology*, *171*(5), 871–881. <https://doi.org/10.1083/JCB.200509172>
- Heng, B. C., Zhang, X., Aubel, D., Bai, Y., Li, X., Wei, Y., Fussenegger, M., & Deng, X. (2020). Role of YAP/TAZ in Cell Lineage Fate Determination and Related Signaling Pathways. *Frontiers in Cell and Developmental Biology*, *8*(July), 1–23. <https://doi.org/10.3389/fcell.2020.00735>
- Hohenester, E. (2019). Structural biology of laminins. *Essays in Biochemistry*, *63*(3), 285–295. <https://doi.org/10.1042/EBC20180075>
- Hohenester, E., & Yurchenco, P. D. (2013). Laminins in basement membrane assembly. *Cell Adhesion & Migration*, *7*(1), 56–63. <https://doi.org/10.4161/CAM.21831>
- Hynes, R. O. (2002). Integrins: Bidirectional, allosteric signaling machines. *Cell*, *110*(6), 673–687. [https://doi.org/10.1016/S0092-8674\(02\)00971-6](https://doi.org/10.1016/S0092-8674(02)00971-6)
- Hynes, R. O. (2009). The extracellular matrix: not just pretty fibrils. *Science (New York, N.Y.)*, *326*(5957), 1216–1219. <https://doi.org/10.1126/SCIENCE.1176009>

Bibliography

- Iadecola, C. (2017). The neurovascular unit coming of age: a journey through neurovascular coupling in health and disease. *Neuron*, *96*(1), 17–42. <https://doi.org/10.1016/j.neuron.2017.07.030>
- Ito, K., & Suda, T. (2014). Metabolic requirements for the maintenance of self-renewing stem cells. *Nature Reviews Molecular Cell Biology* *2014* *15*:4, *15*(4), 243–256. <https://doi.org/10.1038/nrm3772>
- Itoh, S., & ten Dijke, P. (2007). Negative regulation of TGF-beta receptor/Smad signal transduction. *Current Opinion in Cell Biology*, *19*(2), 176–184. <https://doi.org/10.1016/J.CEB.2007.02.015>
- Johnson, R., & Halder, G. (2014). The two faces of Hippo: Targeting the Hippo pathway for regenerative medicine and cancer treatment. *Nature Reviews Drug Discovery*, *13*(1), 63–79. <https://doi.org/10.1038/nrd4161>
- Kalamakis, G., Brüne, D., Ravichandran, S., Bolz, J., Fan, W., Ziebell, F., Stiehl, T., Catalá-Martinez, F., Kupke, J., Zhao, S., Llorens-Bobadilla, E., Bauer, K., Limpert, S., Berger, B., Christen, U., Schmezer, P., Mallm, J. P., Berninger, B., Anders, S., ... Martin-Villalba, A. (2019). Quiescence Modulates Stem Cell Maintenance and Regenerative Capacity in the Aging Brain. *Cell*, *176*(6), 1407-1419.e14. <https://doi.org/10.1016/j.cell.2019.01.040>
- Karakatsani, A., Shah, B., & Ruiz de Almodovar, C. (2019). Blood vessels as regulators of neural stem cell properties. *Frontiers in Molecular Neuroscience*, *12*(April), 1–11. <https://doi.org/10.3389/fnmol.2019.00085>
- Katsimpardi, L., Litterman, N. K., Schein, P. A., Miller, C. M., Loffredo, F. S., Wojtkiewicz, G. R., Chen, J. W., Lee, R. T., Wagers, A. J., & Rubin, L. L. (2014). *Vascular and neurogenic rejuvenation of the aging mouse brain by young systemic factors*. *344*(6184), 630–634. <https://doi.org/10.1126/science.1251141>.Vascular
- Kawaguchi, D., Furutachi, S., Kawai, H., Hozumi, K., & Gotoh, Y. (2013). Dll1 maintains quiescence of adult neural stem cells and segregates asymmetrically during mitosis. *Nature Communications*, *4*. <https://doi.org/10.1038/NCOMMS2895>
- Kazanis, I., & Ffrench-Constant, C. (2011). Extracellular matrix and the neural stem cell niche. *Developmental Neurobiology*, *71*(11), 1006–1017. <https://doi.org/10.1002/DNEU.20970>
- Kazanis, I., Lathia, J. D., Vadakkan, T. J., Raborn, E., Wan, R., Mughal, M. R., Eckley, D. M., Sasaki, T., Patton, B., Mattson, M. P., Hirschi, K. K., Dickinson, M. E., & Ffrench-Constant, C. (2010b). Quiescence and activation of stem and precursor cell populations in the subependymal zone of the mammalian brain are associated with distinct cellular and extracellular matrix signals. *The Journal of Neuroscience : The Official Journal of the Society for Neuroscience*, *30*(29), 9771–9781. <https://doi.org/10.1523/JNEUROSCI.0700-10.2010>
- Kechagia, J. Z., Ivaska, J., & Roca-Cusachs, P. (2019). Integrins as biomechanical sensors of the microenvironment. *Nature Reviews Molecular Cell Biology*, *20*(8), 457–473. <https://doi.org/10.1038/s41580-019-0134-2>

- Kechagia, Z., Sáez, P., Gómez-González, M., Zamarbide, M., Andreu, I., Koorman, T., Beedle, A. E. M., Derksen, P. W. B., Trepas, X., Arroyo, M., & Roca-Cusachs, P. (2022). The laminin-keratin link shields the nucleus from mechanical deformation and signalling. *BioRxiv*, 2022.03.01.482474. <https://doi.org/10.1101/2022.03.01.482474>
- Kerever, A., & Arikawa-Hirasawa, E. (2021). Optimal Extracellular Matrix Niches for Neurogenesis: Identifying Glycosaminoglycan Chain Composition in the Subventricular Neurogenic Zone. *Frontiers in Neuroanatomy*, 15(October), 4–10. <https://doi.org/10.3389/fnana.2021.764458>
- Kerever, A., Mercier, F., Nonaka, R., de Vega, S., Oda, Y., Zalc, B., Okada, Y., Hattori, N., Yamada, Y., & Arikawa-Hirasawa, E. (2014). Perlecan is required for FGF-2 signaling in the neural stem cell niche. *Stem Cell Research*, 12(2), 492–505. <https://doi.org/10.1016/J.SCR.2013.12.009>
- Kerever, A., Nagahara, F., Keino-Masu, K., Masu, M., Van Kuppevelt, T. H., Vivès, R. R., & Arikawa-Hirasawa, E. (2021). Regulation of fractone heparan sulfate composition in young and aged subventricular zone neurogenic niches. *Glycobiology*, 31(11), 1531–1542. <https://doi.org/10.1093/glycob/cwab081>
- Kerever, A., Schnack, J., Vellinga, D., Ichikawa, N., Moon, C., Arikawa-Hirasawa, E., Efrid, J. T., & Mercier, F. (2007). Novel Extracellular Matrix Structures in the Neural Stem Cell Niche Capture the Neurogenic Factor Fibroblast Growth Factor 2 from the Extracellular Milieu. *Stem Cells*, 25(9), 2146–2157. <https://doi.org/10.1634/stemcells.2007-0082>
- Kerever, A., Yamada, T., Suzuki, Y., Mercier, F., & Arikawa-Hirasawa, E. (2015). Fractone aging in the subventricular zone of the lateral ventricle. *Journal of Chemical Neuroanatomy*, 66–67, 52–60. <https://doi.org/10.1016/j.jchemneu.2015.06.001>
- Keung, A. J., De Juan-Pardo, E. M., Schaffer, D. V., & Kumar, S. (2011). Rho GTPases mediate the mechanosensitive lineage commitment of neural stem cells. *Stem Cells (Dayton, Ohio)*, 29(11), 1886–1897. <https://doi.org/10.1002/STEM.746>
- Khalilgharibi, N., & Mao, Y. (2021a). To form and function: On the role of basement membrane mechanics in tissue development, homeostasis and disease. *Open Biology*, 11(2). <https://doi.org/10.1098/rsob.200360>
- Khalilgharibi, N., & Mao, Y. (2021b). To form and function: on the role of basement membrane mechanics in tissue development, homeostasis and disease. *Open Biology*, 11(2). <https://doi.org/10.1098/RSOB.200360>
- Kim, H. J., Lee, E., Nam, M., Chung, J. K., Joo, S., Nam, Y., & Sun, W. (2021). Contribution of Extracellular Matrix Component Landscapes in the Adult Subventricular Zone to the Positioning of Neural Stem/Progenitor Cells. *Experimental Neurobiology*, 30(4), 275–284. <https://doi.org/10.5607/EN21012>
- Kim, N. G., & Gumbiner, B. M. (2015). Adhesion to fibronectin regulates Hippo signaling via the FAK-Src-PI3K pathway. *Journal of Cell Biology*, 210(3), 503–515. <https://doi.org/10.1083/jcb.201501025>

Bibliography

Kjell, J., Fischer-Sternjak, J., Thompson, A. J., Friess, C., Sticco, M. J., Salinas, F., Cox, J., Martinelli, D. C., Ninkovic, J., Franze, K., Schiller, H. B., & Götz, M. (2020). Defining the Adult Neural Stem Cell Niche Proteome Identifies Key Regulators of Adult Neurogenesis. *Cell Stem Cell*, 26(2), 277–293.e8. <https://doi.org/10.1016/j.stem.2020.01.002>

Kobayashi, T., Piao, W., Takamura, T., Kori, H., Miyachi, H., Kitano, S., Iwamoto, Y., Yamada, M., Imayoshi, I., Shioda, S., Ballabio, A., & Kageyama, R. (2019). Enhanced lysosomal degradation maintains the quiescent state of neural stem cells. *Nature Communications*, 10(1), 2–4. <https://doi.org/10.1038/s41467-019-13203-4>

Kokovay, E., Goderie, S., Wang, Y., Lotz, S., Lin, G., Sun, Y., Roysam, B., Shen, Q., & Temple, S. (2010). Adult svz lineage cells home to and leave the vascular niche via differential responses to SDF1/CXCR4 signaling. *Cell Stem Cell*, 7(2), 163–173. <https://doi.org/10.1016/j.stem.2010.05.019>

Kokovay, E., Wang, Y., Kusek, G., Wurster, R., Lederman, P., Lowry, N., Shen, Q., & Temple, S. (2012). VCAM1 is essential to maintain the structure of the SVZ niche and acts as an environmental sensor to regulate SVZ lineage progression. *Cell Stem Cell*, 11(2), 220–230. <https://doi.org/10.1016/J.STEM.2012.06.016>

Lachowski, D., Cortes, E., Robinson, B., Rice, A., Rombouts, K., & Del Río Hernández, A. E. (2018). FAK controls the mechanical activation of YAP, a transcriptional regulator required for durotaxis. *FASEB Journal : Official Publication of the Federation of American Societies for Experimental Biology*, 32(2), 1099–1107. <https://doi.org/10.1096/FJ.201700721R>

Lathia, J. D., Patton, B., Eckley, D. M., Magnus, T., Mughal, M. R., Sasaki, T., Caldwell, M. A., Rao, M. S., Mattson, M. P., & Ffrench-Constant, C. (2007). Patterns of laminins and integrins in the embryonic ventricular zone of the CNS. *The Journal of Comparative Neurology*, 505(6), 630–643. <https://doi.org/10.1002/CNE.21520>

Lawson, C. D., & Burrridge, K. (2014). The on-off relationship of Rho and Rac during integrin-mediated adhesion and cell migration. *Small GTPases*, 5(MAR). <https://doi.org/10.4161/sgtp.27958>

Le Dréau, G. (2022). BuMPing Into Neurogenesis: How the Canonical BMP Pathway Regulates Neural Stem Cell Divisions Throughout Space and Time. *Frontiers in Neuroscience*, 15(January). <https://doi.org/10.3389/fnins.2021.819990>

LeBleu, V. S., MacDonald, B., & Kalluri, R. (2007). Structure and function of basement membranes. *Experimental Biology and Medicine (Maywood, N.J.)*, 232(9), 1121–1129. <https://doi.org/10.3181/0703-MR-72>

Lee, J. H., Lee, J. E., Kahng, J. Y., Kim, S. H., Park, J. S., Yoon, S. J., Um, J. Y., Kim, W. K., Lee, J. K., Park, J., Kim, E. H., Lee, J. H., Lee, J. H., Chung, W. S., Ju, Y. S., Park, S. H., Chang, J. H., Kang, S. G., & Lee, J. H. (2018). Human glioblastoma arises from subventricular zone cells with low-level driver mutations. *Nature*, 560(7717), 243–247. <https://doi.org/10.1038/s41586-018-0389-3>

Leeman, D. S., Hebestreit, K., Ruetz, T., Webb, A. E., McKay, A., Pollina, E. A., Dulken, B. W.,

- Zhao, X., Yeo, R. W., Ho, T. T., Mahmoudi, S., Devarajan, K., Passequé, E., Rando, T. A., Frydman, J., & Brunet, A. (2018). Lysosome activation clears aggregates and enhances quiescent neural stem cell activation during aging. *Science (New York, N.Y.)*, *359*(6381), 1277–1283. <https://doi.org/10.1126/SCIENCE.AAG3048>
- Leonhardt, H., & Desaga, U. (1975). Recent observations on ependyma and subependymal basement membranes. *Acta Neurochirurgica*, *31*(3–4), 153–159. <https://doi.org/10.1007/BF01406287>
- Li, Y., Hibbs, M. A., Gard, A. L., Shylo, N. A., & Yun, K. (2012). Genome-wide analysis of N1ICD/RBPJ targets in vivo reveals direct transcriptional regulation of Wnt, SHH, and hippo pathway effectors by Notch1. *Stem Cells (Dayton, Ohio)*, *30*(4), 741–752. <https://doi.org/10.1002/STEM.1030>
- Liddington, R. C., & Ginsberg, M. H. (2002). Integrin activation takes shape. *The Journal of Cell Biology*, *158*(5), 833–839. <https://doi.org/10.1083/JCB.200206011>
- Lim, D. A., Tramontin, A. D., Trevejo, J. M., Herrera, D. G., García-Verdugo, J. M., & Alvarez-Buylla, A. (2000). Noggin antagonizes BMP signaling to create a niche for adult neurogenesis. *Neuron*, *28*(3), 713–726. [https://doi.org/10.1016/S0896-6273\(00\)00148-3](https://doi.org/10.1016/S0896-6273(00)00148-3)
- Llorens-Bobadilla, E., Zhao, S., Baser, A., Saiz-Castro, G., Zwadlo, K., & Martin-Villalba, A. (2015). Single-Cell Transcriptomics Reveals a Population of Dormant Neural Stem Cells that Become Activated upon Brain Injury. *Cell Stem Cell*, *17*(3), 329–340. <https://doi.org/10.1016/J.STEM.2015.07.002>
- Louissaint, A., Rao, S., Leventhal, C., & Goldman, S. A. (2002). Coordinated interaction of neurogenesis and angiogenesis in the adult songbird brain. *Neuron*, *34*(6), 945–960. [https://doi.org/10.1016/S0896-6273\(02\)00722-5](https://doi.org/10.1016/S0896-6273(02)00722-5)
- Manzari-Tavakoli, A., Babajani, A., Farjoo, M. H., Hajinasrollah, M., Bahrami, S., & Niknejad, H. (2022). The Cross-Talks Among Bone Morphogenetic Protein (BMP) Signaling and Other Prominent Pathways Involved in Neural Differentiation. *Frontiers in Molecular Neuroscience*, *15*. <https://doi.org/10.3389/FNMOL.2022.827275>
- Marjoram, R. J., Lessey, E. C., & Burridge, K. (2014). Regulation of RhoA activity by adhesion molecules and mechanotransduction. *Current Molecular Medicine*, *14*(2), 199–208. <https://doi.org/10.2174/1566524014666140128104541>
- Marqués-Torrejón, M. Á., Williams, C. A. C., Southgate, B., Alfazema, N., Clements, M. P., Garcia-Diaz, C., Blin, C., Arranz-Emparan, N., Fraser, J., Gammoh, N., Parrinello, S., & Pollard, S. M. (2021). LRIG1 is a gatekeeper to exit from quiescence in adult neural stem cells. *Nature Communications*, *12*(1), 1–15. <https://doi.org/10.1038/s41467-021-22813-w>
- Martončíková, M., Matiašová, A. A., Ševc, J., & Račková, E. (2021). Relationship between Blood Vessels and Migration of Neuroblasts in the Olfactory Neurogenic Region of the Rodent Brain. *International Journal of Molecular Sciences*, *22*(21). <https://doi.org/10.3390/IJMS222111506>
- Martynoga, B., Mateo, J. L., Zhou, B., Andersen, J., Achimastou, A., Urbán, N., van den Berg, D.,

Bibliography

Georgopoulou, D., Hadjur, S., Wittbrodt, J., Ettwiller, L., Piper, M., Gronostajski, R. M., & Guillemot, F. (2013). Epigenomic enhancer annotation reveals a key role for NFIX in neural stem cell quiescence. *Genes & Development*, *27*(16), 1769. <https://doi.org/10.1101/GAD.216804.113>

Mateos-White, I., Fabra-Beser, J., de Agustín-Durán, D., & Gil-Sanz, C. (2020). Double In Utero Electroporation to Target Temporally and Spatially Separated Cell Populations. *Journal of Visualized Experiments : JoVE*, *2020*(160), 1–16. <https://doi.org/10.3791/61046>

Mathieu, C., Sii-Felice, K., Fouchet, P., Etienne, O., Haton, C., Mabondzo, A., Boussin, F. D., & Mouthon, M. A. (2008). Endothelial cell-derived bone morphogenetic proteins control proliferation of neural stem/progenitor cells. *Molecular and Cellular Neuroscience*, *38*(4), 569–577. <https://doi.org/10.1016/j.mcn.2008.05.005>

McBeath, R., Pirone, D. M., Nelson, C. M., Bhadriraju, K., & Chen, C. S. (2004). Cell shape, cytoskeletal tension, and RhoA regulate stem cell lineage commitment. *Developmental Cell*, *6*(4), 483–495. [https://doi.org/10.1016/S1534-5807\(04\)00075-9](https://doi.org/10.1016/S1534-5807(04)00075-9)

McKee, K. K., Crosson, S. C., Meinen, S., Reinhard, J. R., Rüegg, M. A., & Yurchenco, P. D. (2017). Chimeric protein repair of laminin polymerization ameliorates muscular dystrophy phenotype. *The Journal of Clinical Investigation*, *127*(3), 1075–1089. <https://doi.org/10.1172/JCI90854>

McKee, K. K., Harrison, D., Capizzi, S., & Yurchenco, P. D. (2007). Role of laminin terminal globular domains in basement membrane assembly. *The Journal of Biological Chemistry*, *282*(29), 21437–21447. <https://doi.org/10.1074/JBC.M702963200>

Mercier, F., & Douet, V. (2014). Bone morphogenetic protein-4 inhibits adult neurogenesis and is regulated by fractone-associated heparan sulfates in the subventricular zone. *Journal of Chemical Neuroanatomy*, *57–58*, 54–61. <https://doi.org/10.1016/j.jchemneu.2014.03.005>

Mercier, F., Kitasako, J. T., & Hatton, G. I. (2002). Anatomy of the brain neurogenic zones revisited: Fractones and the fibroblast/macrophage network. *Journal of Comparative Neurology*, *451*(2), 170–188. <https://doi.org/10.1002/cne.10342>

Mercier, F., Kitasako, J. T., & Hatton, G. I. (2003). Fractones and other basal laminae in the hypothalamus. *The Journal of Comparative Neurology*, *455*(3), 324–340. <https://doi.org/10.1002/CNE.10496>

Merkle, F. T., Fuentealba, L. C., Sanders, T. A., Magno, L., Kessar, N., & Alvarez-Buylla, A. (2014). Adult neural stem cells in distinct microdomains generate previously unknown interneuron types. *Nature Neuroscience*, *17*(2), 207–214. <https://doi.org/10.1038/NN.3610>

Merkle, F. T., Mirzadeh, Z., & Alvarez-Buylla, A. (2007). Mosaic organization of neural stem cells in the adult brain. *Science (New York, N.Y.)*, *317*(5836), 381–384. <https://doi.org/10.1126/SCIENCE.1144914>

Mira, H., Andreu, Z., Suh, H., Chichung Lie, D., Jessberger, S., Consiglio, A., Emeterio, J. S., Hortigüela, R., Marqués-Torrejón, M. Á., Nakashima, K., Colak, D., Götz, M., Fariñas, I., &

- Gage, F. H. (2010). Signaling through BMPR-IA regulates quiescence and long-term activity of neural stem cells in the adult hippocampus. *Cell Stem Cell*, 7(1), 78–89. <https://doi.org/10.1016/J.STEM.2010.04.016>
- Mirzadeh, Z., Merkle, F. T., Soriano-Navarro, M., Garcia-Verdugo, J. M., & Alvarez-Buylla, A. (2008). Neural stem cells confer unique pinwheel architecture to the ventricular surface in neurogenic regions of the adult brain. *Cell Stem Cell*, 3(3), 265–278. <https://doi.org/10.1016/J.STEM.2008.07.004>
- Mitchison, T., & Kirschner, M. (1988). Cytoskeletal dynamics and nerve growth. *Neuron*, 1(9), 761–772. [https://doi.org/10.1016/0896-6273\(88\)90124-9](https://doi.org/10.1016/0896-6273(88)90124-9)
- Morante-Redolat, J. M., & Porlan, E. (2019). Neural stem cell regulation by adhesion molecules within the subependymal niche. *Frontiers in Cell and Developmental Biology*, 7(JUN), 1–8. <https://doi.org/10.3389/fcell.2019.00102>
- Moreno-Layseca, P., Icha, J., Hamidi, H., & Ivaska, J. (2019). Integrin trafficking in cells and tissues. *Nature Cell Biology*, 21(2), 122–132. <https://doi.org/10.1038/s41556-018-0223-z>
- Morgan, M. R., Humphries, M. J., & Bass, M. D. (2007). Synergistic control of cell adhesion by integrins and syndecans. *Nature Reviews Molecular Cell Biology*, 8(12), 957–969. <https://doi.org/10.1038/nrm2289>
- Moya, I. M., & Halder, G. (2019). Hippo–YAP/TAZ signalling in organ regeneration and regenerative medicine. *Nature Reviews Molecular Cell Biology*, 20(4), 211–226. <https://doi.org/10.1038/s41580-018-0086-y>
- Naba, A., Clauser, K. R., Ding, H., Whittaker, C. A., Carr, S. A., & Hynes, R. O. (2016). The extracellular matrix: Tools and insights for the “omics” era. *Matrix Biology*, 49, 10–24. <https://doi.org/10.1016/j.matbio.2015.06.003>
- Naba, A., Clauser, K. R., Hoersch, S., Liu, H., Carr, S. A., & Hynes, R. O. (2012). The matrisome: In silico definition and in vivo characterization by proteomics of normal and tumor extracellular matrices. *Molecular and Cellular Proteomics*, 11(4), 1–18. <https://doi.org/10.1074/mcp.M111.014647>
- Nardone, G., Oliver-De La Cruz, J., Vrbsky, J., Martini, C., Pribyl, J., Skládal, P., Pešl, M., Caluori, G., Pagliari, S., Martino, F., Maceckova, Z., Hajduch, M., Sanz-Garcia, A., Pugno, N. M., Stokin, G. B., & Forte, G. (2017). YAP regulates cell mechanics by controlling focal adhesion assembly. *Nature Communications*, 8. <https://doi.org/10.1038/NCOMMS15321>
- Nascimento, M. A., Sorokin, L., & Coelho-Sampaio, T. (2018). Fractone bulbs derive from ependymal cells and their laminin composition influence the stem cell niche in the subventricular zone. *Journal of Neuroscience*, 38(16), 3880–3889. <https://doi.org/10.1523/JNEUROSCI.3064-17.2018>
- Nguyen, C. D. K., & Yi, C. (2019). YAP/TAZ Signaling and Resistance to Cancer Therapy. *Trends in Cancer*, 5(5), 283–296. <https://doi.org/10.1016/J.TRECAN.2019.02.010>

Bibliography

Nirwane, A., & Yao, Y. (2018). Laminins and their receptors in the CNS. *Biological Reviews of the Cambridge Philosophical Society*, *94*(1), 283–306. <https://doi.org/10.1111/BRV.12454>

Obernier, K., & Alvarez-Buylla, A. (2019). Neural stem cells: Origin, heterogeneity and regulation in the adult mammalian brain. *Development (Cambridge)*, *146*(4). <https://doi.org/10.1242/dev.156059>

Obernier, K., Cebrian-Silla, A., Thomson, M., Parraguez, J. I., Anderson, R., Guinto, C., Rodas Rodriguez, J., Garcia-Verdugo, J. M., & Alvarez-Buylla, A. (2018). Adult Neurogenesis Is Sustained by Symmetric Self-Renewal and Differentiation. *Cell Stem Cell*, 221-234.e8. <https://doi.org/10.1016/j.stem.2018.01.003>

Ohashi, K., Fujiwara, S., & Mizuno, K. (2017). Roles of the cytoskeleton, cell adhesion and rho signalling in mechanosensing and mechanotransduction. *Journal of Biochemistry*, *161*(3), 245–254. <https://doi.org/10.1093/jb/mvw082>

Ortiz-Álvarez, G., Daclin, M., Shihavuddin, A., Lansade, P., Fortoul, A., Faucourt, M., Clavreul, S., Lalioti, M. E., Taraviras, S., Hippenmeyer, S., Livet, J., Meunier, A., Genovesio, A., & Spassky, N. (2019). Adult Neural Stem Cells and Multiciliated Ependymal Cells Share a Common Lineage Regulated by the Geminin Family Members. *Neuron*, *102*(1), 159-172.e7. <https://doi.org/10.1016/J.NEURON.2019.01.051>

Ottone, C., Krusche, B., Whitby, A., Clements, M., Quadrato, G., Pitulescu, M. E., Adams, R. H., & Parrinello, S. (2014). Direct cell-cell contact with the vascular niche maintains quiescent neural stem cells. *Nature Cell Biology*, *16*(11), 1045–1056. <https://doi.org/10.1038/ncb3045>

Pancier, T., Azzolin, L., Cordenonsi, M., & Piccolo, S. (2017). Mechanobiology of YAP and TAZ in physiology and disease. *Nature Reviews. Molecular Cell Biology*, *18*(12), 758–770. <https://doi.org/10.1038/NRM.2017.87>

Pastrana, E., Cheng, L. C., & Doetsch, F. (2009). Simultaneous prospective purification of adult subventricular zone neural stem cells and their progeny. *Proceedings of the National Academy of Sciences of the United States of America*, *106*(15), 6387–6392. <https://doi.org/10.1073/PNAS.0810407106>

Pathak, M. M., Nourse, J. L., Tran, T., Hwe, J., Arulmoli, J., Le, D. T. T., Bernardis, E., Flanagan, L. A., & Tombola, F. (2014). Stretch-activated ion channel Piezo1 directs lineage choice in human neural stem cells. *Proceedings of the National Academy of Sciences of the United States of America*, *111*(45), 16148–16153. <https://doi.org/10.1073/PNAS.1409802111>

Paton, J. A., & Nottebohm, F. N. (1984). Neurons generated in the adult brain are recruited into functional circuits. *Science (New York, N.Y.)*, *225*(4666), 1046–1048. <https://doi.org/10.1126/SCIENCE.6474166>

Perez-Villalba, A., Sirerol-Piquer, M. S., Belenguer, G., Soriano-Cantón, R., Muñoz-Manchado, A. B., Villadiego, J., Alarcón-Arís, D., Soria, F. N., Dehay, B., Bezar, E., Vila, M., Bortolozzi, A., Toledo-Aral, J. J., Pérez-Sánchez, F., & Farías, I. (2018). Synaptic regulator α -synuclein in dopaminergic fibers is essentially required for the maintenance of subependymal neural stem cells. *Journal of Neuroscience*, *38*(4), 814–825. <https://doi.org/10.1523/JNEUROSCI.2276-17.2017>

- Petrik, D., Myoga, M. H., Grade, S., Gerkau, N. J., Pusch, M., Rose, C. R., Grothe, B., & Götz, M. (2018). Epithelial Sodium Channel Regulates Adult Neural Stem Cell Proliferation in a Flow-Dependent Manner. *Cell Stem Cell*, 22(6), 865–878.e8. <https://doi.org/10.1016/J.STEM.2018.04.016>
- Petzold, J., & Gentleman, E. (2021). Intrinsic Mechanical Cues and Their Impact on Stem Cells and Embryogenesis. *Frontiers in Cell and Developmental Biology*, 9(November). <https://doi.org/10.3389/fcell.2021.761871>
- Pineda, J. R., Daynac, M., Chicheportiche, A., Cebrian-Silla, A., Sii Felice, K., Garcia-Verdugo, J. M., Boussin, F. D., & Mouchon, M. A. (2013). Vascular-derived TGF- β increases in the stem cell niche and perturbs neurogenesis during aging and following irradiation in the adult mouse brain. *EMBO Molecular Medicine*, 5(4), 548–562. <https://doi.org/10.1002/EMMM.201202197>
- Pintér, P., & Alpár, A. (2022). The Role of Extracellular Matrix in Human Neurodegenerative Diseases. *International Journal of Molecular Sciences*, 23(19). <https://doi.org/10.3390/IJMS231911085>
- Ponti, G., Obernier, K., Guinto, C., Jose, L., Bonfanti, L., & Alvarez-Buylla, A. (2013). Cell cycle and lineage progression of neural progenitors in the ventricular-subventricular zones of adult mice. *Proceedings of the National Academy of Sciences of the United States of America*, 110(11). <https://doi.org/10.1073/PNAS.1219563110/-/DCSUPPLEMENTAL/PNAS.201219563SI.PDF>
- Porlan, E., Martí-Prado, B., Morante-Redolat, J. M., Consiglio, A., Delgado, A. C., Kypta, R., López-Otín, C., Kirstein, M., & Fariñas, I. (2014). MT5-MMP regulates adult neural stem cell functional quiescence through the cleavage of N-cadherin. *Nature Cell Biology*, 16(7), 629–638. <https://doi.org/10.1038/NCB2993>
- Porlan, E., Morante-Redolat, J. M., Marqués-Torrejón, M. Á., Andreu-Agulló, C., Carneiro, C., Gómez-Ibarlucea, E., Soto, A., Vidal, A., Ferrón, S. R., & Fariñas, I. (2013). Transcriptional repression of *Bmp2* by p21(*Waf1/Cip1*) links quiescence to neural stem cell maintenance. *Nature Neuroscience*, 16(11), 1567–1575. <https://doi.org/10.1038/NN.3545>
- Quaresima, S., Istiaq, A., Jono, H., Cacci, E., Ohta, K., & Lupo, G. (2022). Assessing the Role of Ependymal and Vascular Cells as Sources of Extracellular Cues Regulating the Mouse Ventricular-Subventricular Zone Neurogenic Niche. *Frontiers in Cell and Developmental Biology*, 10(April), 1–15. <https://doi.org/10.3389/fcell.2022.845567>
- Ramírez-Castillejo, C., Sánchez-Sánchez, F., Andreu-Agulló, C., Ferrón, S. R., Aroca-Aguilar, J. D., Sánchez, P., Mira, H., Escribano, J., & Fariñas, I. (2006). Pigment epithelium-derived factor is a niche signal for neural stem cell renewal. *Nature Neuroscience*, 9(3), 331–339. <https://doi.org/10.1038/NN1657>
- Rausch, V., & Hansen, C. G. (2020). The Hippo Pathway, YAP/TAZ, and the Plasma Membrane. *Trends in Cell Biology*, 30(1), 32–48. <https://doi.org/10.1016/j.tcb.2019.10.005>
- Reya, T., Morrison, S. J., Clarke, M. F., & Weissman, I. L. (2001). Stem cells, cancer, and cancer stem cells. *Nature*, 414(6859), 105–111. <https://doi.org/10.1038/35102167>

Bibliography

Reynolds, B. A., & Weiss, S. (1992). Generation of neurons and astrocytes from isolated cells of the adult mammalian central nervous system. *Science (New York, N.Y.)*, *255*(5052), 1707–1710. <https://doi.org/10.1126/SCIENCE.1553558>

Rodgers, J. T., King, K. Y., Brett, J. O., Cromie, M. J., Charville, G. W., Maguire, K. K., Brunson, C., Mastey, N., Liu, L., Tsai, C. R., Goodell, M. A., & Rando, T. A. (2014). mTORC1 controls the adaptive transition of quiescent stem cells from G0 to G(Alert). *Nature*, *510*(7505), 393–396. <https://doi.org/10.1038/NATURE13255>

Rojas-Vázquez, S., Blasco-Chamarro, L., López-Fabuel, I., Martínez-Máñez, R., & Fariñas, I. (2021). Vascular Senescence: A Potential Bridge Between Physiological Aging and Neurogenic Decline. *Frontiers in Neuroscience*, *15*. <https://doi.org/10.3389/FNINS.2021.666881>

Rosa, A. I., Grade, S., Santos, S. D., Bernardino, L., Chen, T. C., Relvas, J., Hofman, F. M., & Agasse, F. (2016). Heterocellular contacts with mouse brain endothelial cells via laminin and $\alpha 6 \beta 1$ integrin sustain subventricular zone (SVZ) stem/progenitor cells properties. *Frontiers in Cellular Neuroscience*, *10*(DEC2016), 1–14. <https://doi.org/10.3389/fncel.2016.00284>

Rosenbluh, J., Nijhawan, D., Cox, A. G., Li, X., Neal, J. T., Schafer, E. J., Zack, T. I., Wang, X., Tsherniak, A., Schinzel, A. C., Shao, D. D., Schumacher, S. E., Weir, B. A., Vazquez, F., Cowley, G. S., Root, D. E., Mesirov, J. P., Beroukhi, R., Kuo, C. J., ... Hahn, W. C. (2012). β -Catenin-driven cancers require a YAP1 transcriptional complex for survival and tumorigenesis. *Cell*, *151*(7), 1457–1473. <https://doi.org/10.1016/J.CELL.2012.11.026>

Ross, K. R., Corey, D. A., Dunn, J. M., & Kelley, T. J. (2007). SMAD3 expression is regulated by mitogen-activated protein kinase kinase-1 in epithelial and smooth muscle cells. *Cellular Signalling*, *19*(5), 923–931. <https://doi.org/10.1016/J.CELLSIG.2006.11.008>

Rozanova, S., Barkovits, K., Nikolov, M., Schmidt, C., Urlaub, H., & Marcus, K. (2021). Quantitative Mass Spectrometry-Based Proteomics: An Overview. *Methods in Molecular Biology (Clifton, N.J.)*, *2228*, 85–116. https://doi.org/10.1007/978-1-0716-1024-4_8

Sato, Y., Kiyozumi, D., Futaki, S., Nakano, I., Shimono, C., Kaneko, N., Ikawa, M., Okabe, M., Sawamoto, K., & Sekiguchi, K. (2019). Ventricular–subventricular zone fractones are speckled basement membranes that function as a neural stem cell niche. *Molecular Biology of the Cell*, *30*(1), 56–68. <https://doi.org/10.1091/mbc.E18-05-0286>

Schaeffer, S., & Iadecola, C. (2021). Revisiting the neurovascular unit. *Nature Neuroscience* *2021* *24*:9, *24*(9), 1198–1209. <https://doi.org/10.1038/s41593-021-00904-7>

Schmierer, B., & Hill, C. S. (2007). TGF β -SMAD signal transduction: Molecular specificity and functional flexibility. *Nature Reviews Molecular Cell Biology*, *8*(12), 970–982. <https://doi.org/10.1038/nrm2297>

Sedlmeier, G., & Sleeman, J. P. (2017). Extracellular regulation of BMP signaling: Welcome to the matrix. *Biochemical Society Transactions*, *45*(1), 173–181. <https://doi.org/10.1042/BST20160263>

- Segarra, M., Aburto, M. R., Hefendehl, J., & Acker-Palmer, A. (2019). Neurovascular Interactions in the Nervous System. *Annual Review of Cell and Developmental Biology*, 35, 615–635. <https://doi.org/10.1146/ANNUREV-CELLBIO-100818-125142>
- Sekiguchi, R., & Yamada, K. M. (2018). Basement Membranes in Development and Disease. *Current Topics in Developmental Biology*, 130, 143–191. <https://doi.org/10.1016/BS.CTDB.2018.02.005>
- Seo, J., & Kim, J. (2018). Regulation of Hippo signaling by actin remodeling. *BMB Reports*, 51(3), 151. <https://doi.org/10.5483/BMBREP.2018.51.3.012>. *BMB Reports*, 51(3), 151. <http://www.ncbi.nlm.nih.gov/pubmed/29353600> <http://www.pubmedcentral.nih.gov/articlerender.fcgi?artid=PMC5882222>
- Shen, Q., Goderie, S. K., Jin, L., Karanth, N., Sun, Y., Abramova, N., Vincent, P., Pumiglia, K., & Temple, S. (2004). Endothelial cells stimulate self-renewal and expand neurogenesis of neural stem cells. *Science*, 304(5675), 1338–1340. <https://doi.org/10.1126/science.1095505>
- Shen, Q., Wang, Y., Kokovay, E., Lin, G., Chuang, S. M., Goderie, S. K., Roysam, B., & Temple, S. (2008). Adult SVZ stem cells lie in a vascular niche: a quantitative analysis of niche cell-cell interactions. *Cell Stem Cell*, 3(3), 289–300. <https://doi.org/10.1016/J.STEM.2008.07.026>
- Shilov, I. V., Seymour, S. L., Patel, A. A., Loboda, A., Tang, W. H., Keating, S. P., Hunter, C. L., Nuwaysir, L. M., & Schaeffer, D. A. (2007). The Paragon Algorithm, a next generation search engine that uses sequence temperature values and feature probabilities to identify peptides from tandem mass spectra. *Molecular & Cellular Proteomics : MCP*, 6(9), 1638–1655. <https://doi.org/10.1074/MCP.T600050-MCP200>
- Silva-Vargas, V., Maldonado-Soto, A. R., Mizrak, D., Codega, P., & Doetsch, F. (2016). Age-Dependent Niche Signals from the Choroid Plexus Regulate Adult Neural Stem Cells. *Cell Stem Cell*, 19(5), 643–652. <https://doi.org/10.1016/j.stem.2016.06.013>
- Simons, B. D., & Clevers, H. (2011). Strategies for homeostatic stem cell self-renewal in adult tissues. *Cell*, 145(6), 851–862. <https://doi.org/10.1016/j.cell.2011.05.033>
- Sirerol-Piquer, M. S., Belenguer, G., Morante-Redolat, J. M., Duart-Abadia, P., Perez-Villalba, A., & Fariñas, I. (2019). Physiological Interactions between Microglia and Neural Stem Cells in the Adult Subependymal Niche. *Neuroscience*, 405, 77–91. <https://doi.org/10.1016/J.NEUROSCIEN.2019.01.009>
- Sun, Yirui, Hu, J., Zhou, L., Pollard, S. M., & Smith, A. (2011). Interplay between FGF2 and BMP controls the self-renewal, dormancy and differentiation of rat neural stem cells. *Journal of Cell Science*, 124(Pt 11), 1867–1877. <https://doi.org/10.1242/JCS.085506>
- Sun, Yubing, Chen, C. S., & Fu, J. (2012). Forcing stem cells to behave: a biophysical perspective of the cellular microenvironment. *Annual Review of Biophysics*, 41(1), 519–542. <https://doi.org/10.1146/ANNUREV-BIOPHYS-042910-155306>
- Sun, Yubing, Yong, K. M. A., Villa-Diaz, L. G., Zhang, X., Chen, W., Philson, R., Weng, S., Xu, H.,

Bibliography

- Krebsbach, P. H., & Fu, J. (2014). Hippo/YAP-mediated rigidity-dependent motor neuron differentiation of human pluripotent stem cells. *Nature Materials*, *13*(6), 599–604. <https://doi.org/10.1038/nmat3945>
- Sun, Zhiqi, Guo, S. S., & Fässler, R. (2016). Integrin-mediated mechanotransduction. *The Journal of Cell Biology*, *215*(4), 445–456. <https://doi.org/10.1083/JCB.201609037>
- Sun, Zhiwei, Cai, S., Zabkiewicz, C., Liu, C., & Ye, L. (2020). Bone morphogenetic proteins mediate crosstalk between cancer cells and the tumour microenvironment at primary tumours and metastases (Review). *International Journal of Oncology*, *56*(6), 1335–1351. <https://doi.org/10.3892/ijo.2020.5030>
- Takada, Y., Ye, X., & Simon, S. (2007). The integrins. *Genome Biology*, *8*(5). <https://doi.org/10.1186/GB-2007-8-5-215>
- Tavazoie, M., Van der Veken, L., Silva-Vargas, V., Louissaint, M., Colonna, L., Zaidi, B., Garcia-Verdugo, J. M., & Doetsch, F. (2008). A Specialized Vascular Niche for Adult Neural Stem Cells. *Cell Stem Cell*, *3*(3), 279–288. <https://doi.org/10.1016/j.stem.2008.07.025>
- Tyler, W. J. (2012). The mechanobiology of brain function. *Nature Reviews. Neuroscience*, *13*(12), 867–878. <https://doi.org/10.1038/NRN3383>
- Urbán, N., Blomfield, I. M., & Guillemot, F. (2019). Quiescence of Adult Mammalian Neural Stem Cells: A Highly Regulated Rest. *Neuron*, *104*(5), 834–848. <https://doi.org/10.1016/j.neuron.2019.09.026>
- Urbán, N., & Guillemot, F. (2014). Neurogenesis in the embryonic and adult brain: same regulators, different roles. *Frontiers in Cellular Neuroscience*, *8*(NOV). <https://doi.org/10.3389/FNCEL.2014.00396>
- van Velthoven, C. T. J., & Rando, T. A. (2019). Stem Cell Quiescence: Dynamism, Restraint, and Cellular Idling. *Cell Stem Cell*, *24*(2), 213–225. <https://doi.org/10.1016/J.STEM.2019.01.001>
- Vescovi, A. L., Reynolds, B. A., Fraser, D. D., & Weiss, S. (1993). bFGF regulates the proliferative fate of unipotent (neuronal) and bipotent (neuronal/astroglial) EGF-generated CNS progenitor cells. *Neuron*, *11*(5), 951–966. [https://doi.org/10.1016/0896-6273\(93\)90124-A](https://doi.org/10.1016/0896-6273(93)90124-A)
- Vidak, E., Javoršek, U., Vizovišek, M., & Turk, B. (2019). Cysteine cathepsins and their extracellular roles: Shaping the microenvironment. *Cells*, *8*(3). <https://doi.org/10.3390/cells8030264>
- Vining, K. H., & Mooney, D. J. (2017). Mechanical forces direct stem cell behaviour in development and regeneration. *Nature Reviews Molecular Cell Biology*, *18*(12), 728–742. <https://doi.org/10.1038/nrm.2017.108>
- Wagh, K., Ishikawa, M., Garcia, D. A., Stavreva, D. A., Upadhyaya, A., & Hager, G. L. (2021). Mechanical Regulation of Transcription: Recent Advances. *Trends in Cell Biology*, *31*(6), 457–472. <https://doi.org/10.1016/j.tcb.2021.02.008>

- Wang, J., Toregrosa-Allen, S., Elzey, B. D., Utturkar, S., Lanman, N. A., Bernal-Crespo, V., Behymer, M. M., Knipp, G. T., Yun, Y., Veronesi, M. C., Sinn, A. L., Pollok, K. E., Brutkiewicz, R. R., Nevel, K. S., & Matosevic, S. (2021). Multispecific targeting of glioblastoma with tumor microenvironment-responsive multifunctional engineered NK cells. *Proceedings of the National Academy of Sciences of the United States of America*, *118*(45), e2107507118. https://doi.org/10.1073/PNAS.2107507118/SUPPL_FILE/PNAS.2107507118.SM02.MOV
- Wang, W., Zuidema, A., Molder, L. te, Nahidiazar, L., Hoekman, L., Schmidt, T., Coppola, S., & Sonnenberg, A. (2020). Hemidesmosomes modulate force generation via focal adhesions. *Journal of Cell Biology*, *219*(2), 1–19. <https://doi.org/10.1083/jcb.201904137>
- Weickert, C. S., Webster, M. J., Colvin, S. M., Herman, M. M., Hyde, T. M., Weinberger, D. R., & Kleinman, J. E. (2000). Localization of epidermal growth factor receptors and putative neuroblasts in human subependymal zone. *Journal of Comparative Neurology*, *423*(3), 359–372. [https://doi.org/10.1002/1096-9861\(20000731\)423:3<359::AID-CNE1>3.0.CO;2-0](https://doi.org/10.1002/1096-9861(20000731)423:3<359::AID-CNE1>3.0.CO;2-0)
- Whitman, M. C., Fan, W., Rela, L., Rodriguez-Gil, D. J., & Greer, C. A. (2009). Blood vessels form a migratory scaffold in the rostral migratory stream. *The Journal of Comparative Neurology*, *516*(2), 94–104. <https://doi.org/10.1002/CNE.22093>
- Xu, Y., Zhou, J., Liu, C., Zhang, S., Gao, F., Guo, W., Sun, X., Zhang, C., Li, H., Rao, Z., Qiu, S., Zhu, Q., Liu, X., Guo, X., Shao, Z., Bai, Y., Zhang, X., & Quan, D. (2021). Understanding the role of tissue-specific decellularized spinal cord matrix hydrogel for neural stem/progenitor cell microenvironment reconstruction and spinal cord injury. *Biomaterials*, *268*. <https://doi.org/10.1016/J.BIOMATERIALS.2020.120596>
- Yousef, H., Morgenthaler, A., Schlesinger, C., Bugaj, L., Conboy, I. M., & Schaffer, D. V. (2015). Age-Associated Increase in BMP Signaling Inhibits Hippocampal Neurogenesis. *Stem Cells (Dayton, Ohio)*, *33*(5), 1577–1588. <https://doi.org/10.1002/STEM.1943>
- Yurchenco, P. D., Amenta, P. S., & Patton, B. L. (2004). Basement membrane assembly, stability and activities observed through a developmental lens. *Matrix Biology*, *22*(7), 521–538. <https://doi.org/10.1016/j.matbio.2003.10.006>
- Yuzwa, S. A., Borrett, M. J., Innes, B. T., Voronova, A., Ketela, T., Kaplan, D. R., Bader, G. D., & Miller, F. D. (2017). Developmental Emergence of Adult Neural Stem Cells as Revealed by Single-Cell Transcriptional Profiling. *Cell Reports*, *21*(13), 3970–3986. <https://doi.org/10.1016/j.celrep.2017.12.017>
- Zappaterra, M. W., & Lehtinen, M. K. (2012). The cerebrospinal fluid: regulator of neurogenesis, behavior, and beyond. *Cellular and Molecular Life Sciences : CMLS*, *69*(17), 2863–2878. <https://doi.org/10.1007/S00018-012-0957-X>
- Zhu, C., Yao, W. L., Tan, W., & Zhang, C. H. (2017). SDF-1 and CXCR4 play an important role in adult SVZ lineage cell proliferation and differentiation. *Brain Research*, *1657*, 223–231. <https://doi.org/10.1016/J.BRAINRES.2016.06.011>

Bibliography

Zhu, Y., Li, X., Janairo, R. R. R., Kwong, G., Tsou, A. D., Chu, J. S., Wang, A., Yu, J., Wang, D., & Li, S. (2019). Matrix stiffness modulates the differentiation of neural crest stem cells in vivo. *Journal of Cellular Physiology*, *234*(5), 7569–7578. <https://doi.org/10.1002/jcp.27518>

Zimmermann, L. M. A., Correns, A., Furlan, A. G., Spanou, C. E. S., & Sengle, G. (2021). Controlling BMP growth factor bioavailability: The extracellular matrix as multi skilled platform. *Cellular Signalling*, *85*(July), 110071. <https://doi.org/10.1016/j.cellsig.2021.110071>

Annex

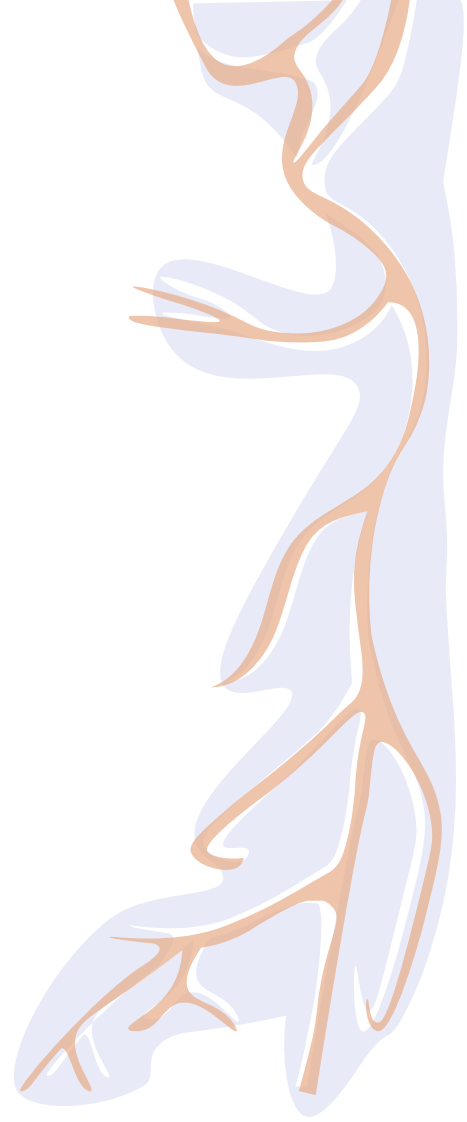


Table 1-Primary antibodies

<i>Antibody</i>	<i>Host</i>	<i>Dilution</i>	<i>Source, ref.</i>	<i>Application</i>
AQP4	rabbit	1: 500	Sigma, HPA014784	IHC
CD31	rat	1:100	BD, 550274	IHC, ICC
GFAP	chicken	1:800	Millipore, AB5541	IHC, ICC
GFP	chicken	1:500	Aveslab, GFP-1020	IHC, TEM
Laminin	rabbit	1:500	Novus, NB300-144	IH/CC, FC, WB
Nestin	mouse	1:3	Hibridoma bank, rat-401	ICC
S100b	mouse	1:400	Sigma, S2532	IHC
CD45-BV421	rat	1:200	BD, 563890	FC <i>in vivo</i>
O4-Biotin	mouse	1:30	Miltenyi, 130-095-895	FC <i>in vivo</i>
CD31-BV421	rat	1:100	BD, 563356	FC <i>in vivo</i>
TER-119-BV42	rat	1:200	BD, 563998	FC <i>in vivo</i>
A647 streptavidin		1:300	BD, 563259	FC <i>in vivo</i>
CD24-PerCP-Cy5.5	rat	1.300	BD, 562360	FC <i>in vivo</i>
CD9-APC-VIO770	rat	1:20	Miltenyi, 130-102-384	FC <i>in vivo</i>
GLAST-PE	mouse	1:100	Miltenyi, 130-118-344	FC <i>in vivo/in vitro</i>
EGF-A488	rat	1:300	Molecular probes, E13345	FC <i>in vivo/in vitro</i>
EGF-A647	rat	1:300	Molecular probes, E35351	FC <i>in vivo/in vitro</i>
DAPI		0.1 µg/ml	Sigma, D9542	IHC, ICC; FC

Table 2- Secondary antibodies

<i>Fluorescence</i>	<i>Specificity</i>	<i>Dilution</i>	<i>Source, ref.</i>	<i>Application</i>
Alexa Fluor® 488	chicken	1: 800	Jackson Imm., HPA014784	IHC, ICC
Alexa Fluor® 488	mouse	1:800	Molecular probes, A21202	ICC
Alexa Fluor® 488	rabbit	1:800	Jackson Imm., 711-547-003	IHC, ICC
Alexa Fluor® 647	rabbit	1:800	Molecular probes, A31573	IHC, FC
Cy3	rabbit	1:800	Jackson Imm., 711-165-152	IHC, ICC
Cy3	rat	1:800	Jackson Imm., 712-165-153	ICC
HRP	rabbit	1:5000	Dako, P0449	WB

Annex

Table 3- FACS buffer

<i>Reagent</i>	<i>Concentration</i>	<i>Stock</i>	<i>Source</i>	<i>Ref.</i>
HBSS*	1X	10X	Gibco	14185052
HEPES	10mM	1M	Biowest	L0180-100
EDTA	2mM	20mM	Sigma	E6511
BSA	0.5%	Powder	Sigma	B4287

*Without Ca²⁺ and Mg²⁺

Table 4- EC isolation buffer

<i>Reagent</i>	<i>Concentration</i>	<i>Stock</i>	<i>Source</i>	<i>Ref.</i>
HBSS*	1X	10X	Gibco	14185052
Piruvate	1 mM	100 mM	Biowest	L0180-100
Glucose	0.6%	30%	Panreac	141341
BSA	0.5%	Powder	Sigma	B4287

* With Ca²⁺ and Mg²⁺

Table 5- HUVEC media

<i>Reagent</i>	<i>Conc.</i>	<i>Volume (100ml)</i>	<i>Source</i>	<i>Ref.</i>
EndoGRO-LS*	1X	91.4ml	Millipore	SCME-001
LS supplement	0.2%	200µl		
rhEGF	5 ng/ml	100µl		
L-Glutamine	10mM	5ml		
Hydrocortisone Hemisuccinate	1 µg/ml	100µl		
Heparan sulfate	0.75U/ml	100µl		
Ascorbic Acid	50 µg/ml	100µl		
FBS	5%	2ml		
Antibiotic/antimycotic	1X	1ml	Gibco	15240-062

* All components (except for antibiotics) are included in EndoGRO-LS complete culture media kit and are freshly added when prepared. Working concentrations are listed.

Table 6- Primary EC media

<i>Reagent</i>	<i>Conc.</i>	<i>Volume (50 ml)</i>	<i>Source</i>	<i>Ref.</i>
Endothelial cell growth medium MV2*	1X	46.8	Promo-cell	C-22022
Antibiotic/antimycotic	1X	0.5mL		
Supplement mix:		2.7mL		
VEGF	0.5 ng/ml			
EGF	5 ng/ml			
bFGF	10 ng/ml			
IGF	20 ng/ml			
Ascorbic Acid	1 µg/ml			
Heparin	22.5 µg/ml			
Hydrocortisone	0.2 µg/ml			
Fetal Calf Serum	0.02 ml/ml			

* Growth medium MV2 (Ready-to-use) contains a supplement mix that is already prepared with all the components. Supplement mix and antibiotics are added before its use.

Annex

Table 7- NSC control media

<i>Reagent</i>	<i>Concentration</i>	<i>Stock</i>	<i>Source</i>	<i>Ref.</i>
DMEM/F12	1X	10X	Gibco	11320-074
HEPES	5mM	1M	Biowest	L0180-100
Sodium bicarbonate	0.1%	7.5%	Biowest	L0680-500
L-Glutamine	2 mM	200 mM	Gibco	25030-081
Heparin sodium salt	0.7 U/ml	350 U/ml	Sigma	H3149
Antibiotic/Antimycotic	1X	100X	Gibco	15240-062
B27 supplement *	1X	50X	Gibco	1750404
Hormone mix:	1X	10X		
DMEM/F12	1X	10X	Gibco	11320-074
HEPES	5mM	1M	Biowest	L0180-100
Sodium bicarbonate	0.1%	7.5%	Biowest	L0680-500
Apo-transferrin	1 mg/ml	Powder	Sigma	T2252
Bovine Insulin	0.05 mg/ml	8.3 mg/ml	Sigma	I6634
Putrescine	160 µg/ml	96.5 mg/ml	Sigma	P7505
Progesterone	0.2 nM	2 µM	Sima	P6149
Sodium selenite	0.3 µM	3 mM	Gibco	S9133
BSA	0.5 mg/ml	75 mg/ml	Sigma	B4287

*B27 supplement was only added in NSC nucleofections and sorting experiments

Table 8- NSC growth media

<i>Reagent</i>	<i>Concentration</i>	<i>Stock</i>	<i>Source</i>	<i>Ref.</i>
NSC control media	1X	1X		
EGF	20 ng/ml	4 µg/ml	Gibco	53003-018
bFGF	10 ng/ml	25 µg/ml	Sigma	F0291

Table 9- Gelling solution

<i>Reagent</i>	<i>Concentration</i>	<i>Stock</i>
4HT	1 mg/ml	5 mg/ml
TEMED	20 mg/ml	100 mg/ml
APS	20 mg/ml	100 mg/ml
Stock X:	NA	NA
Sodium acrylate	86 mg/ml	380 mg/ml
Acrylamide	25 mg/ml	290 mg/ml
N,N-methylenebisacrylamide	1.5 mg/ml	20 mg/ml
NaCl	117 mg/ml	5M
PBS	1X	10X

Table 10- Digestion solution

<i>Reagent</i>	<i>Concentration</i>	<i>Stock</i>
Triton X-100	5 mg/ml	powder
EDTA, disodium	2 µl/ml	0.5M
Tris-Cl	5ml	1M
NaCl	46.7mg/mL	powder
Proteinase K	8U/ml	800U/ml

Table 11- Taqman probes

<i>Gene</i>	<i>TaqMan probe Ref.</i>
<i>Gapdh</i>	Mm99999915_g1
<i>18S</i>	Hs99999901_s1
<i>Lama3</i>	Mm01254735_m1
<i>Lama5</i>	Mm01222029_m1
<i>Lamb2</i>	Mm00493080_m1
<i>Lamb3</i>	Mm00493108_m1
<i>Itga6</i>	Mm00434375_m1

Annex

Table 12- Laemmli buffer

<i>Reagent</i>	<i>Concentration</i>
Tris-HCl (pH 6.8)	62.5 mM
Glycerol	10%
SDS	1%
DTT	100 mM
Bromophenol blue	0,02%

Table 13- Transfer buffer

<i>Reagent</i>	<i>Concentration</i>
Tris base	25 mM
Glycine	200 mM
Methanol	20%
SDS	0,01%

Table 14- Tris buffer saline

<i>Reagent</i>	<i>Concentration</i>
Tris-HCl (pH 7.5)	0.1 M
NaCl	0.9 %
Tween-20	0.1%

T

Figure 1- ROCK1 WT and $\Delta 5$ constructs for nucleofections

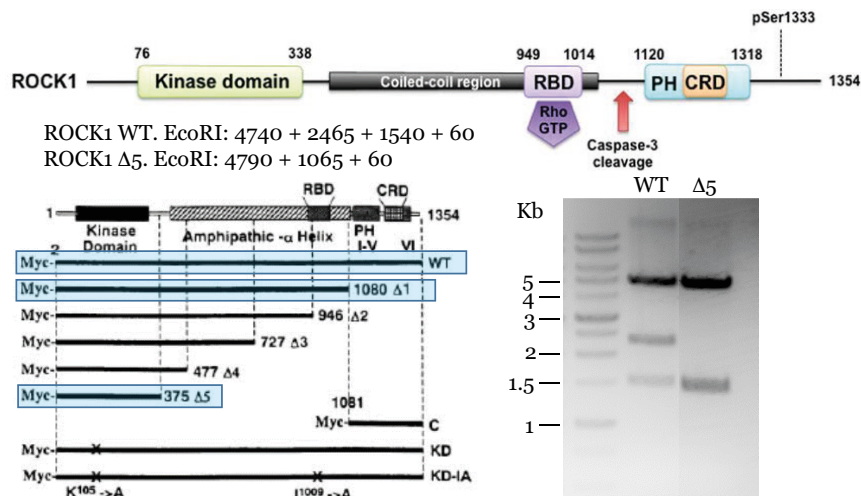
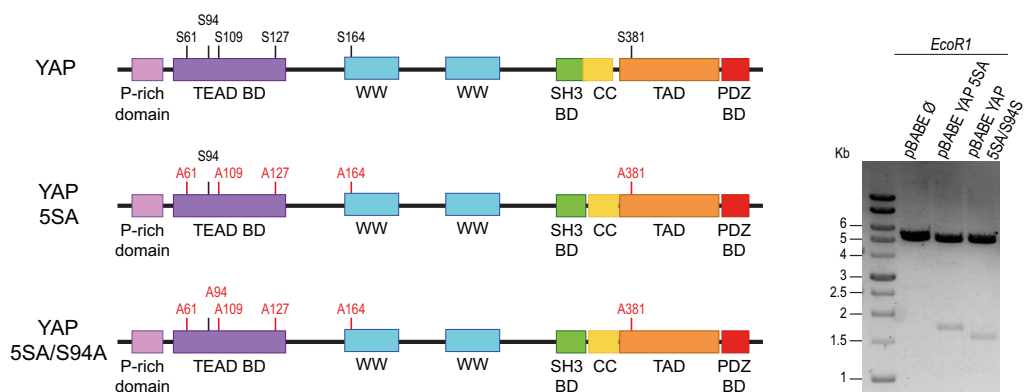


Figure 2- YAP constructs for nucleofections



Agradecimientos



Si vuelvo a la primera página de la historia que he ido escribiendo a lo largo de estos años, todavía consigo verme. Con la mochila cargada de ilusión, ganas de aprender y, por qué no decirlo, la inseguridad de alguien que elige un camino con la incertidumbre de no conocer lo que se va a encontrar en él. Veo a una persona diferente a la que está escribiendo esto. La de ahora tiene la misma ilusión y las mismas ganas, eso sí, pero es distinta. Más segura y orgullosa de sí misma, y con la resiliencia que da haber aprendido que los fracasos solo te acercan un paso más a tus objetivos. Para mí, la investigación te despierta algo por dentro. Hacer un descubrimiento con tus experimentos, por muy pequeño que sea, te inspira a seguir queriendo entender la vida a través de la lente de un microscopio. Y cuando empiezas, es difícil encontrar algo más estimulante que las ganas de descubrir. Si vuelvo de nuevo a esa primera página, lo que nunca hubiese podido llegar a imaginar es que las personas con las que compartiría el camino serían, sin duda, mi mejor descubrimiento.

Isabel, gracias por confiar en mí. Me has conseguido contagiar tu pasión por la ciencia, y has sabido guiarme y motivarme en cada paso del camino. Gracias por darme tanta libertad para crecer, así como los medios y el apoyo para conseguirlo. Gracias por haber sabido encontrar el equilibrio perfecto entre la exigencia y la cercanía. Eres un gran ejemplo a seguir.

Mi familia científica, Neuromol. Los que ya terminaron, y los que todavía me acompañan. Muchísimas gracias a cada una de las personas que habéis hecho de la rutina algo estimulante y divertido. Habéis sido un apoyo constante y me habéis enseñado el significado de la palabra equipo. Me llevo grandes recuerdos y amigos con los que, sin duda, espero vivir muchas otras aventuras. Gracias, también, a las personas con las que compartí mi tiempo en Frankfurt, que hicieron de la estancia una experiencia personal y profesional única.

A mis amigas y amigos. Los que han estado cerca, y los que han estado a una pantalla de distancia. Gracias por formar parte de ese gran *et al.* que me acompaña también en la vida.

Pere, siete letras se quedan más que cortas, pero GRACIAS. Así, en mayúsculas. Si tuviese que agradecerte con palabras todo lo que has hecho y haces por mí, podría escribir un libro entero. No solo me has acompañado en cada paso, sino que has dado todos y cada uno de ellos conmigo de la mano. Viviendo cada éxito y cada fracaso, como propios. Gracias por dejarme aprender de ti, y por quererme en todas mis versiones.

Por último, a mi familia, especialmente a mis tres incondicionales. A mis padres, Ángela y Óscar, y a mi hermana, Sara. Las personas que confían en mí muchísimo más que yo misma. A quienes nunca he tenido que pedir nada, porque siempre se han anticipado para ofrecerme, en cada momento, lo que he necesitado. Gracias por escucharme, entenderme y apoyarme en esta etapa y siempre. Gracias por ser mi trampolín, y ayudarme a saltar cada vez más alto. Sin duda, esta tesis es también vuestra.

Este trabajo de Tesis Doctoral ha sido posible gracias a una beca predoctoral del Programa de Formación de Profesorado Universitario (FPU), financiada por el Ministerio de Universidades (MIU), un contrato como investigadora no doctora financiado por el Plan Nacional de I+D+I del Ministerio de ciencia e innovación (MICINN) La investigación ha sido financiada por los siguientes proyectos de investigación a cargo de Isabel Fariñas:

- 2014-2018. Estudio de células madre en el ámbito de las investigaciones básicas en terapia celular. Fundación Botín-Banco de Santander
- 2015-2017. Regulación molecular de la quiescencia: células madre neurales. MINECO (SAF2014-54581-R).
- 2018-2021. Regulación del comportamiento de las células madre neurales por el medio sistémico: el nicho extendido. MINECO (SAF2017-86690-R).
- 2016-Vigente. CIBER en Enfermedades Neurodegenerativas (CIBERNED). ISCIII (Programa de Investigación Cooperativa, CB06/05/0086).
- 2017-2021. Efectos directos y remotos de la respuesta inflamatoria sobre las células madre neurales. Generalitat Valenciana (Proyectos de Excelencia, PROMETEO/2017/030).
- 2017-2021. RETIC de terapia celular ISCIII (RD16/0011/0017).
- 2021-2024 Regulación molecular de la heterogeneidad celular en los nichos neurogénicos adultos MICINN (PID2020- 117937GB-I00).

